Doctoral Dissertation

Dispersion and Interfacial Management for Designing Polypropylene Nanocomposites

Zhu Dongzhi

Supervisor: Toshiaki Taniike

Graduate School of Advanced Science and Technology

Japan Advanced Institute of Science and Technology

Materials Science

September 2022

Dispersion and interfacial management for designing polypropylene nanocomposites

Zhu Dongzhi (1920417)

Along with the worldwide trend toward more energy-efficient structure and reduced emissions in industry and transportation, there is an increasing demand for developing lightweight, high-performance, and low-cost materials. Plastics are among the material of choices, which not only provide the light-weight structure, but also require less energy manufacturing processes into the final products as compared to other materials such as metals and glass. Currently, nanofillers are widely used to enhance mechanical and thermomechanical performances of polymers. However, the addition of nanofillers often results in a considerable loss in the toughness and elongation at break due to the rigidity of the embedded nanoparticles as well as loose interfaces. Thus, it is essential to explore a way to alleviate these problems in order to devise high-performant polymer nanocomposites. In this dissertation, I exploited different strategies, with the aim to fabricate polymer nanocomposites bearing desired properties without sacrificing the toughness. The main research results are as follows:

In **Chapter 2**, organically modified SiO_2 was used to prepare graft-type polypropylene (PP) nanocomposites, where PP containing less than one functional group per chain prepared by catalyzed copolymerization between propylene and 7-octenyltrimethoxysilane (PP-OTMS) was used as a reactive matrix. It was found that surface modification of SiO_2 with silane coupling agents enhanced the hydrophobicity of SiO_2 surfaces to improve the dispersion of SiO_2, which in turn promoted the in-situ grafting of PP-OTMS onto filler surfaces via hydrolysis/condensation. The modification with long alkyl chains led to efficient grafting to strengthen the interfacial interaction, and recovered the deterioration in the elongation at break from its plasticizing ability. This provided an opportunity to balance the reinforcement and the toughness of the materials, which is hardly achieved by the in-situ grafting or surface modification alone.

In **Chapter 3**, a novel PP matrix bearing methoxy-phenyl side-functional groups (PP-ADMB) was synthesized by copolymerization of propylene with 4-allyl-1,2-dimethoxybenzene. The introduction of methoxy-phenyl side-functional groups even at a trace amount not only improved the compatibility between the matrix and fillers to promote the dispersion of SiO_2, but also softened the polymer, which dramatically improved the elongation at break and the toughness without deteriorating the reinforcement of PP nanocomposites. These functions of PP-ADMB make it advantageous over the homo PP in balancing the mechanical properties of nanocomposites.

In **Chapter 4**, reactor granule technology (RGT), where TiO_2 nanoparticles were in-situ formed in the porous structure of PP granules, was used to fabricate biaxially oriented polypropylene (BOPP) nanocomposites. Benefitted from highly dispersed TiO_2 nanoparticles, biaxial stretching without breakage was achieved. The permittivity of nanocomposites was greatly enhanced beyond the classical mixing rule by a small amount of TiO_2. This suggested the critical role of the interphase around nanoparticles.

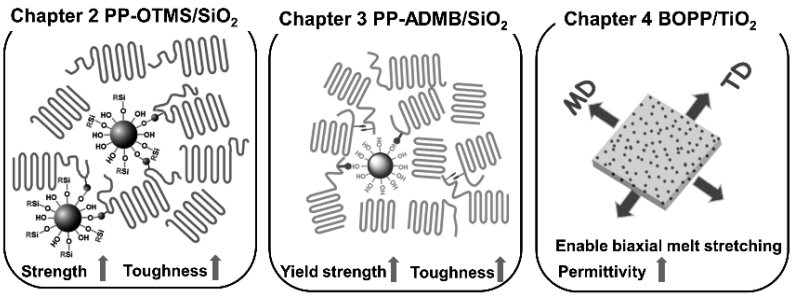

Fig. 1. Materials design implemented in this thesis.

In conclusion, three different strategies were successfully implemented to fabricate PP nanocomposites (Fig. 1), which facilitated desired properties without sacrificing the ductility of the material. These developed strategies are believed to be promising for designing high-performance polymer nanocomposites.

Keywords: Polymer nanocomposites; Mechanical properties; Reactor granule technology; Biaxially oriented polypropylene; Dielectric properties

Referee-in-chief: Professor Toshiaki Taniike
Japan Advanced Institute of Science and Technology

Referees: Professor Masayuki Yamaguchi
Japan Advanced Institute of Science and Technology

Professor Kazuaki Matsumura
Japan Advanced Institute of Science and Technology

Associate Professor Eijiro Miyako
Japan Advanced Institute of Science and Technology

Professor Wen-Hua Sun
Institute of Chemistry Chinese Academy of Sciences

Preface

The present thesis is submitted for the Degree of Doctor of Philosophy at Japan Advanced Institute of Science and Technology, Japan. The thesis is consolidation of results of the research work on the topic "Dispersion and interfacial management for designing polypropylene nanocomposites" and implemented during October 2019–September 2022 under the supervision of Prof. Dr. Toshiaki Taniike at Graduate School of Advanced Science and Technology, Japan Advanced Institute of Science and Technology.

Chapter 1 provides a general introduction of the research field, and accordingly the objective of this thesis. **Chapter 2** combines the surface modification of silica nanoparticles (SiO_2) with in situ grafting and the mechanical properties of resultant polypropylene (PP)/SiO_2 nanocomposites. **Chapter 3** describes the design of functionalized PP/SiO_2 nanocomposites for balanced toughness and stiffness. **Chapter 4** reports the design of biaxially oriented polypropylene (BOPP)/TiO_2 nanocomposites by applying the reactor granule technology (RGT) for the dielectric properties. Finally, **Chapter 5** describes the general conclusions of this thesis. The work is original, and no part of this thesis has been plagiarized.

Zhu Dongzhi

Graduate School of Advanced Science and Technology

Japan Advanced Institute of Science and Technology

September 2022

Acknowledgements

I would like to express my sincere gratitude to my supervisor, Prof. Dr. Toshiaki Taniike, Graduate School of Advanced Science and Technology, Japan Advanced Institute of Science and Technology, who has offered me a kind guidance and whose valuable suggestions, incisive comment, constructive criticism, and heartfelt encouragement have contributed greatly to the completion of this thesis. I am grateful to him for his tremendous assistance in developing the framework and revising the draft of this thesis several times. His patience, encouragement, and professional instructions helped me in all the time of research and writing of this thesis. I am deeply grateful to Senior Lecturer Dr. Chammingkwan Patchanee for her helpful discussion and many suggestions about experiments. I would like to thank the nanocomposites research group of Taniike laboratory for stimulating discussions and constant help. I am also heartily grateful to all the members of Taniike laboratory for their valuable suggestions, cooperation and support.

I would also take this opportunity to thank Prof. Noriyoshi Matsumi and Prof. Tatsuo Kaneko in JAIST for their guidance and encouragement for me. Without their kind support and help, the completion of the present thesis would not have been possible. I would also like to thank the members of my review committee, Prof. Masayuki Yamaguchi (JAIST), Prof. Kazuaki Matsumura (JAIST), Assoc. Prof. Eijiro

Miyako (JAIST), and Prof. Wen-Hua Sun (Institute of Chemistry Chinese Academy of Sciences), who have spent their valuable time to read the thesis and provided their insightful comments and remarks to enhance the quality of this thesis from various perspectives.

I am also grateful for the scholarship of China Scholarship Council during my doctoral course studying. Last but not the least, my gratitude also extends to my family who has been assisting, supporting, and caring for all my life. Special thanks should go to my friends for their utmost care and moral support.

Zhu Dongzhi

Graduate School of Advanced Science and Technology

Japan Advanced Institute of Science and Technology

September 2022

Table of contents

Chapter 1

General Introduction

Chapter 1

1.1. Polymer nanocomposites

Polymer materials have been one of the most important parts in the development of materials science, due to their lightweight, low cost, and easy processing, which cover a wide range of applications from daily life to aerospace [1–13]. In particular, polymer composites, containing fillers with at least one dimension less than 100 nm [14] are called polymer nanocomposites. Since its discovery for nylon6/clay hybrids [15,16], they have attracted increasing interests due to that a small proportion of nanoparticles dispersed in polymer matrices not only leads to reinforcements but also new functionalities which are not present in the original polymers [17–25]. Significant increases in the particle number density and the interfacial area due to the small size allow polymer nanocomposites to attain favorable properties at a considerably lower filler loading than conventional micro-sized based polymer composites [26–35]. At present, polymers such as polyamide (PA), polyphenylene sulfide (PPS), and polypropylene (PP) are extensively reinforced with nanofillers to improve their mechanical and thermomechanical performance as a cost-effective replacement for traditional engineering materials in demanding applications such as automotives, aerospace, marine, and electronics, and so on [35]. Hereafter, a brief introduction of polymer matrices, nanofillers, and the process of nanocomposites is described.

1.1.1. Polymer matrices

The polymer matrix is the most important component of a polymer nanocomposites [36]. When compared to other materials such as metals and ceramics, polymers have lower strength, modulus, electric permittivity, and so on. With the effort to overcome these limitations, polymers are reinforced with appropriate nanofillers to satisfy specific application demands [37]. Among the multiple polymer matrices, polyolefin-based nanocomposites are considered as one of the most commonly used thermoplastics matrix for fabricating nanocomposites [38,39].

1.1.2. Nanofillers

Nanofillers play important roles in modifying desirable properties of polymers with lower cost [40] As illustrated in Fig. 1.1. based on their dimensions, nanofillers are classed as zero-dimensional (spherical particles), one-dimensional (nanowires), and two-dimensional (nanosheet) ones. There is a number study reporting that the size, shape, and the loading of nanofillers have significant effects of the final properties on the nanocomposites [14,41–44]. The size reduction of the nanoparticles leads to a dramatic increase in the interfacial area as compared to traditional composites [42]. This interfacial area creates a significant volume fraction of interfacial polymer with properties different from the bulk polymer even at low loadings (Fig. 1.2). Nanofillers are available in a variety of shapes, including spherical, triangular, needles, rods, cubic, etc., which enables

them to be employed in a variety of applications, including device manufacturing, optics, biofuel cells, electronics, and so on [14,43,44].

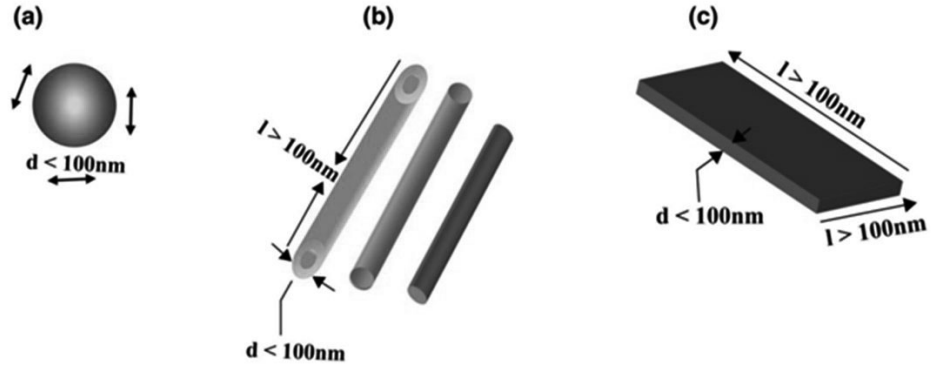

Fig. 1.1. Schematic illustration of different types of nanofillers a) zero-dimensional, b) one-dimensional and c) two-dimensional. Reproduced from Ref. [41].

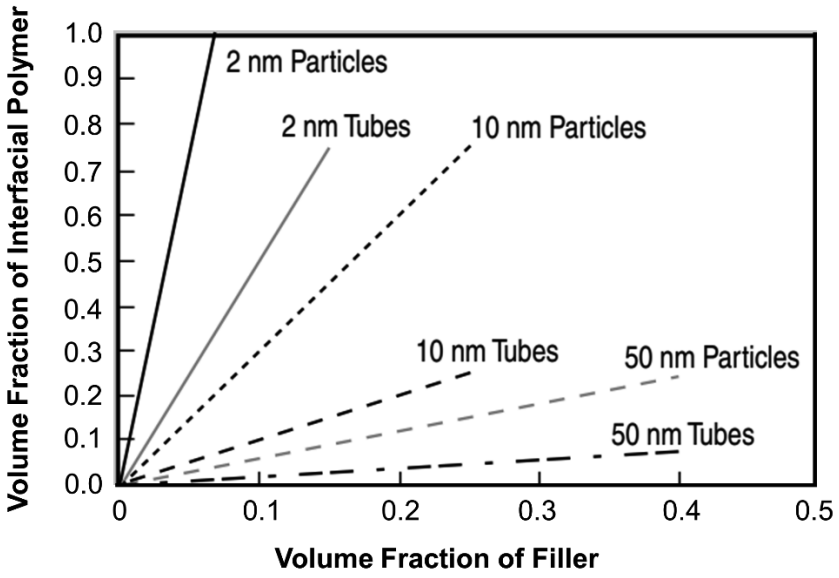

Fig. 1.2. Schematic illustration showing the volume fraction of interfacial polymer based on a 10-nm thick interfacial region surrounding each nanoparticle. Reproduced from Ref. [42].

1.1.3. Processing

Three basic techniques for making polymer nanocomposites are described here: In-situ polymerization, solution blending, and melt mixing [45]. The process for synthesizing polymer nanocomposites is mostly determined by the type of polymeric matrices, nanofiller, and desired final product properties [46].

1.1.3.1. In-situ polymerization

The in-situ polymerization method was developed to provide good nanofiller dispersion in a polymer matrix [47]. The nanofillers are disperse into the monomers or pre-polymers first, and then in such a circumstance, polymerization takes place, as shown in Fig. 1.3. When nanofillers are included in the polymerization process, the viscosity of the nanocomposites tends to increase significantly [48], making them difficult to manipulate and preventing further advancement of the polymer nanocomposites performance [49–51].

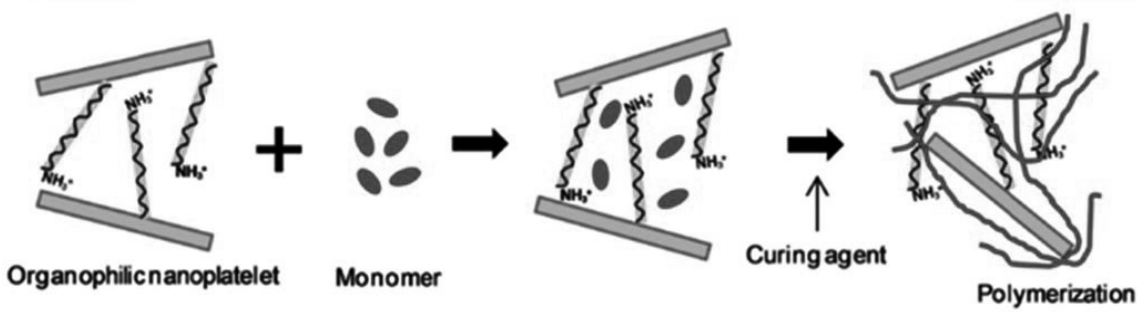

Fig. 1.3. Schematic illustration of the in-situ polymerization method.
Reproduced from Ref. [47].

1.1.3.2. Solution blending

Solution blending is a simple and effective way to produce polymer nanocomposites. The entire procedure might be divided into three steps (Fig. 1.4) [52–54]. To begin with, the nanofillers and polymer need to be dispersed and dissolved in a solution, respectively. Second, sonication or other mechanical stirring methods are used to mix the nanofillers and polymer solution. Finally, the solvent is evaporated from the well-dispersed mixing solution, giving polymer nanocomposites. This method will most likely be limited to dispersing the polymers in the solution [47], and more importantly, cost of using and removing a solvent.

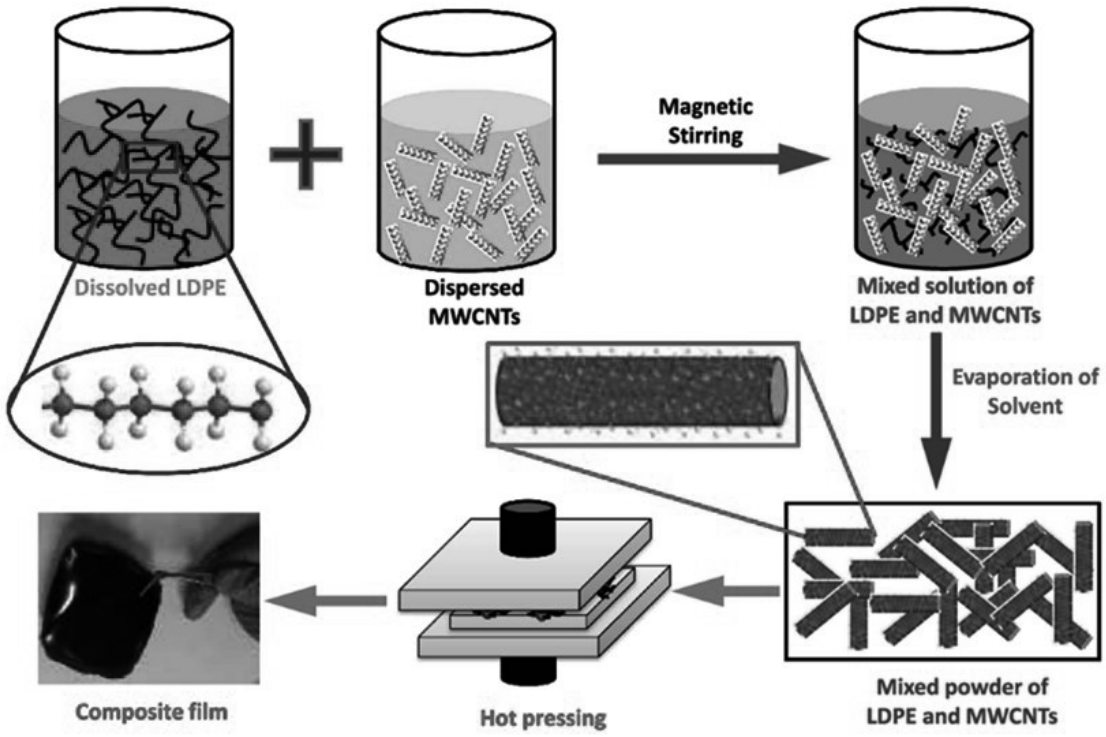

Fig. 1.4. Schematic illustration the solution blending method for preparing polymer nanocomposites. Reproduced from Ref. [52].

1.1.3.3. Melt mixing

Due to its simplicity, melt mixing is the most common and practical method for creating polymer nanocomposites [55]. Melt mixing is a technique in which the nanofillers are mixed directly with the polymer while it is still molten, as shown in Fig. 1.5 [56] The most important advantages of melt mixing are that it can be well-matched with several industrial processes (extrusion and injection molding), the improvement of mechanical properties [57–59], and effectiveness as well as environmental friendliness.

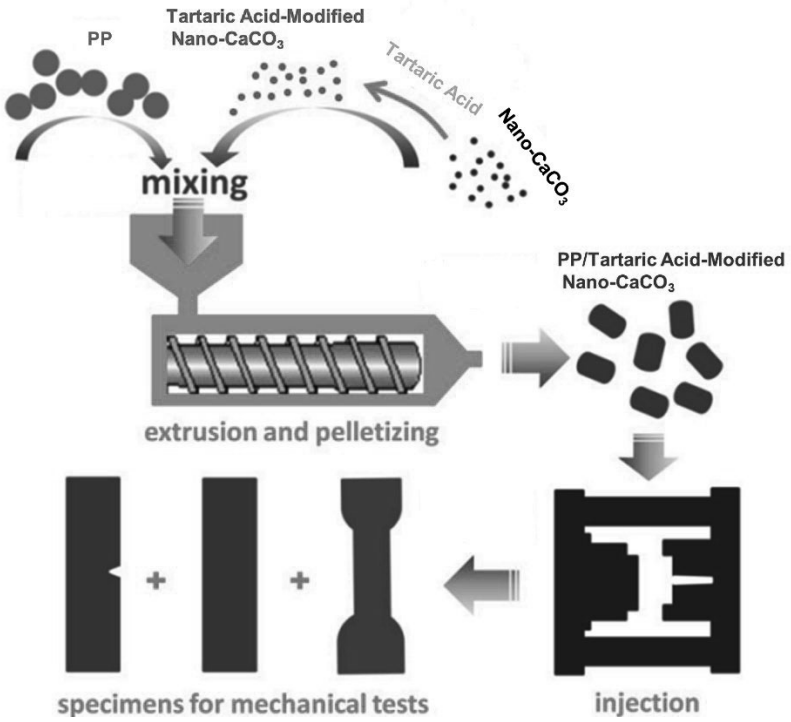

Fig.1.5. Schematic illustration of the melt mixing method for preparing polymer nanocomposites. Reproduced from Ref. [55].

1.2. Polypropylene (PP)-based nanocomposites

Around 380 million tons of plastics are nowadays produced worldwide per the year [60]. Among these, polypropylene (PP) is one of the most important ones with a wide range of applications and tremendous commercial success owing to its low cost, lightweight, ease of processing, low environmental load, and chemical resistance and so on (Fig. 1.6) [61–69]. PP is generally obtained by catalyzed polymerization of gaseous propylene, where stereochemical as well as regiochemical control is essential, unlike in ethylene polymerization. The methine

carbon in the polymer structure is chiral, which creates a variety of stereoisomeric possibilities. If the neighboring methine carbons are predominantly situated in the same chiral configuration, the polymer is designated “isotactic”. Isotactic PP is by far the mostly used commercial important stereoisomer of PP [70]. If the chirality of the neighboring methine carbons alternates from side to side along the polymer chain, the stereoisomeric form is termed “syndiotactic” (Fig. 1.7), and like isotactic, also contains a substantial crystalline content. If the methyl group is randomly oriented, the polymer is termed “atactic” and is a rubbery, amorphous, tacky material, generally considered to be undesirable.

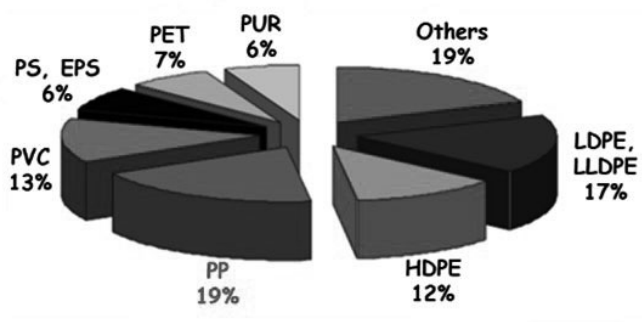

Fig. 1.6. World plastics demand by resin types in 2006. Reproduced from Ref. [61].

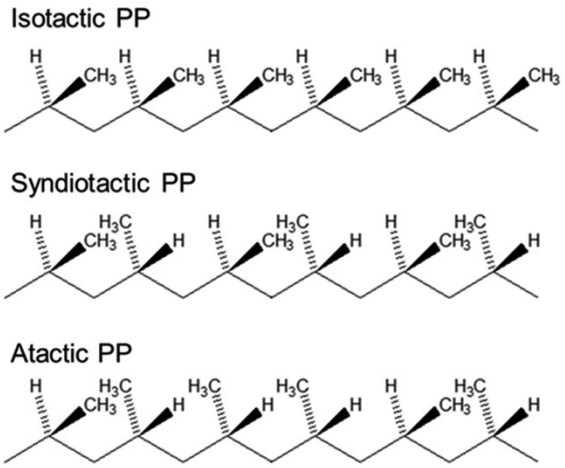

Fig. 1.7. Stereo configuration of polypropylene.

Due to the advantages of PP, PP-based nanocomposites have attracted great attention as a way to enhance their applicability and explore a new specialty. However, the nonpolar and chemically inert nature of PP against inorganic nanoparticles makes practical applications of PP-based nanocomposites extremely challenging compared to other polar polymers [71]. Therefore, studying the key factors that affect the final properties of PP-based nanocomposites is very important.

1.3. Key factors for fabricating PP-based nanocomposites

1.3.1. Dispersion of nanoparticles

To improve the efficiency of the addition of nanoparticles, some crucial issues need to be considered. The first one is the dispersion of nanoparticles. In most cases, nanoparticles do not disperse well in PP and instead form huge and compact aggregates

due to the poor compatibility, as shown in the Fig. 1.8 [72]. The existence of these agglomerates inevitably causes a reduction in reinforcement and negatively affects the ductility. This is due to that nanoparticle aggregations operate as weak points where a destructive process can start, resulting in mechanical properties deterioration [73]. Polymer nanocomposites need to have sufficient stiffness, strength and toughness for practical applications purposes. Thus, the uniform dispersion of nanoparticles at a nano scale is the first prerequisite for preparing performant nanocomposites.

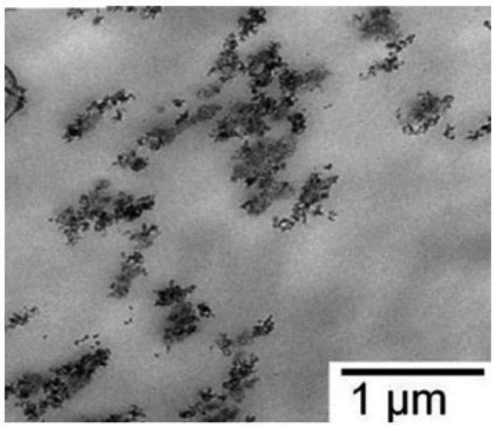

Fig. 1.8. Example of the agglomeration of nanoparticles in PP.

Reproduced from Ref. [72].

1.3.2. Interfacial bonding between the nanoparticles and PP matrix

The second factor to be considered is the interfacial bonding of nanofillers with the polymer matrix. Thus, structural optimization of the interracial bonding of fillers and polymer would be essential, which is particularly important for improving the strength

and toughness of composites [74]. Strong interfacial bonding between nanoparticles and the matrix is favorable for effective load transfer [75]. As such, enhancement of the interfacial adhesion is a promising way to improve the ductility in PP-based nanocomposites [74,76–78].

1.4. Main strategies for fabricating PP-based nanocomposites

For a range of current and future applications of PP-based nanocomposites, controlling the dispersion and managing the interfacial interaction between nanoparticles and PP is crucial. The main research efforts are presented below and divided into three categories: compatibilizers, surface modification, polymer grafting, and in-situ formation of nanoparticles.

1.4.1. Compatibilizers

Adding a compatibilizer, such as maleic anhydride-grafted PP (PP-*g*-MA), is the most common and cost-effective way to alleviate incompatibility [79–81]. Vladimirov et al., for example, used a twin-screw co-rotating extruder to create polypropylene/flumed silica nanocomposites. The dispersion of fillers improved when PP-*g*-MA was introduced as a compatibilizer, leading to an increase in the mechanical properties [81]. Lonkar et al. have prepared compatibilized PP/organo-layered double hydroxide hybrid

nanocomposites [82], as shown in Fig. 1.9. They found that when PP-*g*-MA content increased, tensile strength and modulus improved, while elongation at break declined. The results showed that a compatibilizer content of 10 wt% is optimal for producing high-performance nanocomposites. A demerit of PP-*g*-MA is also known: It generally accelerates the oxidative degradation of the matrix [82,83].

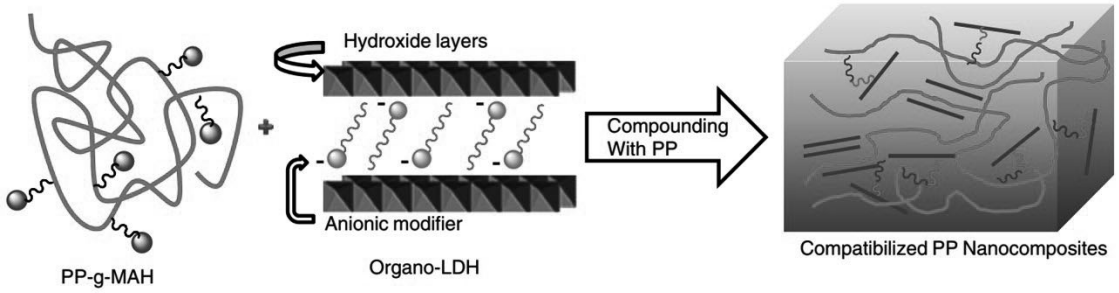

Fig. 1.9. Schematic illustration of compatibilized PP/organo-layered double hydroxide hybrid nanocomposites. Reproduced from Ref. [83].

1.4.2. Surface modification

Surface modification of nanoparticles help to avoid agglomeration caused by the incompatibility between hydrophilic inorganic fillers and hydrophobic polymer matrices. Surface modification of nanoparticles with silane coupling agents is the most straightforward approach for weakening interconnections between adjacent nanoparticles and improving their compatibility with polymer matrices [84–88]. However, one disadvantage of surface modification is that it creates a soft interfacial layer between the

matrix and the fillers, sacrificing reinforcement [88]. For instance, Zhou et al. fabricated PP/SiO_2 nanocomposites by mixing untreated and surface treated SiO_2 nanoparticles with different alkyl chain lengths on particle surface with isotactic PP [88]. They found that when introduce the modified SiO_2 nanoparticles, the yield strain and toughness increased, while the modulus decreased (Fig. 1.10).

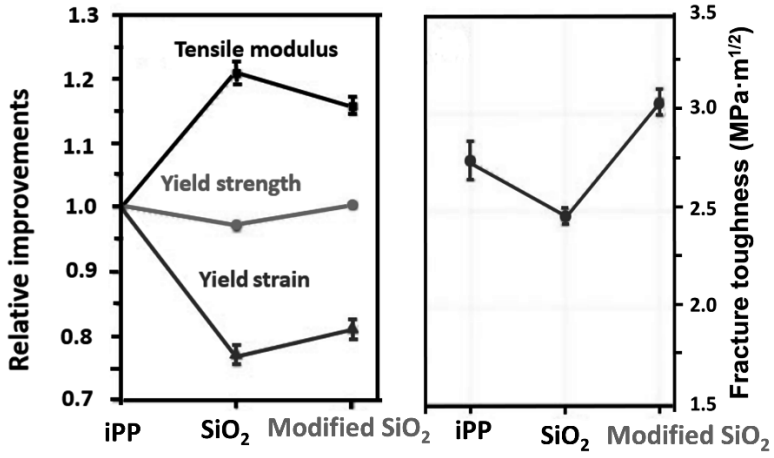

Fig. 1.10. Relative tensile properties of iPP/SiO_2 nanocomposites containing 2.3 vol% of nanoparticles. Reproduced from Ref. [88].

1.4.3. Polymer grafting

Many strategies have been proposed to overcome the poor dispersion of nanoparticles and weak interfacial bonding of the fillers and matrix. Indeed, most these strategies can achieve well dispersed nanoparticles. However, because PP lacks any functional groups that can interact with polar groups, improving interfacial interactions

in PP nanocomposites remains a considerable challenge. In recent years, developing functionalized PP with polar or reactive functional groups has been an attractive topic [89–98]. As grafting functionalized PP chain onto nanoparticles is a promising way to alleviate agglomeration due to the improvement in compatibility and to offer improved mechanical properties of nanocomposites due to entanglement [71]. For example, our research group have employed terminally hydroxylated PP (PP-*t*-OH) with various chain lengths [99]. PP-*t*-OH was grafted onto silica nanoparticles (SiO_2) and the grafted nanoparticles were melt-mixed with a PP matrix. The resultant nanocomposites had good nanoparticle dispersion and considerable strengthening due to physical crosslinking based on co-crystallization (Fig. 1.11). However, the complexity of the synthesis of PP-*t*-OH makes it less practical.

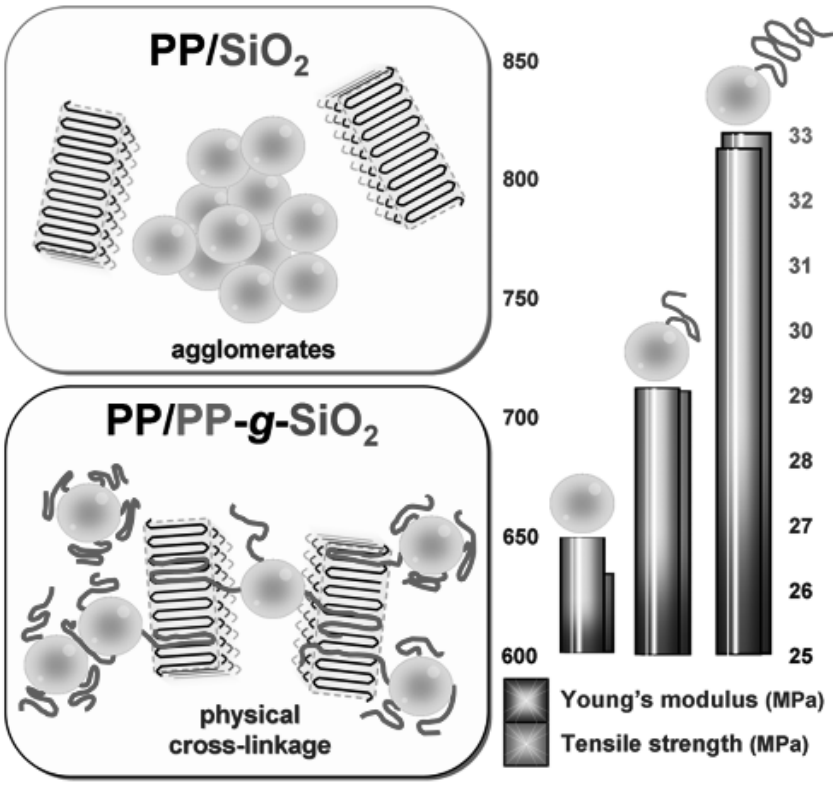

Fig. 1.11. Schematic illustration of PP/PP-*g*-SiO_2 nanocomposites.

Reproduced from Ref. [71].

There are four main methods for fabricating functionalized PP, including post-treatment, reactive intermediate, chain transfer reaction, and direct copolymerization with polar comonomers. Among these methods, direct copolymerization of propylene with polar comonomers appears to be the most straightforward method for obtaining functionalized PP in one step. For example, by copolymerizing propylene with 7-octenyltrimethoxysilane (OTMS), our research group has developed a functionalized PP matrix (PP-OTMS) [100]. In the preparation of PP-OTMS/SiO_2 nanocomposites, PP-

OTMS undergoes in-situ grafting onto SiO_2 during melt mixing, which improves dispersion and reinforcement by a reaction between methoxy groups on a side chain and silanol groups on SiO_2 surfaces, similar to ex situ grafting but more effectively (Fig. 1.12). Furthermore, the interchain interaction between methoxy groups generates a crosslink network that helps to increase the mechanical properties of nanocomposites.

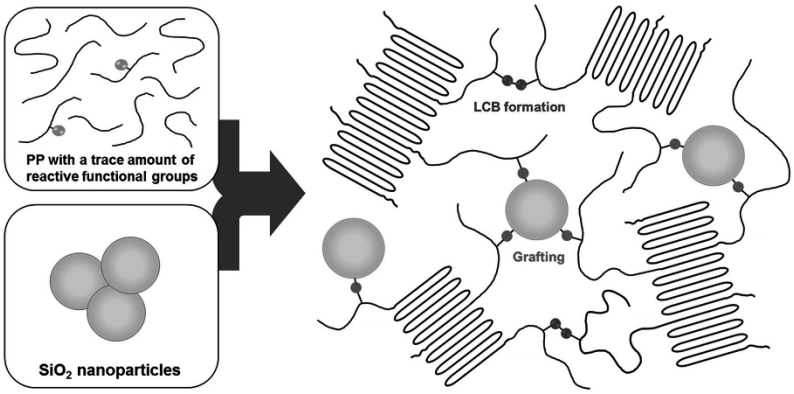

Fig. 1.12. Schematic illustration of PP-OTMS/SiO_2 nanocomposites.

Reproduced from Ref. [100].

1.4.4. In-situ formation of nanoparticles

Polymer nanocomposites can also be created based on a sol-gel process to synthesize inorganic fillers in-situ in the polymer matrix. Such a process, metal alkoxides are hydrolyzed and condensation reactions occur within a polymer matrix. Inorganic nanoparticles are formed as a result of these reactions and are dispersed throughout the polymer matrix. Bahloul et al. used the sol-gel process to make PP/TiO_2 nanocomposites

from titanium alkoxide inorganic precursors that were premixed with PP under molten conditions. The TiO_2 nanoparticles was highly dispersed throughout the polymer matrix [101–103].

Our research group has developed a novel in-situ method, called reactor granule technology (RGT). Reactor granule is a porous polyolefin powder obtained directly after catalyzed olefin polymerization and before shipment pelletization. RGT is a process for converting precursors impregnated in polyolefin reactor granules into highly dispersed nanoparticles at melt compounding temperatures, as seen in Fig. 1.13. Many PP-based nanocomposites, including PP/TiO_2, PP/Al_2O_3 PP/$Mg(OH)_2$, PP/Au, PP/Ag, have been developed based on RGT [72,104–109]. The RGT is applicable to preparing polyolefin nanocomposites filled with nanoparticles from low to high content up to 20 wt% without the need of a compatibilizer and without seriously sacrificing the mechanical properties of PP nanocomposites [72].

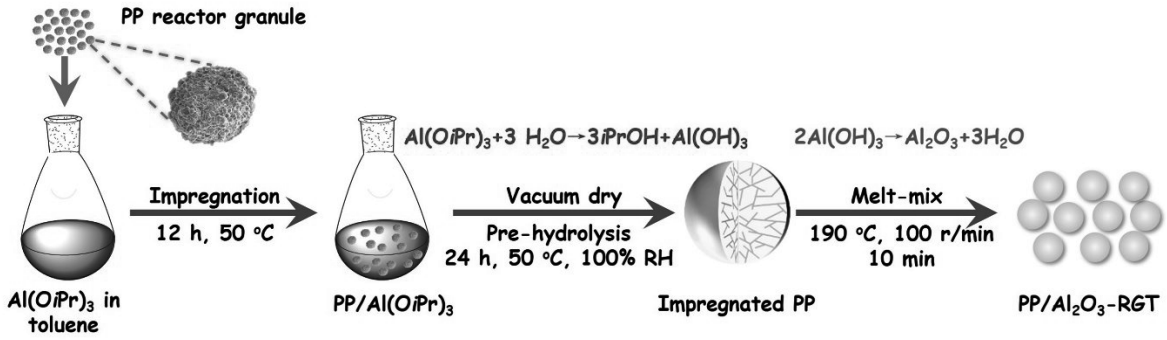

Fig. 1.13. Schematic illustrations for the reactor granule technology.

Reproduced from Ref. [108].

1.5. Toughness of PP nanocomposites

In many cases, the introduction of rigid fillers to a matrix always results in reinforcement at the expense of significantly reducing the toughness [41,74]. It was reported that the agglomeration and loose interface make the problem more significant [18,110,111]. In particular, the agglomeration and loose interface become much more evident when fillers are nano-sized. This concern may be alleviated by the significant interfacial interaction between nanofillers and the polymer matrix [112]. Kim and Michler [113,114] have studied the micromechanical deformation processes in PP/$Al(OH)_3$ composites. They described that because of the stiffness inorganic particles, particles cannot be deformed by external stress in the specimen and instead operate as stress concentrators during deformation processes. Debonding occurs easily on both sides in a parallel direction to the applied stress due to the weak interfacial adhesion between the $Al(OH)_3$ filler particles and the PP matrix, whereas highest stress concentration is at the poles of rigid particles. The matrix material between the voids deforms more easily during these debonding processes, resulting in shear yielding. The main methods for improving the toughness of PP-based nanocomposites are shown below, including adding elastomer, hybrid fillers, and adding β nucleating agent.

1.5.1. Elastomer

The main strategies that have been developed to improve the toughness of PP nanocomposites are incorporating elastomer [41,115]. Generally, the elastomer volume fraction of 5 to 20% is needed to realize the significant toughening of PP. However, the high loading of elastomer dramatically decreases the strength and stiffness of PP, even up to 50%. For example, Lim et al., studied rubber-toughened polypropylene (PP)/orgmontmorillonite (org-MMT) nanocomposite [115]. They found that polyethylene octene elastomer (POE) was very effective in converting brittle PP nanocomposites into tough nanocomposites (Fig. 1.14). However, the Young's modulus and tensile strength of the blends decreased with respect to the PP nanocomposites (Fig. 1.15).

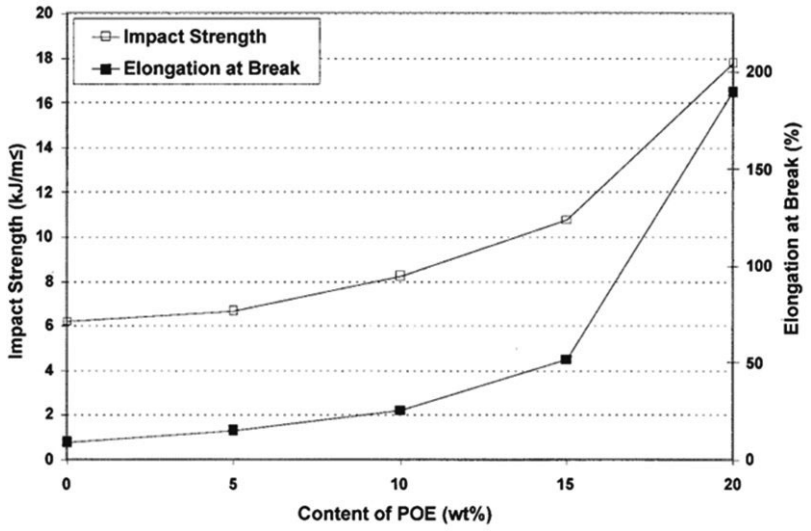

Fig. 1.14. Effect of the POE copolymer content on the impact strength and elongation at break of PP nanocomposites. Reproduced from Ref. [115].

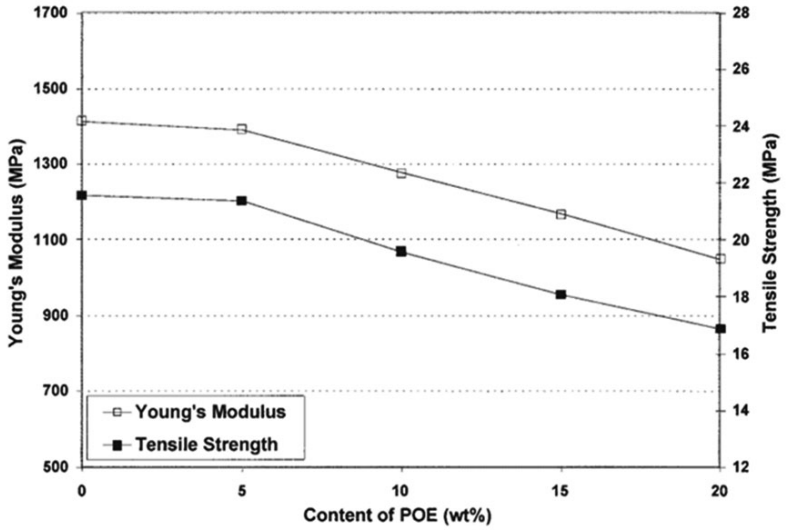

Fig. 1.15. Effect of POE copolymer content on the tensile strength and Young's modulus of PP nanocomposites. Reproduced from Ref. [115].

Hong et al. [116] synthesized PP-based RTPO (or in reactor made TPO), which is a blend of PP and poly(ethyleneco-propylene) (serving as the rubber phase) by bulk polymerization of propylene followed by gas-phase copolymerization of ethylene and propylene driven by a $TiCl_4/MgCl_2$-based catalyst system. Then, using PP-MA as a compatibilizer, they fabricated PP-based RTPO/clay nanocomposites. Table 1 shows the detailed tensile data of nanocomposites. Although the elongation at break drops as the clay content increases to 437%, which is significantly greater than the value of PP/clay nanocomposites reported elsewhere. They believed that elongational properties of PP-based RTPO/clay nanocomposites are unique and promising for a variety of applications.

Table 1. Tensile results of PP-based RTPO/PP-MA/clay nanocomposites. Reproduced

from Ref. [116].

Sample	PP-based RTPO (wt.%)	PP-MA	Clay (wt.%)	Tensile modulus (MPa)	Elongation at break (%)
RTPO	100	0	0	46.0	1390
RTPO NC3	88	9	3	71.2	980
RTPO NC5	80	15	5	78.3	859
RTPO NC10	60	30	10	251	437

1.5.2. Hybrid fillers

Some studies have examined the synergistic effects of nanoparticles and traditional reinforcements like short fibers. The use of two or more fillers of different sizes or shapes has been shown to have a synergistic effect on the toughness of PP-based nanocomposites [18,117,118]. This is because fillers with a high aspect ratio can serve as bridges between other fillers in the hybrid system. For example, Junaedi et al. found that adding 2.5 wt% TiO_2 nanoparticles to a 10 wt% short carbon fiber reinforced PP composite increased the strain at break by 15% when compared to simply adding 10 wt% short carbon fiber to PP composites [117]. Gabr et al. [118] fabricated carbon fiber/nano-clay/polypropylene nanocomposites. They reported that the fracture toughness of nanocomposites increased at 3 wt% adding of nano-clay, as shown in the Fig. 1.16. However, the synergistic effect of fillers is limited to specific combinations.

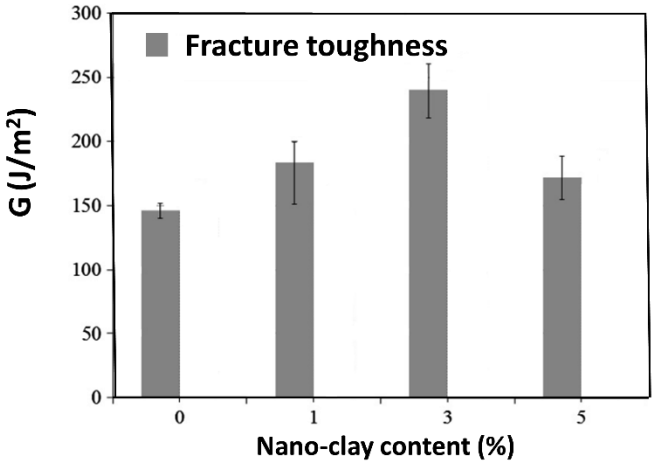

Fig. 1.16. Effect of nano-clay content on the fracture toughness of PP nanocomposites. Reproduced from Ref. [118].

1.5.3. β nucleating agent

iPP is a semi-crystalline polymer with four different crystal forms: α, β, λ, and smectic [119–122]. Due to its superior toughness and elongation at break, β crystal garnered the most attention when compared to other crystal forms. As a result, introducing β nucleating agent to a nanocomposite system may provide a useful benefit for toughening. For instance, Xie et al. observed that 1.0 wt% content of β nucleating agent could enhance the impact toughness of iPP/glass fiber composites from 9.3 kJ/m^2 (without a nucleating agent) to 14.6 kJ/m^2. Chen et al. reported that the toughness of glass fiber reinforced isotactic polypropylene composites increased with the addition of a β nucleating agent [123]. However, the addition of β nucleating agent also slightly

decreased the corresponding tensile strength and modulus [124].

1.6. Aim of thesis

The demand to develop lightweight, high-value, low-cost materials to replace traditional materials is increasing owing to global trends for higher fuel efficiency and lower emissions in industry and automation transportation. For this purpose, PP is considered one of the most plastics, but challenges arising from the chemical inertness of PP must be addressed. In particular, the main weakness of PP-based nanocomposites is the reinforcement accompanies reduction in the toughness. To obtain polymer nanocomposites with desired properties, many strategies have been proposed. It is known that the surface modification of nanoparticles with short aliphatic alkyl chains could be a facile way to increase the toughness of PP nanocomposites. However, due to the plasticizer effect of short aliphatic alkyl chains, this compensates the modulus. Therefore, it is very important to improve existing strategies in a way to be more versatile to prepare nanocomposites with desired properties but not significantly decrease the toughness of the matrix. In this dissertation, I aim to fabricate PP-based nanocomposites with improved desired properties without significantly sacrificing the toughness of the PP matrix. For this, the strategies of chemically modifying both the nanoparticles and the PP chain, as well as reactor granule technology (RGT), are applied to prepare PP nanocomposites for the purpose of optimizing the dispersion and interfacial bonding in PP nanocomposites. My research is mainly comprised of the following three chapters:

In Chapter 2, catalyzed copolymerization between propylene and 7-octenyltrimethoxysilane (OTMS) was used to prepare PP with less than one functional group per chain. Silica nanoparticles (SiO_2) was selected as a filler. It was expected that the surface modification of SiO_2 with silane coupling agents would help to enhance the dispersion of SiO_2 and offer more opportunity for in-situ grafting during melt mixing of the reactive matrix with nanofillers. By combining the surface modification of SiO_2 with in-situ grafting, the dispersion of nanoparticles and interface interaction were optimized, resulting in improved mechanical properties.

In Chapter 3, by direct copolymerization of propylene with 4-Allyl-1,2-dimethoxybenzene (ADMB) using a Ziegler-Natta catalyst, functionalized PP (PP-ADMB) containing methoxy-phenyl side-functional groups was prepared. The functionalized PP (PP-ADMB) was employed as a matrix for fabricating PP/SiO_2 nanocomposites. The introduction of ADMB was expected to help improve the dispersion of SiO_2 and to balance the stiffness and toughness of PP/SiO_2 nanocomposites.

In Chapter 4, the reactor granule technology (RGT) was applied to prepare biaxially oriented polypropylene (BOPP) nanocomposites to effectively improve the dielectric properties of PP. Titania nanoparticles (TiO_2) was chosen not only for its low price, but also for its high relative permittivity. The effects of various factors, such as the TiO_2 content, interfacial design, and drawing ratio on the permittivity, breakdown voltage, and dielectric loss of the nanocomposites were investigated in detail.

References

[1] Y. Ishiguro, S. Inagi, T. Fuchigami. Site-controlled application of electric potential on a conducting polymer “canvas”. J. Am. Chem. Soc. 2012, 134, 4034–4036.

[2] C. Wu, D. Chiu. Highly fluorescent semiconducting polymer dots for biology and medicine. Angew. Chem. Int. Ed. 2013, 52, 3086–3109.

[3] M.K. Nguyen, E. Alsberg. Bioactive factor delivery strategies from engineered polymer hydrogels for therapeutic medicine. Prog. Polym. Sci. 2014, 39, 1235–1265.

[4] Maitz, F. Manfred. Applications of synthetic polymers in clinical medicine. Biosurf. Biotribol. 2015, 1, 161–176.

[5] L. Nyholm, G. Nyström, A. Mihranyan, M. Strømme. Toward flexible polymer and paper-based energy storage devices. Adv. Mater. 2011, 23, 3751–3769.

[6] Y. Zhang, C. Zhang, Y. Feng, T. Zhang, Q. Chen, Q. Chi, L. Liu, G. Li, Y. Cui, X. Wang. Excellent energy storage performance and thermal property of polymer-based composite induced by multifunctional one-dimensional nanofibers oriented in-plane direction. Nano energy 2019, 56, 138–150.

[7] X. Zhang, X. Zheng, D. Ren, Z. Liu, W. Yang, M. Yang. Unusual positive temperature coefficient effect of polyolefin/carbon fiber conductive composites. Mater. Lett. 2016, 164, 587–590.

[8] X. Yang, C. Liang, T. Ma, Y. Guo, J. Kong, J. Gu, M. Chen, J. Zhu. A review on thermally conductive polymeric composites: classification, measurement, model and

equations, mechanism and fabrication methods. Adv. Compos. Hybrid Mater. 2018, 1, 207–230.

[9] M. Vadivelu, C.R. Kumar, G.M. Joshi. Polymer composites for thermal management: a review. Compos. Interfaces 2016, 23, 847–872.

[10] S. Sternstein, S. Amanuel, M.L. Shofner. Reinforcement mechanisms in nanofilled polymer melts and elastomers. Rubber Chem. Technol. 2010, 83, 181–198.

[11] T. Witten, M. Rubinstein, R. Colby. Reinforcement of rubber by fractal aggregates. J. Phys. II 1993, 3, 367–383.

[12] A. Bouty, L. Petitjean, J. Chatard, R. Matmour, C. Degrandcourt, R. Schweins, F. Meneau, P. Kwasńiewski, F. Boué, M. Couty. Interplay between polymer chain conformation and nanoparticle assembly in model industrial silica/rubber nanocomposites. Faraday Discuss. 2016, 186, 325–343.

[13] C.G. Robertson, N.J. Hardman. Nature of carbon black reinforcement of rubber: perspective on the original polymer nanocomposite. Polymers 2021, 13, 538.

[14] S. Fu, Z. Sun, P. Huang, Y. Li, N. Hu. Some basic aspects of polymer nanocomposites: a critical review. Nano Mater. Sci. 2019, 1, 2–30.

[15] A.P. More, A.M. Donald. Mechanical properties of nylon-6 after treatment with metal halides. Polymer 1993, 34, 5093–5098.

[16] Y. Kojima, A. Usuki, M. Kawasumi. Synthesis and mechanical properties of nylon 6-clay hybrid. J. Mater. Life Soc. 1993, 11, 1179–1185.

[17] A.A. Azeez, K.Y. Rhee, S.J. Park, D. Hui. Epoxy clay nanocomposites-processing,

properties and applications: a review. Composites Part B 2013, 45, 308–320.

[18] S. Pavlidou, C. Papaspyrides. A review on polymer-layered silicate nanocomposites. Prog. Polym. Sci. 2008, 33, 1119–1198.

[19] S. Sprenger. Epoxy resins modified with elastomers and surface-modified silica nanoparticles. Polymer 2013, 54, 4790–4797.

[20] Y. Tang, L. Ye, Z. Zhang, K. Friedrich. Interlaminar fracture toughness and CAI strength of fibre-reinforced composites with nanoparticles-a review. Compos. Sci. Technol. 2013, 86, 26–37.

[21] Y. Zeng, H.-Y. Liu, Y.-W. Mai, X.-S. Du. Improving interlaminar fracture toughness of carbon fibre/epoxy laminates by incorporation of nano-particles. Composites Part B 2012, 43, 90–94.

[22] C. Ma, H.-Y. Liu, X. Du, L. Mach, F. Xu, Y.-W. Mai. Fracture resistance, thermal and electrical properties of epoxy composites containing aligned carbon nanotubes by low magnetic field. Compos. Sci. Technol. 2015, 114, 126–135.

[23] L.-X. Gong, L. Zhao, L.-C. Tang, H.-Y. Liu, Y.-W. Mai. Balanced electrical, thermal and mechanical properties of epoxy composites filled with chemically reduced graphene oxide and rubber nanoparticles. Compos. Sci. Technol. 2015, 121, 104–114.

[24] M.S. Islam, R. Masoodi, H. Rostami. The effect of nanoparticles percentage on mechanical behavior of silica-epoxy nanocomposites. J. Nanosci. 2013, 2013, 1–10.

[25] D. Puglia, M.A.S. Al-Maadeed, J.M. Kenny, S. Thomas. Elastomer/thermoplastic modified epoxy nanocomposites: the hybrid effect of “micro”and “nano”scale. Mater.

Sci. Eng. R Rep. 2017, 116, 1–29.

[26] T. Kashiwagi, E. Grulke, J. Hilding, K. Groth, R. Harris, K. Butler, J. Shields, S. Kharchenko, J. Douglas. Thermal and flammability properties of polypropylene/carbon nanotube nanocomposites. Polymer 2004, 45, 4227–4239.

[27] H.U. Zaman, P.D. Hun, R.A. Khan, K.-B. Yoon. Morphology, mechanical, and crystallization behaviors of micro-and nano-ZnO filled polypropylene composites. J. Reinf. Plast. Compos. 2012, 31, 323–329.

[28] E. Manias, A. Touny, L. Wu, K. Strawhecker, B. Lu, T. Chung. Polypropylene/montmorillonite nanocomposites. Review of the synthetic routes and materials properties. Chem. Mater. 2001, 13, 3516–3523.

[29] A. Fina, D. Tabuani, A. Frache, G. Camino. Polypropylene-polyhedral oligomeric silsesquioxanes (POSS) nanocomposites. Polymer 2005, 46, 7855–7866.

[30] M. Zanetti, G. Camino, D. Canavese, A.B. Morgan, F.J. Lamelas, C.A. Wilkie. Fire retardant halogen-antimony-clay synergism in polypropylene layered silicate nanocomposites. Chem. Mater. 2002, 14, 189–193.

[31] T. Sun, J.M. Garces. High-performance polypropylene-clay nanocomposites by in-situ polymerization with metallocene/clay catalysts. Adv. Mater. 2002, 14, 128–130.

[32] M.A. Hood, C.S. Gold, F.L. Beyer, J.M. Sands, C.Y. Li. Extraordinarily high plastic deformation in polyurethane/silica nanoparticle nanocomposites with low filler concentrations. Polymer 2013, 54, 6510–6515.

[33] W. Yuan, H. Zhao, H. Hu, S. Wang, G.L. Baker. Synthesis and characterization of the

hole-conducting silica/polymer nanocomposites and application in solid-state dye-sensitized solar cell. ACS Appl. Mater. Interfaces 2013, 5, 4155–4161.

[34] J. Qian, G. Cheng, H. Zhang, Y. Xu. Preparation and characterization of polypropylene/silica nanocomposites by gamma irradiation via ultrafine blend. J. Polym. Res. 2011, 18, 409–417.

[35] A.M. Díez-Pascual, M. Naffakh. Polypropylene/glass fiber hierarchical composites incorporating inorganic fullerene-like nanoparticles for advanced technological applications. ACS Appl. Mater. Interfaces 2013, 5, 9691–9700.

[36] A.J. Crosby, J.Y. Lee. Polymer nanocomposites: the “nano” effect on mechanical properties. Polym. Rev. 2007, 47, 217–229.

[37] I.O. Oladele, S.O. Adelani, O.G. Agbabiaka, M.H. Adegun. Applications and aisposal of polymers and polymer composites: a. Eur. J. Adv. Eng. Technol. 2022, 9, 65–89.

[38] D.W. Sauter, M. Taoufik, C. Boisson. Polyolefins, a success story. Polymers 2017, 9, 185.

[39] S. Paszkiewicz, K. Pypeć, I. Irska, E. Piesowicz. Functional polymer hybrid nanocomposites based on polyolefins: a review. Processes 2020, 8, 1475.

[40] M. Adnan, Z. Abdul-Malek, K.Y. Lau, M. Tahir. Polypropylene-based nanocomposites for HVDC cable insulation. IET Nanodielectr. 2021, 4, 84–97.

[41] B. Cotterell, J. Chia, K. Hbaieb. Fracture mechanisms and fracture toughness in semicrystalline polymer nanocomposites. Eng. Fract. Mech. 2007, 74, 1054–1078.

[42] L. Schadler, L. Brinson, W. Sawyer. Polymer nanocomposites: a small part of the

story. JOM 2007, 59, 53–60.

[43] R.S. Hamida, M.A. Ali, A. Redhwan, M.M. Bin-Meferij. Cyanobacteria-a promising platform in green nanotechnology: a review on nanoparticles fabrication and their prospective applications. Int. J. Nanomed. 2020, 15, 6033.

[44] Z. Wu, S. Yang, W. Wu. Shape control of inorganic nanoparticles from solution. Nanoscale 2016, 8, 1237–1259.

[45] Z. Teo, W. Chow. Impact, thermal, and morphological properties of poly (lactic acid)/poly (methyl methacrylate)/halloysite nanotube nanocomposites. Polym. Plast. Technol. Eng. 2016, 55, 1474–1480.

[46] A. Seko, K. Toyoura, S. Muto, T. Mizoguchi, S. Broderick. Progress in nanoinformatics and informational materials science. MRS Bull. 2018, 43, 690–695.

[47] C. Huang, Q. Cheng. Learning from nacre: constructing polymer nanocomposites. Compos. Sci. Technol. 2017, 150, 141–166.

[48] D. Qi, C. Liu, Z. Chen, G. Dong, Z. Cao. In situ emulsion copolymerization of methyl methacrylate and butyl acrylate in the presence of SiO_2 with various surface coupling densities. Colloid. Polym. Sci. 2015, 293, 463–471.

[49] C.I. Jo, J. Ko, Z. Yin, Y.-J. Kim, Y.S. Kim. Solvent-free and highly transparent SiO_2 nanoparticle-polymer composite with an enhanced moisture barrier property. Ind. Eng. Chem. Res. 2016, 55, 9433–9439.

[50] X. Wang, L. Wang, Q. Su, J. Zheng. Use of unmodified SiO_2 as nanofiller to improve mechanical properties of polymer-based nanocomposites. Compos. Sci. Technol.

2013, 89, 52–60.

[51] S.O. Adeosun, G. Lawal, S.A. Balogun, E.I. Akpan. Review of green polymer nanocomposites. J. Miner. Mater. Charact. Eng. 2012, 11, 385.

[52] T.K. Gupta, S. Kumar, A.Z. Khan, K.M. Varadarajan, W. Cantwell. Self-sensing performance of MWCNT-low density polyethylene nanocomposites. Mater. Res. Express 2018, 5, 015703.

[53] M. Bhattacharya. Polymer nanocomposites-a comparison between carbon nanotubes, graphene, and clay as nanofillers. Materials 2016, 9, 262.

[54] H. Geng, R. Rosen, B. Zheng, H. Shimoda, L. Fleming, J. Liu, O. Zhou. Fabrication and properties of composites of poly (ethylene oxide) and functionalized carbon nanotubes. Adv. Mater. 2002, 14, 1387–1390.

[55] J. Yao, H. Hu, Z. Sun, Y. Wang, H. Huang, L. Gao, X. Jiang, X. Wang, C. Xiong. Synchronously strengthen and toughen polypropylene using tartaric acid-modified nano-$CaCO_3$. Nanomaterials 2021, 11, 2493.

[56] S. Mallakpour, M. Naghdi. Polymer/SiO_2 nanocomposites: production and applications. Prog. Mater Sci. 2018, 97, 409–447.

[57] M. Garcia, G. Van Vliet, S. Jain, B. Schrauwen, A. Sarkissov, W. Van Zyl, B. Boukamp. Polypropylene/SiO_2 nanocomposites with improved mechanical properties. Rev. Adv. Mater. Sci. 2004, 6, 169–175.

[58] O.H. Lin, H.M. Akil, Z. Mohd Ishak. Surface-activated nanosilica treated with silane coupling agents/polypropylene composites: mechanical, morphological, and thermal

studies. Polym. Compos. 2011, 32, 1568–1583.

[59] S. Etienne, C. Becker, D. Ruch, B. Grignard, G. Cartigny, C. Detrembleur, C. Calberg, R. Jérôme. Effects of incorporation of modified silica nanoparticles on the mechanical and thermal properties of PMMA. J. Therm. Anal. Calorim. 2007, 87, 101–104.

[60] R. Geyer, J.R. Jambeck, K.L. Law. Production, use, and fate of all plastics ever made. Sci. Adv. 2017, 3, e1700782.

[61] H.A. Maddah. Polypropylene as a promising plastic: a review. Am. J. Polym. Sci 2016, 6, 1–11.

[62] D. Tan, L. Zhang, Q. Chen, P. Irwin. High-temperature capacitor polymer films. J. Electron. Mater. 2014, 43, 4569–4575.

[63] J.L. Nash. Biaxially oriented polypropylene film in power capacitors. Polym. Eng. Sci. 1988, 28, 862–870.

[64] I. Rytöluoto, A. Gitsas, S. Pasanen, K. Lahti. Effect of film structure and morphology on the dielectric breakdown characteristics of cast and biaxially oriented polypropylene films. Eur. Polym. J. 2017, 95, 606–624.

[65] N. Zhang, J. Ho, J. Runt, S. Zhang. Light weight high temperature polymer film capacitors with dielectric loss lower than polypropylene. J. Mater. Sci. Mater. Electron. 2015, 26, 9396–9401.

[66] J. Xiong, X. Wang, X. Zhang, Y. Xie, J. Lu, Z. Zhang. How the biaxially stretching mode influence dielectric and energy storage properties of polypropylene films. J.

Appl. Polym. Sci. 2021, 138, 50029.

[67] Z. Li, X. Chen, C. Zhang, E. Baer, D. Langhe, M. Ponting, M. Brubaker, T. Hosking, R. Li, M. Fukuto. High dielectric constant polycarbonate/nylon multilayer films capacitors with self-healing capability. ACS Appl. Polym. Mater. 2019, 1, 867–875.

[68] Y. Wang, X. Zhou, Q. Chen, B. Chu, Q. Zhang. Recent development of high energy density polymers for dielectric capacitors. IEEE Trans. Dielectr. Electr. Insul. 2010, 17, 1036–1042.

[69] M. Ritamäki, I. Rytöluoto, K. Lahti. Performance metrics for a modern BOPP capacitor film. IEEE Trans. Dielectr. Electr. Insul. 2019, 26, 1229–1237.

[70] R. Paukkeri, A. Lehtinen. Thermal behaviour of polypropylene fractions: 1. Influence of tacticity and molecular weight on crystallization and melting behaviour. Polymer 1993, 34, 4075–4082.

[71] T. Taniike, M. Toyonaga, M. Terano. Polypropylene-grafted nanoparticles as a promising strategy for boosting physical properties of polypropylene-based nanocomposites. Polymer 2014, 55, 1012–1019.

[72] B. Maira, P. Chammingkwan, M. Terano, T. Taniike. Reactor granule technology for fabrication of functionally advantageous polypropylene nanocomposites with oxide nanoparticles. Compos. Sci. Technol. 2017, 144, 151–159.

[73] J. Liu, Y. Gao, D. Cao, L. Zhang, Z. Guo. Nanoparticle dispersion and aggregation in polymer nanocomposites: insights from molecular dynamics simulation. Langmuir 2011, 27, 7926–7933.

[74] R. Watanabe, M. Kunioka, J. Mizukado, H. Suda, H. Hagihara. Highly ductile polypropylene-based nanocomposites by dispersing monodisperse silica nanospheres in functionalized polypropylene containing hydroxyl groups. Polymer 2016, 99, 63–71.

[75] H. Lu, Z. Chen, C. Ma. Bioinspired approaches for optimizing the strength and toughness of graphene-based polymer nanocomposites. J. Mater. Chem. 2012, 22, 16182–16190.

[76] W. Zuiderduin, C. Westzaan, J. Huetink, R. Gaymans. Toughening of polypropylene with calcium carbonate particles. Polymer 2003, 44, 261–275.

[77] S.C. Tjong. Structural and mechanical properties of polymer nanocomposites. Mater. Sci. Eng. R Rep. 2006, 53, 73–197.

[78] J. Wang, X. Jin, C. Li, W. Wang, H. Wu, S. Guo. Graphene and graphene derivatives toughening polymers: toward high toughness and strength. Chem. Eng. J. 2019, 370, 831–854.

[79] M.A. Poothanari, J. Abraham, N. Kalarikkal, S. Thomas. Excellent electromagnetic interference shielding and high electrical conductivity of compatibilized polycarbonate/polypropylene carbon nanotube blend nanocomposites. Ind. Eng. Chem. Res. 2018, 57, 4287–4297.

[80] X. Wen, J. Min, H. Tan, D. Gao, X. Chen, K. Szymańska, B. Zielińska, E. Mijowska, T. Tang. Reactive construction of catalytic carbonization system in PP/C_{60}/$Ni(OH)_2$ nanocomposites for simultaneously improving thermal stability, flame retardancy

and mechanical properties. Composites Part A 2020, 129, 105722.

[81] V. Vladimirov, C. Betchev, A. Vassiliou, G. Papageorgiou, D. Bikiaris. Dynamic mechanical and morphological studies of isotactic polypropylene/fumed silica nanocomposites with enhanced gas barrier properties. Compos. Sci. Technol. 2006, 66, 2935–2944.

[82] S.P. Lonkar, S. Therias, F. Leroux, J.L. Gardette, R.P. Singh. Influence of reactive compatibilization on the structure and properties of PP/LDH nanocomposites. Polym. Int. 2011, 60, 1688–1696.

[83] B. Mailhot, S. Morlat, J.-L. Gardette, S. Boucard, J. Duchet, J.-F. Gérard. Photodegradation of polypropylene nanocomposites. Polym. Degrad. Stab. 2003, 82, 163–167.

[84] S. Kango, S. Kalia, A. Celli, J. Njuguna, Y. Habibi, R. Kumar. Surface modification of inorganic nanoparticles for development of organic-inorganic nanocomposites-a review. Prog. Polym. Sci. 2013, 38, 1232–1261.

[85] F. Ahangaran, A.H. Navarchian. Recent advances in chemical surface modification of metal oxide nanoparticles with silane coupling agents: a review. Adv. Colloid Interface Sci. 2020, 286, 102298.

[86] S. Hu, Y. Zhou, C. Yuan, W. Wang, J. Hu, Q. Li, J. He. Surface-modification effect of MgO nanoparticles on the electrical properties of polypropylene nanocomposite. High Voltage 2020, 5, 249–255.

[87] Y. Zhou, J. Hu, B. Dang, J. He. Effect of different nanoparticles on tuning electrical

properties of polypropylene nanocomposites. IEEE Trans. Dielectr. Electr. Insul. 2017, 24, 1380–1389.

[88] R.-J. Zhou, T. Burkhart. Polypropylene/SiO_2 nanocomposites filled with different nanosilicas: thermal and mechanical properties, morphology and interphase characterization. J. Mater. Sci. 2011, 46, 1228–1238.

[89] T. Chung, D. Rhubright. Synthesis of functionalized polypropylene. Macromolecules 1991, 24, 970–972.

[90] N. Gomathi, R. Rajasekar, R.R. Babu, D. Mishra, S. Neogi. Development of bio/blood compatible polypropylene through low pressure nitrogen plasma surface modification. Mater. Sci. Eng., C 2012, 32, 1767–1778.

[91] R. Nakano, K. Nozaki. Copolymerization of propylene and polar monomers using Pd/IzQO catalysts. J. Am. Chem. Soc. 2015, 137, 10934–10937.

[92] X. Wang, Y. Wang, X. Shi, J. Liu, C. Chen, Y. Li. Syntheses of well-defined functional isotactic polypropylenes via efficient copolymerization of propylene with ω-Halo-α-alkenes by post-metallocene hafnium catalyst. Macromolecules 2014, 47, 552–559.

[93] M.C. Hsiao, S.H. Liao, Y.F. Lin, C.A. Wang, N.W. Pu, H.M. Tsai, C.C. Ma. Preparation and characterization of polypropylene-graft-thermally reduced graphite oxide with an improved compatibility with polypropylene-based nanocomposite. Nanoscale 2011, 3, 1516–1522.

[94] X.Y. Wang, Y.Y. Long, Y.X. Wang, Y.S. Li. Insights into propylene/ω-halo-α-alkenes

copolymerization promoted by rac-Et(Ind)$_2$ZrCl$_2$ and (pyridyl-amido) hafnium catalysts. J. Polym. Sci., Part A: Polym. Chem. 2014, 52, 3421–3428.

[95] D. Zhang, L. Pan, Y. Li, B. Wang, Y. Li. Synthesis and reaction of anthracene-containing polypropylene: a promising strategy for facile, efficient functionalization of isotactic polypropylene. Macromolecules 2017, 50, 2276–2283.

[96] R. Watanabe, H. Shinzawa, M. Kunioka, J. Mizukado, H. Suda, H. Hagihara. Reinforcement mechanism of functionalized polypropylene containing hydroxyl group nanocomposites studied by rheo-optical near-infrared spectroscopy. Eur. Polym. J. 2017, 92, 86–96.

[97] W. Ryota, H. Hideaki, S. Hiroaki. Structure-property relationships of polypropylene-based nanocomposites obtained by dispersing mesoporous silica into hydroxyl-functionalized polypropylene (Part 1) toughness, stiffness and transparency. Polym. J. 2018, 50.

[98] Watanabe, Ryota, Kunioka, Masao, Sato, Hiroaki, Mizukado, Junji, Hagihara, Hideaki. Management of both toughness and stiffness of polypropylene nanocomposites using poly(5-hexen-1-ol-co-propylene) and silica nanospheres. Polym. Adv. Technol. 2018, 29, 417–423.

[99] M. Toyonaga, P. Chammingkwan, M. Terano, T. Taniike. Well-defined polypropylene/polypropylene-grafted silica nanocomposites: roles of number and molecular weight of grafted chains on mechanistic reinforcement. Polymers 2016, 8, 300.

[100] E. Kurahashi, T. Wada, T. Nagai, P. Chammingkwan, M. Terano, T. Taniike. Synthesis of polypropylene functionalized with a trace amount of reactive functional groups and its utilization in graft-type nanocomposites. Polymer 2018, 158, 46–52.

[101] W. Bahloul, F. Mélis, V. Bounor-Legaré, P. Cassagnau. Structural characterisation and antibacterial activity of PP/TiO_2 nanocomposites prepared by an in situ sol-gel method. Mater. Chem. Phys. 2012, 134, 399–406.

[102] M.M. Adnan, A.R.M. Dalod, M.H. Balci, J. Glaum, M.A. Einarsrud. In situ synthesis of hybrid inorganic-polymer nanocomposites. Polymers 2018, 10, 1129.

[103] Q. Guo, R. Ghadiri, T. Weigel, A. Aumann, E.L. Gurevich, C. Esen, O. Medenbach, W. Cheng, B. Chichkov, A. Ostendorf. Comparison of in situ and ex situ methods for synthesis of two-photon polymerization polymer nanocomposites. Polymers 2014, 6, 2037–2050.

[104] A. Qiagedeer, B. Maira, R. Strauss, Y. Zhao, P. Chammingkwan, G. Mizutani, T. Taniike. Preparation and characterization of polypropylene/noble metal nanocomposites based on reactor granule technology. Polymer 2017, 127, 251–258.

[105] B. Maira, P. Chammingkwan, M. Terano, T. Taniike. New reactor granule technology for highly filled nanocomposites: effective flame retardation of polypropylene/magnesium hydroxide nanocomposites. Macromol. Mater. Eng. 2015, 300, 679–683.

[106] B. Maira, K. Takeuchi, P. Chammingkwan, M. Terano, T. Taniike. Thermal

conductivity of polypropylene/aluminum oxide nanocomposites prepared based on reactor granule technology. Compos. Sci. Technol. 2018, 165, 259–265.

[107] X. Zhang, B. Maira, Y. Hashimoto, T. Wada, P. Chammingkwan, A. Thakur, T. Taniike. Selective localization of aluminum oxide at interface and its effect on thermal conductivity in polypropylene/polyolefin elastomer blends. Composites Part B 2019, 162, 662–670.

[108] X. Zhang, T. Wada, P. Chammingkwan, A. Thakur, T. Taniike. Cooperative influences of nanoparticle localization and phase coarsening on thermal conductivity of polypropylene/polyolefin elastomer blends. Composites Part A 2019, 126, 105602.

[109] X. Zhang, X. Xia, H. You, T. Wada, P. Chammingkwan, A. Thakur, T. Taniike. Design of continuous segregated polypropylene/Al_2O_3 nanocomposites and impact of controlled Al_2O_3 distribution on thermal conductivity. Composites Part A 2020, 131, 105825.

[110] M.L. Kaneko, R.B. Romero, R.E. de Paiva, M.I. Felisberti, M.C. Goncalves, I.V. Yoshida. Improvement of toughness in polypropylene nanocomposite with the addition of organoclay/silicone copolymer masterbatch. Polym. Compos. 2013, 34, 194–203.

[111] A. Ramsaroop, K. Kanny, T. Mohan. Fracture toughness studies of polypropylene-clay nanocomposites and glass fibre reinfoerced polypropylene composites. Mater. Sci. Appl. 2010, 1, 301.

[112] A.S. Zerda, A.J. Lesser. Intercalated clay nanocomposites: morphology, mechanics,

and fracture behavior. J. Polym. Sci., Part B: Polym. Phys. 2001, 39, 1137–1146.

[113] G.-M. Kim, G. Michler. Micromechanical deformation processes in toughened and particle-filled semicrystalline polymers: part 1. Characterization of deformation processes in dependence on phase morphology. Polymer 1998, 39, 5689–5697.

[114] G.-M. Kim, G. Michler. Micromechanical deformation processes in toughened and particle filled semicrystalline polymers: part 2. model representation for micromechanical deformation processes. Polymer 1998, 39, 5699–5703.

[115] J. Lim, A. Hassan, A. Rahmat, M. Wahit. Rubber-toughened polypropylene nanocomposite: effect of polyethylene octene copolymer on mechanical properties and phase morphology. J. Appl. Polym. Sci. 2006, 99, 3441–3450.

[116] C.H. Hong, Y.B. Lee, J.W. Bae, J.Y. Jho, B.U. Nam, G.J. Nam, K.J. Lee. Tensile and flammability properties of polypropylene-based RTPO/clay nanocomposites for cable insulating material. J. Appl. Polym. Sci. 2005, 97, 2375–2381.

[117] H. Junaedi, M. Baig, A. Dawood, E. Albahkali, A. Almajid. Mechanical and physical properties of short carbon fiber and nanofiller-reinforced polypropylene hybrid nanocomposites. Polymers 2020, 12, 2851.

[118] M.H. Gabr, W. Okumura, H. Ueda, W. Kuriyama, K. Uzawa, I. Kimpara. Mechanical and thermal properties of carbon fiber/polypropylene composite filled with nano-clay. Composites Part B 2015, 69, 94–100.

[119] A.T. Jones, J.M. Aizlewood, D. Beckett. Crystalline forms of isotactic polypropylene. Die Makromolekulare Chemie 1964, 75, 134–158.

[120] S. Brückner, S.V. Meille, V. Petraccone, B. Pirozzi. Polymorphism in isotactic polypropylene. Prog. Polym. Sci. 1991, 16, 361–404.

[121] S. Tjong, J. Shen, R. Li. Morphological behaviour and instrumented dart impact properties of β-crystalline-phase polypropylene. Polymer 1996, 37, 2309–2316.

[122] S. Tjong, J. Shen, R. Li. Mechanical behavior of injection molded β-crystalline phase polypropylene. Polym. Eng. Sci. 1996, 36, 100–105.

[123] Y.-H. Chen, Z.-Y. Huang, Z.-M. Li, J.-H. Tang, B.S. Hsiao. Simultaneous improvement of strength and toughness in fiber reinforced isotactic polypropylene composites by shear flow and a β-nucleating agent. RSC Adv. 2014, 4, 14766–14776.

[124] H.Q. Xie, S. Zhang, D. Xie. An efficient way to improve the mechanical properties of polypropylene/short glass fiber composites. J. Appl. Polym. Sci. 2005, 96, 1414–1420.

Chapter 2

Enhancing Mechanical Properties of Graft-type Nanocomposites Using Organically Modified SiO_2 and Polypropylene Containing Reactive Methoxy Groups

Chapter 2

Abstract

In situ grafting of a reactive matrix and nanofillers is a promising strategy to fabricate graft-type polypropylene (PP)-based nanocomposites, where the grafting efficiency is affected by the initial dispersion of nanofillers in the matrix. In this work, influences of surface organic modification of nanofillers were investigated on properties of PP/SiO_2 nanocomposites using poly(propylene-co-octenyltrimethoxysilane) as a reactive matrix. The surface modification of SiO_2, especially with longer alkyl chains, led to improved dispersion of nanoparticles, thus promoting the grafting reaction and mechanical properties. The combination of in situ grafting and surface modification of nanofillers provided several benefits, most notably in balancing the strength and the toughness, which could not be achieved by the grafting alone.

Keywords: PP nanocomposites; in-situ grafting; reactive matrix; surface modification

2.1. Introduction

Polymer nanocomposites, consisting of at least one phase having dimensions smaller than 100 nm [1], have attracted great interest owing to their potential applications in different industrial sectors. Significant increases in the particle number density and interfacial area due to the small size enable nanocomposites to achieve desired properties at a much smaller loading of fillers compared to conventional microcomposites [2].

Meanwhile, strong interparticle attraction in comparison to weak interfacial interaction with polymer matrices constitutes one of the main impediments in the development of high-performance nanocomposites.

Polypropylene (PP), one of the most abundant thermoplastics, has been employed for fabricating polymer nanocomposites using a wide variety of nanofillers [3–16]. The hydrophobicity and chemical innerness of PP make uniform dispersion of nanoparticles challenging, for which various strategies have been reported. These include the use of a compatibilizer such as maleic anhydride-grafted PP [17–25], surface modification by organic compounds [26–28], polymer grafting [29–33], propylene polymerization in presence of nanofillers [34], in situ formation of nanofillers [35–37], and so on. Among these, the polymer grafting, especially using PP as the graft chain, is the most promising [38]. Grafted PP chains not only improve the compatibility between nanofillers and the PP matrix, they also co-crystallize with the matrix to strengthen interfacial interaction [37,38]. It has been reported that various functional groups have been introduced to PP chains as a reactive site for grafting reaction [38–43]. For example, we exploited terminally hydroxylated PP (PP-*t*-OH) with different chain lengths, which was synthesized through controlled chain transfer reaction during metallocene-catalyzed propylene polymerization, followed by hydroxylation. PP-*t*-OH was grafted onto silica nanoparticles (SiO_2) and subsequently used for melt mixing with a PP matrix [38]. The resultant nanocomposites exhibited excellent dispersion of nanoparticles and significant reinforcement arisen from co-crystallization-based physical crosslinkage. Nonetheless,

elaboration in the synthesis of PP-*t*-OH as well as ex situ grafting makes the process less practical. In a more recent publication, efficient synthesis of reactive PP with less than one functional group per chain by virtue of catalyzed copolymerization between propylene and 7-octenyltrimethoxysilane (OTMS) was reported [39]. During melt mixing, PP-OTMS undergoes in situ grafting onto SiO_2 through the reaction between methoxy groups at a side chain and silanol groups on SiO_2 surfaces, leading to improved dispersion and reinforcement, similar to ex situ grafting but more efficiently. In addition, interchain re-action among methoxy groups creates a crosslink network, which also co-contributes to the improvement in mechanical properties.

Despite the effective reinforcing of PP-OTMS/SiO_2 nanocomposites, due to particle-particle interactions and the high surface energy of SiO_2, uniform dispersion of neat SiO_2 in the early stages of melt mixing remains a challenge [26,44]. The shear forces during melt mixing were unable to break down this agglomeration of SiO_2 in the matrix. Surface modification of SiO_2 with inert functional groups, such as alkyl chains, is the most convenient method for weakening connections between adjacent nanoparticles and decreasing moisture absorption by lowering the surface energy [44]. As the grafting reaction and interchain reaction are competing reactions that consume the reactive functional group [39], good control of SiO_2 dispersion in the early stage would provide more opportunities to control the grafting reaction and to maximize the resultant properties.

Here, I report a method to further improve the physical properties of graft-type

nanocomposites using PP-OTMS as reactive matrix. Specifically, organically modified SiO_2 nanoparticles were used in combination with PP-OTMS. The organic modification improved the dispersion of the nanoparticles in the early stage of melt mixing and consequently improved the grafting efficiency. This, together with the plasticizing effect of aliphatic chains, resulted in improved mechanical properties compared to the nanocomposites using unmodified nanoparticles. In particular, the improvement in toughness was quite remarkable.

2.2. Materials and methods

2.2.1. Materials

PP (M_n = 6.3 × 10^4, M_w/M_n = 3.9, stereoregularity (*mmmm*) = 95 mol%) and PP-OTMS (M_n = 7.3 × 10^4, M_w/M_n = 3.7, *mmmm* = 98 mol%) were synthesized using a 5th-generation Ziegler-Natta catalyst according to previous study [39]. *n*-Heptane was dried by N_2 bubbling in the presence of molecular sieve 3Å prior to use. Propylene of polymerization grade was donated by Japan Polypropylene Corporation (Tokyo, Japan) and used as received. Triethylaluminum (TEA, donated by Tosoh Finechem Corporation, ToykoYamaguchi, JapanCo.) was used as a dilution in heptane. 7-octenyltrimethoxysilane (OTMS, purity >90%, Tokyo Chemical Industry Co., Ltd., Toyko, Japan) was used as a comonomer without further purification. Based on a gas chromatographymass spectrometry analysis, the impurities in OTMS were OTMS isomers with different double

bond positions. These impurities are similarly or less poisonous to the catalyst as compared to OTMS. Therefore, they are assumed to have insignificant effects on the catalytic properties. SiO_2 nanoparticles (average diameter = 26 nm, specific surface area = 110 m^2 g^{-1}) were purchased from Kanto Chemical Co., Inc. (Tokyo, Japan). Octadecyl-3-(3,5-di-tert-butyl-4-hydroxyphenyl) propionate (AO-50, donated by ADEKA Corporation, Tokyo, Japan) was used as a stabilizer. Trichlorohexylsilane, trichlorododecylsilane, and trichlorohexadecylsilane were purchased from Tokyo Chemical Industry Co., Ltd. (Tokyo, Japan). According to the alkyl chain length, they are denoted as C6, C12, and C16, respectively. Toluene (Kanto Chemical Co., Inc., Tokyo, Japan) was dried and deoxygenated by N_2 bubbling in the presence of molecular sieve 3Å.

2.2.2. Synthesis of PP-OTMS

PP-OTMS was synthesized by copolymerization of propylene and OTMS using a $MgCl_2$-supported Ziegler-Natta catalyst [39]. The polymerization was performed in a 1 L stainless steel reactor in a semi-batch mode. To the reactor blanked by N_2, 500 mL of heptane as a solvent, 15 mmol of TEA as a cocatalyst, and 10 mmol of OTMS as a comonomer were introduced. The solvent was saturated with 0.5 MPa of propylene at 50 °C for 30 min. Followed by the introduction of 16 mmol of H_2, catalyst powder (50 mg) was injected to initiate the polymerization. The polymerization was continued at

50 °C and 0.5 MPa for 60 min, followed by depressurization. The solvent was removed by decantation, and the resultant polymer powder was washed repetitively with ethanol and acetone under N_2. Finally, the powder was purified by reprecipitation (xylene to acetone) and dried in vacuum at room temperature. PP homopolymer (HomoPP) was synthesized in the absence of OTMS under the same conditions, except 5.0 mmol of TEA used as a cocatalyst.

2.2.3. Surface modification of SiO_2

Surface modification of SiO_2 was performed according to a previously reported method [45]. SiO_2 (0.3 g) was added in 30 mL of toluene in a round-bottom flask, and sonicated for 30 min. A specified amount of a silane coupling agent (0.01, 0.1, or 1 mmol) was added under N_2. The mixture was stirred at room temperature for 1 h. The obtained product was collected by centrifugation, repetitively washed with anhydrous ethanol, and dried in a vacuum oven at 80 °C for 24 h. The modified SiO_2 samples are denoted as C*x*-*y*-SiO_2, where x and y represent the alkyl chain length and the amount (mmol) of the silane coupling agents (per 0.3 g of SiO_2), respectively. For example, C6-0.1-SiO_2 stands for SiO_2 modified with 0.1 mmol of trichlorohexylsilane.

2.2.4. Preparation of PP-OTMS/SiO_2 nanocomposites

PP-OTMS/SiO_2 nanocomposites were prepared by the following procedure: First, PP-OTMS (3.7 g) was pre-impregnated with 1.0 wt% of AO-50 in 100 mL of acetone. After evaporation of the solvent under N_2 flow, the polymer was dried at room temperature under vacuum for 12 h. The dried polymer was melt-mixed with 5.0 wt% of unmodified SiO_2 or modified SiO_2 using Micro Compounder MC5 (Xplore) at 185 °C and 100 rpm for 15 min under N_2 atmosphere. The extrudate was hot-pressed into a 200 μm-thick film at 230 °C and 20 MPa for 5 min, followed by quenching at 100 °C for 5 min and then cooling at 0 °C for 3 min. For comparison, a nanocomposite (HomoPP/SiO_2) was also prepared using HomoPP and unmodified SiO_2 according to the same procedure.

2.2.5. Characterizations

Fourier transform infrared (FTIR) spectra were recorded on a Perkin Elmer Spectrum 100 spectrometer (PerkinElmer, Inc., Waltham, USA) in the transmission mode between 4000 cm^{-1} and 450 cm^{-1} with a resolution of 4 cm^{-1}. The scans of each FTIR experiment are 64. A sample was mixed with dried KBr and pressed into a disc for the measurement. Water contact angle (WCA) measurements were carried out on SiO_2 samples using a contact angle goniometer (SImageAUTO 100, Excimer. Inc., Kanagawa, Japan). At room temperature, 10.0 μL of deionized water was dropped on a sample surface pressed on a glass slide. The WCA was determined by the tangent method. The weight

loss of unmodified and modified SiO_2 was measured by thermal gravimetric analysis (TGA, Thermo plus evo, Rigaku, Tokyo, Japan). A sample was heated from 25 °C to 600 °C at the heating rate of 10 °C min^{-1} under dry air flow. The weight loss below 200 °C corresponds to the evaporation of physisorped water and surface hydroxyl groups, while the weight loss in a range of 200–600 °C corresponds to thermal decomposition of organic groups for modified SiO_2.

The methoxy (OMe) content in PP-OTMS before and after melt mixing was analyzed by 1H NMR (Bruker 400 MHz) operated at 120 °C with 1000 scans. Ca. 60 mg of a sample was dissolved in 0.2 mL of 1,1,2,2-tetrachloroethane-d_2 (an internal lock and a reference) and 0.5 mL of 1,2,4-trichlorobenzene containing 0.006 wt% of 2,6-di-tert-butyl-4-methylphenol (anti-oxidant). The OMe content was calculated using Equation (2-1),

$$\text{OMe content (mol\%)} = \frac{H^a/3}{H^c} \times 100 \qquad (2\text{-}1),$$

where H^a and H^c are the peak areas for the methyl protons of the methoxy group and the methine protons of the polymer backbone, respectively. A typical NMR spectrum of PP-OTMS and peak assignment are provided in Fig. 2.1.

The dispersion of SiO_2 nanoparticles was observed on a transmission electron microscope (TEM, Hitachi H-7650, Hitachi High-Tech Corporation, Tokyo, Japan) operated at an acceleration voltage of 100 kV. A 100-nm-thick specimen was cut from a nanocomposite film using an ultramicrotome instrument (Leica ULTRACUTS FCS, Leica Microsystems GmbH, Wetzlar, Germany) equipped with a diamond knife. The

dispersion of SiO_2 in the matrix was quantitatively evaluated based on a dispersion parameter (D) defined in Equation (2-2),

$$D = \frac{0.2}{\sqrt{2\pi}} \times \frac{\mu}{\sigma} \quad (2\text{-}2),$$

where μ and σ are the average size and its standard deviation of SiO_2 domains (SiO_2 particles or their aggregates) [46]. The analysis of TEM images was performed using ImageJ software, and covered at least 200 domains of SiO_2, which corresponded to 3 TEM images taken at different regions and were sufficient to obtain stable D values.

Differential scanning calorimetry (DSC) measurements were performed on Mettler Toledo DSC 822 under N_2 atmosphere. Ca. 8 mg of a sample was added in an aluminum pan, and heated to 230 °C at the heating rate of 20 °C min^{-1}. The melting temperature (T_m) and the crystallinity (X_c) were determined from the melting endotherm. After holding 230 °C for 10 min, the sample was cooled down to 25 °C at the cooling rate of 20 °C min^{-1} for acquiring the crystallization temperature (T_c), or to 144 °C at the rate of 50 °C min^{-1} for isothermal crystallization. In the latter case, the crystallization rate was calculated as the inverse of the half time of the crystallization (denoted as $t_{1/2}^{-1}$).

Tensile properties were measured using a tensile tester (Abecks Inc., Dat-100, Tokyo, Japan) at a crosshead speed of 1 mm min^{-1} at room temperature. Dumbbell-shaped specimens were die-cut from a 200-μm-thick film. The tensile properties were reported as an average from at least four measurements per sample.

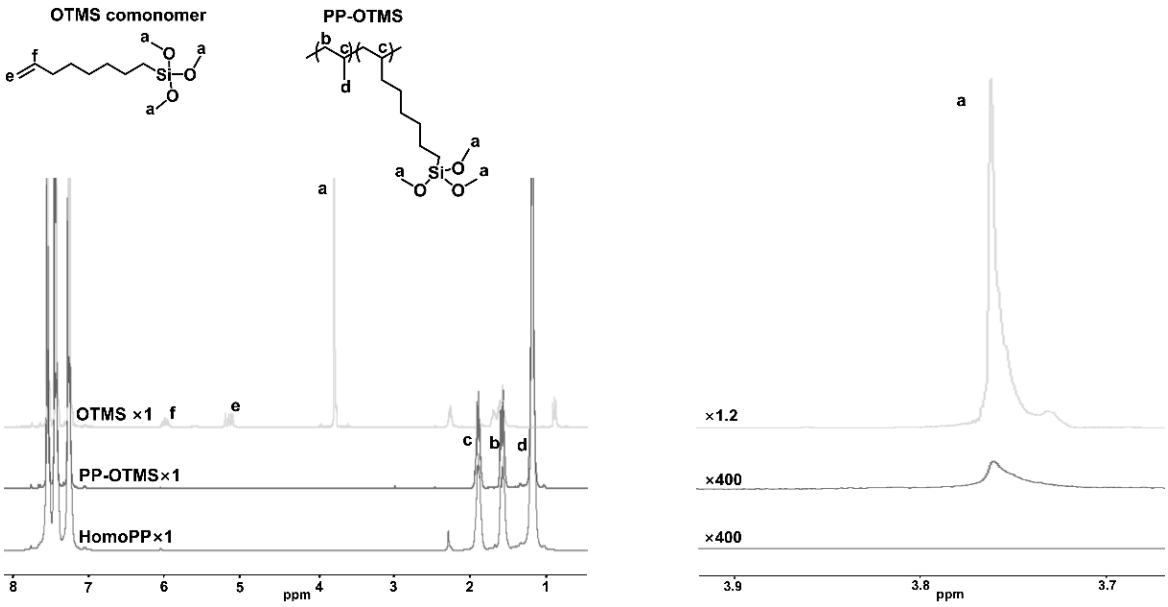

Fig. 2.1. ^{1}H NMR spectra of HomoPP and PP-OTMS.

The right figure enlarges the methoxy region.

2.3. Results and discussion

2.3.1. Surface modification of SiO_2

Successful organic modification of SiO_2 was confirmed by FTIR. As shown in Fig. 2.2a, unmodified SiO_2 exhibited broad peaks at around 3500 cm^{-1} and 1617 cm^{-1}, which are characteristics of surface hydroxyl groups and physisorbed water [47]. The most intense peak around 1100 cm^{-1} and the sharp peak at 804 cm^{-1} are respectively attributed to Si-OH/Si–O–Si stretching and Si–O–Si bending [48,49]. After surface modification, new peaks appeared at 2962 cm^{-1}, 2921 cm^{-1}, 2847 cm^{-1}, and 1466 cm^{-1}. These correspond to asymmetric stretching of $–CH_3$, asymmetric stretching of $–CH_2–$,

symmetric stretching of $-CH_2-$, and C–H bending [48–50]. It is also noted that the peak ratio between the asymmetric stretching of $-CH_2-$ and $-CH_3$ changed in line with the CH_2/CH_3 ratio of the alkyl chain [47,48]. The morphology of the neat and surface modified SiO_2 was conducted. It was found that the shape and size of the SiO_2 before and after modification do not have changed (Fig. 2.3).

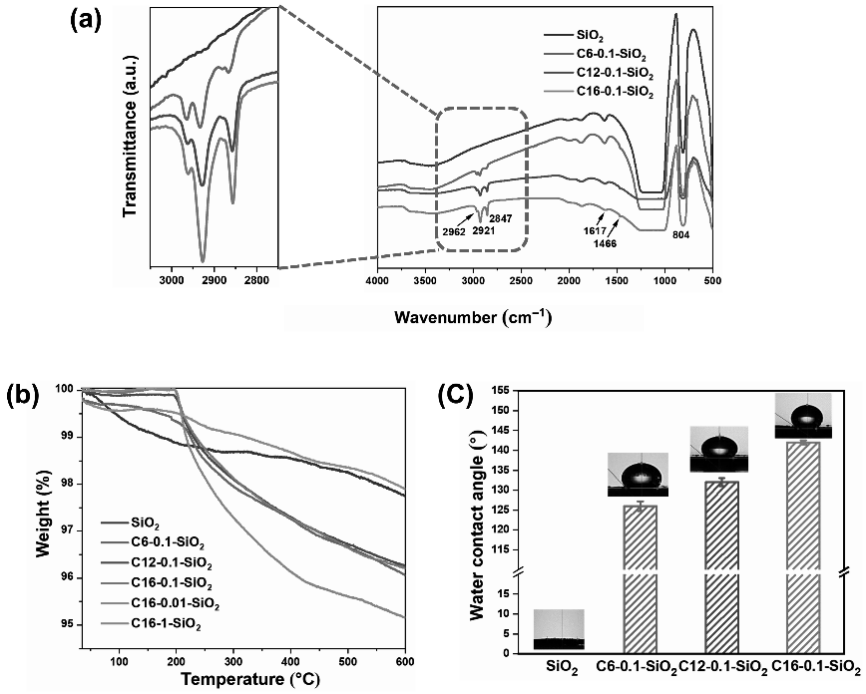

Fig. 2.2. Characterization of unmodified and organically modified SiO_2 nanoparticles: a) FTIR spectra, b) TG curves, and c) water contact angles.

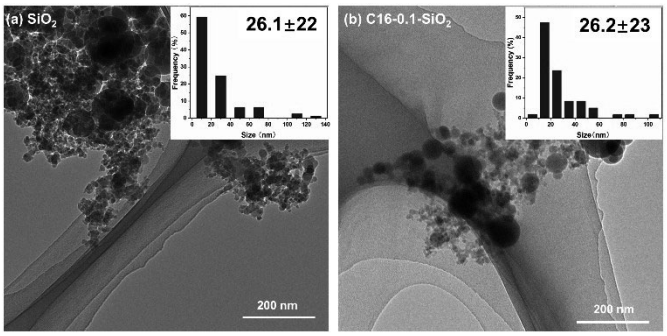

Fig. 2.3. TEM images of neat and surface modified SiO_2 nanoparticles.

TGA was implemented to determine the amount of silanes grafted on SiO_2 surfaces. For unmodified SiO_2, the weight loss gradually occurred upon heating to 600 °C, due to the vaporization of physisorbed water and the loss of surface hydroxyl groups [51]. For modified SiO_2, a sharp weight loss was observed at around 200 °C, as shown in Fig. 2.2b. According to literature, the weight loss of silane-modified SiO_2 starts at around 200 °C via dissociative combustion of the alkyl chain, leaving the siloxy groups on the SiO_2 surface [52]. The following equation (3-3) was used to estimate the amount of grafted silanes from the weight loss in the range of 200–600 °C,

$$m\% = \frac{1}{1 + \frac{M_{\text{Silane}}}{M_{\text{SiO}_2}} \times \left(\frac{r_{\text{a/s}}}{\Delta W} - 1\right)} \times 100 \quad (3\text{-}3),$$

where $m\%$ is the molar percentage of silanes with respect to SiO_2. M_{silane} and M_{SiO_2} are the molecular weights of silane coupling agents and SiO_2, respectively. ΔW is the weight loss of modified SiO_2 between 200–600 °C minus that of unmodified SiO_2. $r_{\text{a/s}}$ is the weight ratio of the alkyl chain in the correspondent silane coupling agent [52]. For example, ΔW is calculated as 3.27 wt% for C6-0.1-SiO_2. The $r_{\text{a/s}}$ and M_{silane} values for

trichlorohexylsilane are 0.39 and 219.61 g mol^{-1}, respectively. According to Equation (3), the molar percentage of the grafted silane is calculated as 1.57 mol%. Considering the surface area of SiO_2, the silane grafting density can be further calculated as 1.43 nm^{-2}. Table 2.1 summarizes the silane molar percentage and the grafting density when silane coupling agents having different alkyl chain lengths were employed. It can be seen that at the fixed mole of silane coupling agents (0.1 mmol), the grafting amount decreased with the increase in the alkyl chain length. It is considered that the adsorption and reaction of a molecule of a bulky silane coupling agent inhibits the approach of a new molecule to the surrounding silanols. By increasing the amount of the silane coupling agent (C16), the grafting density increased and reached 0.94 nm^{-2} at 1 mmol of the silane addition. It must be noted that the grafting density was sufficiently lower than the original OH density (ca. 4–5 nm^{-2}) for all cases, i.e., the OH sites remained available for grafting to PP-OTMS.

Table 2.1. Silane grafting amounts derived from TGA.

Sample	*m*(%) [a]	Silane grafting density (nm^{-2})[b]
C6-0.1-SiO_2	1.57	1.43
C12-0.1-SiO_2	0.89	0.81
C16-0.1-SiO_2	0.72	0.66
C16-0.01-SiO_2	0.13	0.12
C16-1-SiO_2	1.03	0.94

[a] Calculated based on Equation (3); [b] The surface area of SiO_2 was measured as 110 m^2

g^{-1}.

Fig. 2.2c depicts the results of WCA measurements for SiO_2 samples. Without organic modification, the SiO_2 surface was highly hydrophilic (WCA = 0°) due to the presence of surface hydroxyl groups. The modification with silane coupling agents significantly increased WCAs to 126–142°, indicating that the original hydrophilic surface changed to hydrophobic one due to the presence of aliphatic chains. The WCAs were found to be larger when the chain length increased from C6 to C12 regardless of a lower grafting density. These results pointed out that it is easier for a longer alkyl chain to shield the surface from water by forming a hydrophobic network [53].

2.3.2. TEM images of PP and PP-OTMS nanocomposites

A series of nanocomposites were prepared by melt compounding 5.0 wt% of unmodified or modified SiO_2. Fig. 2.4 shows TEM images of the resultant nanocomposites and the dispersion parameter (*D*) calculated based on Equation (2). Generally, a higher *D* value indicates better dispersion [46]. As known from literature, SiO_2 nanoparticles have poor compatibility with the PP matrix and easily form agglomerates due to strong particle-particle interactions (Fig. 2.4a). The incorporation of a small amount of OTMS in PP chains helped to improve the dispersion as evidenced by the decrease in the size of SiO_2 domains (Fig. 2.4b). In our previous paper, the improved

dispersion was ascribed to the presence of polar functional groups as well as the in situ grafting of OTMS to SiO_2 surfaces to strengthen the interfacial interaction [39]. When modified SiO_2 nanoparticles were employed, the dispersion of SiO_2 in the PP-OTMS matrix further improved (Fig. 2.4c–e). In Fig. 2.4f, the *D* value increases along the alkyl chain length. These results are explained by the decrease in the cohesive attraction among SiO_2 nanoparticles and improved compatibility with the matrix due to organic modification, and/or the prevention of re-agglomeration due to more efficient grafting of PP-OTMS (described below).

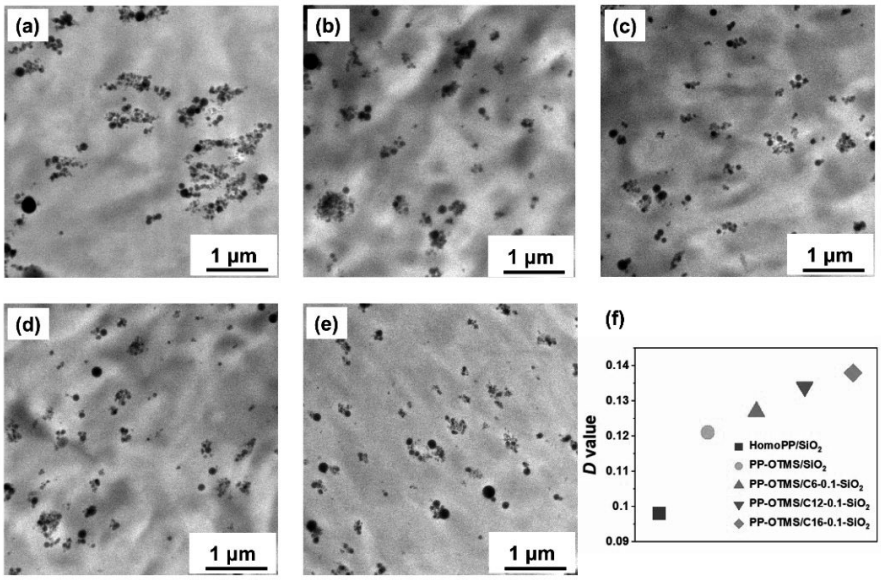

Fig. 2.4. TEM images of nanocomposites: (a) HomoPP/SiO_2, (b) PP-OTMS/SiO_2, (c) PP-OTMS/C6-0.1-SiO_2, (d) PP-OTMS/C12-0.1-SiO_2, and (e) PP-OTMS/C16-0.1-SiO_2. The SiO_2 content was 5.0 wt% for all the samples. (f) The dispersion parameter (*D*) acquired from TEM images.

2.3.3. OMe content before and after melt mixing

During the melt mixing process, the OMe groups of PP-OTMS can react with surface silanol groups of SiO_2 to form Si-O-Si bonds, by which PP-OTMS grafts to the SiO_2 nanoparticles [39]. To confirm the occurrence of in situ grafting, the OMe content before and after melt mixing was analyzed by ^1H NMR (Fig. 2.5). As shown in Fig. 2.6, even in the absence of SiO_2, a part of OMe groups was consumed during melt mixing. This suggests that the OMe groups belonging to different chains can react with each other, most plausibly via hydrolysis/condensation with the aid of residual water. In the presence of SiO_2, the decrease in the OMe content became more pronounced, which indicated the occurrence of in situ grafting. The consumption of the OMe group was greater for modified SiO_2 as compared to unmodified one, even though surface silanol groups were partially consumed by the organic modification. This result evidenced the importance of initial dispersion on the efficiency of the in situ grafting. The consumption of the OMe groups increased along with the alkyl chain length, in agreement with the improved dispersion parameter in Fig. 2.4f. It is plausible that the improved dispersion of modified SiO_2 provided more contact interfaces to promote the grafting reaction.

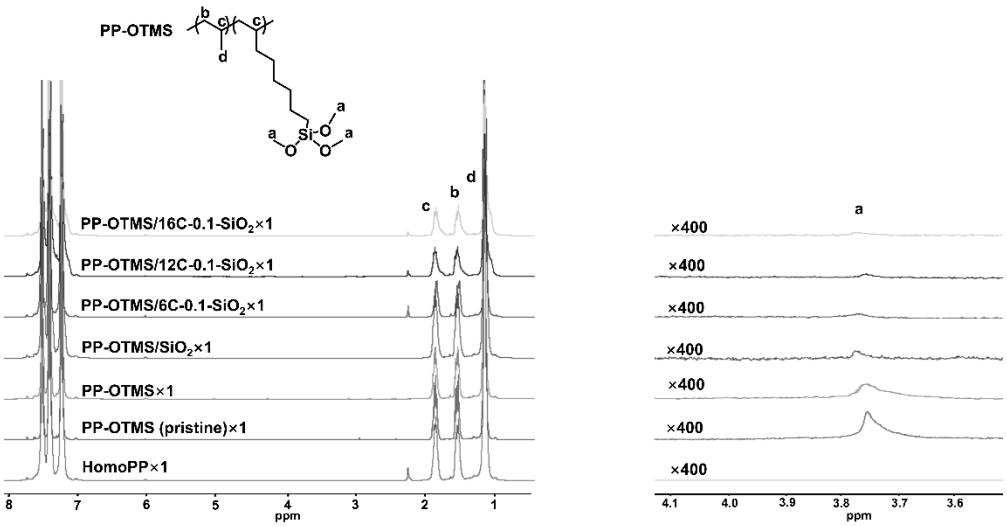

Fig. 2.5. ^{1}H NMR of PP-OTMS and its nanocomposites before and after melt mixing.

The right figure enlarges the methoxy region.

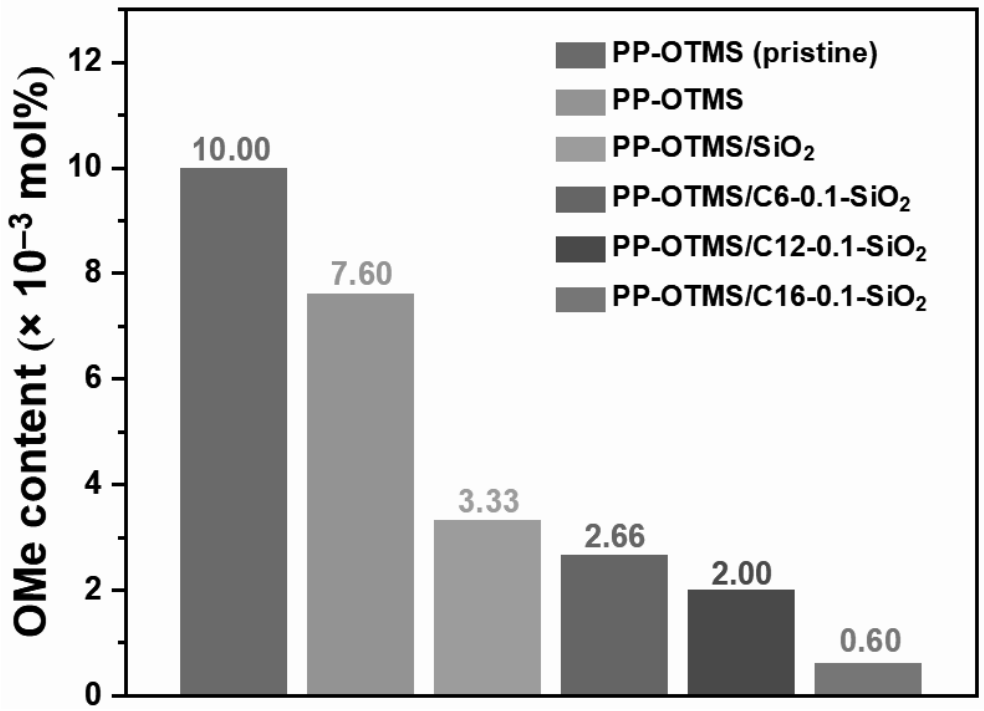

Fig. 2.6. The OMe content analyzed by ^{1}H NMR before and after melt mixing.

2.3.4. DSC results of polymer and nanocomposites

The influences of SiO_2 and its surface modification on the melting and crystallization behaviors of nanocomposites were investigated by DSC. The acquired parameters, such as the melting temperature (T_m), crystallization temperature (T_c), and crystallinity (X_c) of the nanocomposites, are summarized in Table 2.2. The DSC profiles during heating and cooling are respectively provided in Fig. 2.7 and 2.8. In Table 2.2, Tm and X_c of PP-OTMS were slightly higher than those of HomoPP due to slightly higher isotacity of PP-OTMS (98 mol% *mmmm* for PP-OTMS vs. 95 mol% for HomoPP). On the other hand, T_c and $t_{1/2}^{-1}$ were obviously higher for PP-OTMS. This is due to the nucleation ability of PP-OTMS, which forms a long-chain branched (LCB) structure by interchain reaction during melt mixing and shows a nucleation ability similar to LCBPP [39]. The introduction of SiO_2 to HomoPP did not cause any significant change in the thermal properties and the crystallinity of the resultant nanocomposite. Contrary, the introduction of SiO_2 to the PP-OTMS matrix increased T_c by 3 °C and doubled the crystallization rate. The significant crystallization acceleration has been reported for the other grafted-type nanocomposites, where grafted PP chains with lower mobility facilitate nucleation [54,55]. The crystallization acceleration was also observed with modified SiO_2, and became more pronounced for a longer alkyl chain. These results are in perfect agreement with the TEM and NMR results that the surface modification improved the dispersion of SiO_2 nanoparticles and made the grafting reaction more efficient, in particular for a longer

alkyl chain.

Table 2.2. Melting and crystallization behaviors of nanocomposites analyzed by DSC.

Sample	T_m (°C)	X_c (%)	T_c (°C)	$t_{1/2}^{-1}$ [a] ($\times 10^{-3}$ s^{-1})
HomoPP	161	49	117	0.13
HomoPP/SiO_2	161	48	118	0.21
PP-OTMS	163	53	126	2.11
PP-OTMS/SiO_2	164	52	129	4.63
PP-OTMS/C6-0.1-SiO_2	164	50	129	4.59
PP-OTMS/C12-0.1-SiO_2	164	49	129	4.90
PP-OTMS/C16-0.1-SiO_2	164	49	129	5.21

[a] Inverse of the half time of isothermal crystallization at 144 °C.

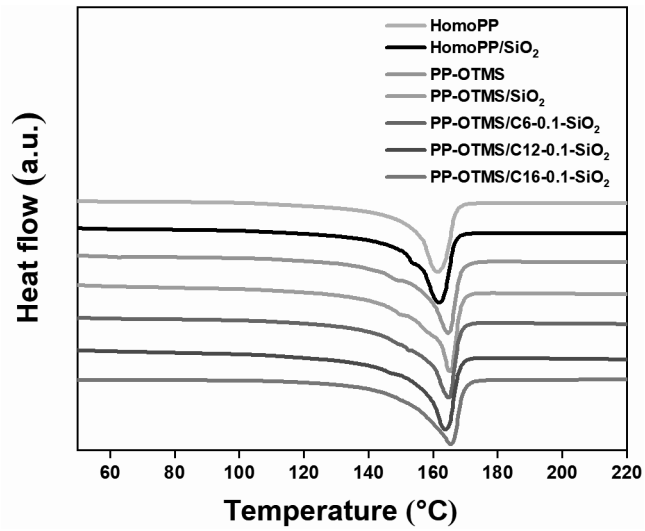

Fig. 2.7. DSC profiles during heating.

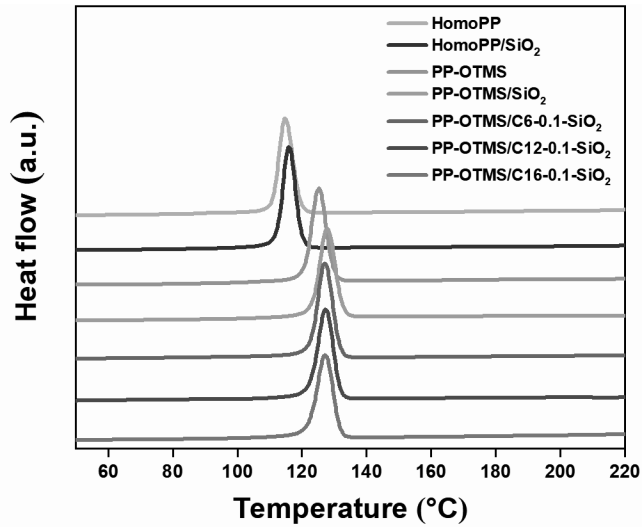

Fig. 2.8. DSC profiles during cooling.

Profiles are vertically shifted for visual clarity

2.3.5. Mechanical properties of polymer and nanocomposites

Tensile properties of nanocomposites were acquired using a uniaxial tensile tester. The representative stress–strain curves of the nanocomposites are provided in Fig. 2.9. From Table 2.3 and Fig. 2.10, the yield strength and elongation at break of PP-OTMS were higher than HomoPP as a consequence of LCBPP formation [56]. The addition of SiO_2 to HomoPP did not cause the improvement in the mechanical properties, but rather deteriorated the elongation at break due to the nanoparticle agglomeration and poorly connected interfaces [38,39]. On the other hand, the introduction of SiO_2 to PP-OTMS improved both of the Young's modulus and yield strength as compared to PP-OTMS. Such the improvement was associated with the improved dispersion and the successful grafting of PP-OTMS onto SiO_2 surfaces. The grafting not only improves the dispersion

of SiO_2 in PP, but also improves the interfacial bonding (hence the yield strength). Grafted chains co-crystallize with the matrix, and SiO_2 acts as a physical crosslinker, which disappears above the melting point, so nanocomposites are melt processible [38]. This is the largest advantage of graft-type nanocomposites with identical matrix and grafted chains. In contrast, the physical crosslink structure with SiO_2 as the core is much less flexible to deformation, which leads to a large decrease in elongation at break. This is a common disadvantage of the graft-type nanocomposites [38–40], and the significant decrease in the elongation at break and the toughness was also observed in PP-OTMS/SiO_2. By exploiting modified SiO_2 (C*x*-0.1-SiO_2), the elongation at break was partially recovered in addition to further improvement in the yield strength. The degree of the recovery/improvement was found to be greater for a longer alkyl chain (Table 2.3). In general, the yield strength is largely determined by the dispersion and interfacial interactions between the polymer matrix and fillers. Hence, the higher yield strength for a longer alkyl chain reasonably arose from better SiO_2 dispersion as well as from a larger extent of in situ grafting. Meanwhile, the elongation at break depends on the incidental presence of agglomerates or defects and the ductility of the original materials. In this light, a long alkyl chain not only provided homogeneous dispersion, but also behaved as a plasticizer to enhance the ductility of the materials, leading to the recovery of the elongation at break [26,28]. With the improvement in the yield strength and the recovery of the elongation at break, the toughness of the resultant nanocomposites was greatly enhanced along with the alkyl chain length (Table 2.3). The influence of the silane

grafting density on mechanical properties of nanocomposites was also studied for C16 (Table 2.3). It was found that an excessive addition of the silane coupling agent rather deteriorated the mechanical properties. This was likely associated with the formation of a soft organic layer, which hampered the stress transfer to hard nanoparticles.

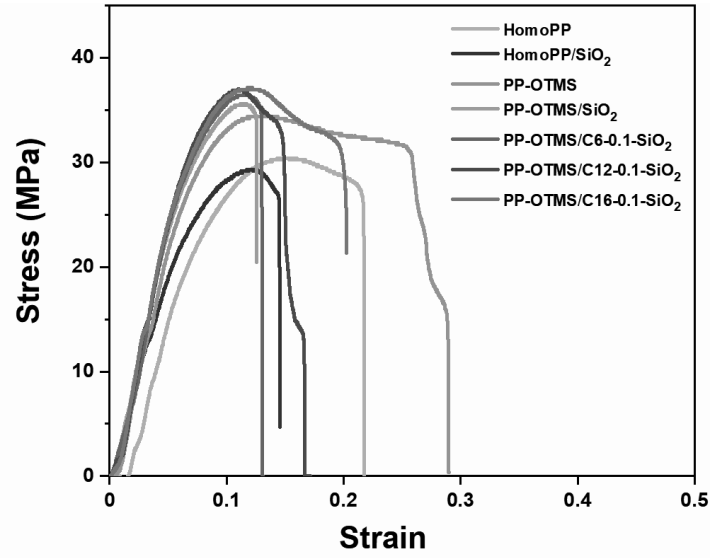

Fig. 2.9. Stress-strain curves.

Table 2.3. Tensile properties of nanocomposites.

Sample	Young's modulus (MPa)	Yield strength (MPa)	Elongation at break (%)	Toughness (MJ/m^3)
HomoPP	576 ± 18	30.2 ± 0.3	24.3 ± 2.7	5.4 ± 0.8
HomoPP/SiO_2	617 ± 46	29.6 ± 0.4	13.9 ± 1.1	2.8 ± 0.2
PP-OTMS	621 ± 30	34.8 ± 0.5	32.0 ± 6.5	7.9 ± 0.9

PP-OTMS/SiO_2	639 ± 39	36.5 ± 1.5	12.2 ± 0.2	2.9 ± 0.2
PP-OTMS/C6-0.1-SiO_2	646 ± 40	36.8 ± 0.6	14.4 ± 1.6	3.1 ± 0.6
PP-OTMS/C12-0.1-SiO_2	657 ± 28	37.6 ± 1.1	18.1 ± 4.1	4.3 ± 1.2
PP-OTMS/C16-0.1-SiO_2	662 ± 52	37.8 ± 1.0	20.1 ± 2.2	5.8 ± 0.7
PP-OTMS/C16-0.01-SiO_2	633 ± 56	36.7 ± 0.8	13.8 ± 0.7	3.5 ± 0.2
PP-OTMS/C16-1-SiO_2	620 ± 46	35.8 ± 2.8	12.9 ± 3.9	3.1 ± 1.2

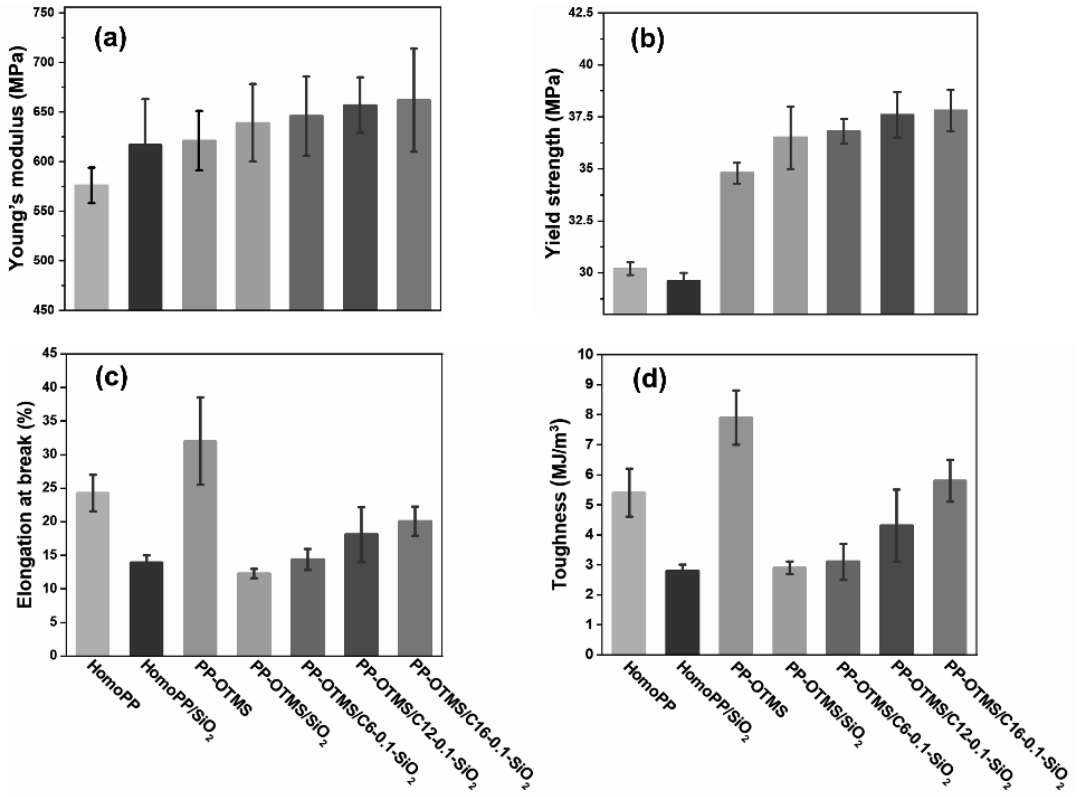

Fig. 2.10. Tensile properties: a) Young's modulus, b) yield strength, c) elongation at break, and d) toughness of nanocomposites.

2.4. Conclusions

In this study, organically modified SiO_2 was exploited for the fabrication of graft-type polymer nanocomposites using polypropylene having reactive functional groups (PP-OTMS) as a matrix. It was shown that the surface modification of SiO_2 with silane coupling agents helped the dispersion of SiO_2 to promote the in situ grafting during melt compounding of the reactive matrix with nanofillers. The influences of the alkyl chain length of silane coupling agents and the grafting amount on the properties of resultant nanocomposites were also studied. It was found that the dispersion improved with the increase in the alkyl chain length due to the improved hydrophobicity of SiO_2 surfaces. This offered a more opportunity for the reactive groups at the PP side chain to react with the remaining surface silanol groups during melt mixing and thus to in situ graft onto nanofiller surfaces. This grafting reaction was confirmed by the significant reduction in the amount of the reactive functional groups and the observed crystallization acceleration in the resultant nanocomposites. The advantage of the combination of surface modification and in situ grafting was evidenced for the mechanical properties, in which the efficient grafting strengthened the interfacial interaction between the matrix and SiO_2 to improve the reinforcement. Furthermore, the modification with plasticizing alkyl chains also helped to recover the toughness deterioration caused by the grafting itself. This provided the opportunity to balance the reinforcement and the toughness of the materials, which is difficult to achieve by in situ grafting alone.

References

[1] D.R. Paul, L.M. Robeson. Polymer nanotechnology: nanocomposites. Polymer 2008, 49, 3187–3204.

[2] F. Gao. Clay/polymer composites: the story. Mater. Today 2004, 7, 50–55.

[3] H. Liu, S. Gu, H. Cao, X. Li, X. Jiang, Y. Li. Modification of MWNTs by the combination of Li-TFSI and MAPP: novel strategy to high performance PP/MWNTs nanocomposites. Compos. Part B Eng. 2019, 176, 107268.

[4] P.-C. Ma, N.A. Siddiqui, G. Marom, J.-K. Kim. Dispersion and functionalization of carbon nanotubes for polymer-based nanocomposites: a review. Compos. Part A Appl. Sci. Manuf. 2010, 41, 1345–1367.

[5] H. Palza, J. Vera, M. Wilhelm, P. Zapata. Spherulite growth rate in polypropylene/silica nanoparticle composites: effect of particle morphology and compatibilizer. Macromol. Mater. Eng. 2011, 296, 744–751.

[6] H. Mao, B. He, W. Guo, L. Hua, Q. Yang. Effects of nano-$CaCO_3$ content on the crystallization, mechanical properties, and cell structure of PP nanocomposites in microcellular injection molding. Polymers 2018, 10, 1160.

[7] N.-V. Stanciu, F. Stan, I.-L. Sandu, C. Fetecau, A.-M. Turcanu. Thermal, rheological, mechanical, and electrical properties of polypropylene/multi-walled carbon nanotube nanocomposites. Polymers 2021, 13, 187.

[8] I.O. Navas, M. Kamkar, M. Arjmand, U. Sundararaj. Morphology evolution, molecular simulation, electrical properties, and rheology of carbon nanotube/polypropylene/polystyrene blend nanocomposites: effect of molecular interaction between styrene-butadiene block copolymer and carbon nanotube. Polymers 2021, 13, 230.

[9] J.F. Castro-Landinez, F. Salcedo-Galan, J.A. Medina-Perilla. Polypropylene/ethylene-and polar-monomer-based copolymers/montmorillonite nanocomposites: morphology, mechanical properties, and oxygen permeability. Polymers 2021, 13, 705.

[10] M.N.F. Norrrahim, H. Ariffin, T. Arisyah, T.A.T. Yasim-Anuar, M.A. Hassan, N.A. Ibrahim, W.M.Z.W. Yunus, H. Nishida. Performance evaluation of cellulose nanofiber with residual hemicellulose as a nanofiller in polypropylene-based nanocomposite. Polymers 2021, 13, 1064.

[11] E. Velásquez, S. Espinoza, X. Valenzuela, L. Garrido, M.J. Galotto, A. Guarda, C.L.D. Dicastillo. Effect of organic modifier types on the physical mechanical properties and overall migration of postconsumer polypropylene/clay nanocomposites for food packaging. Polymers 2021, 13, 1502.

[12] B. Constant-Mandiola, H. Aguilar-Bolados, J. Geshev, R. Quíjada. Study of the influence of magnetite nanoparticles supported on thermally reduced graphene oxide as filler on the mechanical and magnetic properties of polypropylene and polylactic acid nanocomposites. Polymers 2021, 13, 1635.

[13] N. Vidakis, M. Petousis, E. Velidakis, L. Tzounis, N. Mountakis, A. Korlos, P.E. Fischer-Griffiths, S. Grammatikos. On the mechanical response of silicon dioxide nanofiller concentration on fused filament fabrication 3D printed isotactic polypropylene nanocomposites. Polymers 2021, 13, 2029.

[14] V. Titone, M.C. Mistretta, L. Botta, F.P.L. Mantia. Investigation on the properties and on the photo-oxidation behaviour of polypropylene/fumed silica nanocomposites. Polymers 2021, 13, 2673.

[15] B.-N. Jung, H.-W. Jung, D.-H. Kang, G.-H. Kim, J.-K. Shim. A study on the oxygen permeability behavior of nanoclay in a polypropylene/nanoclay nanocomposite by biaxial stretching. Polymers 2021, 13, 2760.

[16] S. Naseem, S. Wießner, I. Kühnert, A. Leuteritz. Layered double hydroxide (MgFeAl-LDH)-based polypropylene (PP) nanocomposite: mechanical properties and thermal degradation. Polymers 2021, 13, 3452.

[17] D.N. Bikiaris, A. Vassiliou, E. Pavlidou, G.P. Karayannidis. Compatibilisation effect of PP-g-MA copolymer on iPP/SiO_2 nanocomposites prepared by melt mixing. Eur. Polym. J. 2005, 41, 1965–1978.

[18] W. Li, J. Karger-Kocsis, R. Thomann. Compatibilization effect of TiO_2 nanoparticles on the phase structure of PET/PP/TiO_2 nanocomposites. J. Polym. Sci. Part B Polym. Phys. 2009, 47, 1616–1624.

[19] F.-C. Chiu, H.-Z. Yen, C.-E. Lee. Characterization of PP/HDPE blend-based nanocomposites using different maleated polyolefins as compatibilizers. Polym. Test.

2010, 29, 397–406.

[20] P. Liborio, V.A. Oliveira, M.d.F.V. Marques. New chemical treatment of bentonite for the preparation of polypropylene nanocomposites by melt intercalation. Appl. Clay Sci. 2015, 111, 44–49.

[21] M. Ataeefard, S. Moradian. Surface properties of polypropylene/organoclay nanocomposites. Appl. Surf. Sci. 2011, 257, 2320–2326.

[22] P. Peng, Z. Yang, M. Wu, Q. Zhang, G. Chen. Effect of montmorillonoite modification and maleic anhydride-grafted polypropylene on the microstructure and mechanical properties of polypropylene/montmorillonoite nanocomposites. J. Appl. Polym. Sci. 2013, 130, 3952–3960.

[23] P. Maiti, P.H. Nam, M. Okamoto. Influence of crystallization on intercalation, morphology, and mechanical properties of polypropylene/clay nanocomposites. Macromolecules 2002, 35, 2042–2049.

[24] M.A. Al-Saleh, A.A. Yussuf, S. Al-Enezi, R. Kazemi, M.U. Wahit, T. Al-Shammari, A. Al-Banna. Polypropylene/graphene nanocomposites: effects of GNP loading and compatibilizers on the mechanical and thermal properties. Materials 2019, 12, 3924.

[25] M. Ataeefard, S. Moradian. Polypropylene/organoclay nanocomposites: effects of clay content on properties. Polym. Plast. Technol. Eng. 2011, 50, 732–739.

[26] S.H. Ahn, S.H. Kim, S.G. Lee. Surface-modified silica nanoparticle reinforced poly(ethylene 2,6-naphthalate). J. Appl. Polym. Sci. 2004, 94, 812–818.

[27] O.H. Lin, H.M. Akil, Z.A. Mohd Ishak. Surface-activated nanosilica treated with

silane coupling agents/polypropylene composites: mechanical, morphological, and thermal studies. Polym. Compos. 2011, 32, 1568–1583.

[28] R.-J. Zhou, T. Burkhart. Polypropylene/SiO_2 nanocomposites filled with different nanosilicas: thermal and mechanical properties, morphology and interphase characterization. J. Mater. Sci. 2010, 46, 1228–1238.

[29] A. Rungta, B. Natarajan, T. Neely, D. Dukes, L.S. Schadler, B.C. Benicewicz. Grafting bimodal polymer brushes on nanoparticles using controlled radical polymerization. Macromolecules 2012, 45, 9303–9311.

[30] C. Li, B.C. Benicewicz. Synthesis of well-defined polymer brushes grafted onto silica nanoparticles via surface reversible addition-fragmentation chain transfer polymerization. Macromolecules 2005, 38, 5929–5936.

[31] R. Ranjan, W.J. Brittain. Synthesis of high density polymer brushes on nanoparticles by combined RAFT polymerization and click chemistry. Macromol. Rapid Commun. 2008, 29, 1104–1110.

[32] H. Wang, Z. Fu, X. Zhao, Y. Li, J. Li. Reactive nanoparticles compatibilized immiscible polymer blends: synthesis of reactive SiO_2 with long poly(methyl methacrylate) chains and the in situ formation of janus SiO_2 nanoparticles anchored exclusively at the interface. ACS Appl. Mater. Interfaces 2017, 9, 14358–14370.

[33] H. Wang, X. Yang, Z. Fu, X. Zhao, Y. Li, J. Li. Rheology of nanosilica-compatibilized immiscible polymer blends: formation of a “heterogeneous network” facilitated by interfacially anchored hybrid nanosilica. Macromolecules 2017, 50, 9494−9506.

[34] M.A. Milani, D. González, R. Quijada, N.R.S. Basso, M.L. Cerrada, D.S. Azambuja, G.B. Galland. Polypopylene/graphene nanosheet nanocomposites by in situ polymerization: synthesis, characterization and fundamental properties. Compos. Sci. Technol. 2013, 84, 1–7.

[35] X. Zhang, T. Wada, P. Chammingkwan, A. Thakur, T. Taniike. Cooperative influences of nanoparticle localization and phase coarsening on thermal conductivity of polypropylene/polyolefin elastomer blends. Compos. Part A Appl. Sci. Manuf. 2019, 126, 105602.

[36] X. Zhang, X. Xia, H. You, T. Wada, P. Chammingkwan, A. Thakur, T. Taniike. Design of continuous segregated polypropylene/Al_2O_3 nanocomposites and impact of controlled Al_2O_3 distribution on thermal conductivity. Compos. Part A Appl. Sci. Manuf. 2020, 131, 105825.

[37] X. Zhang, B. Maira, Y. Hashimoto, T. Wada, P. Chammingkwan, A. Thakur, T. Taniike. Selective localization of aluminum oxide at interface and its effect on thermal conductivity in polypropylene/polyolefin elastomer blends. Compos. Part B Eng. 2019, 162, 662–670.

[38] T. Taniike, M. Toyonaga, M. Terano. Polypropylene-grafted nanoparticles as a promising strategy for boosting physical properties of polypropylene-based nanocomposites. Polymer 2014, 55, 1012–1019.

[39] E. Kurahashi, T. Wada, T. Nagai, P. Chammingkwan, M. Terano, T. Taniike. Synthesis of polypropylene functionalized with a trace amount of reactive functional groups

and its utilization in graft-type nanocomposites. Polymer 2018, 158, 46–52.

[40] G. Zhang, H. Li, M. Antensteiner, T.C. Mike Chung. Synthesis of functional polypropylene containing hindered phenol stabilizers and applications in metallized polymer film capacitors. Macromolecules 2015, 48, 2925–2934,

[41] Y. Jing, H. Niu, Y. Li. Improved ethylene-propylene rubber/silica interface via in-situ polymerization. Polymer 2019, 172, 117–125.

[42] M. Toyonaga, P. Chammingkwan, M. Terano, T. Taniike. Well-defined polypropylene/polypropylene-grafted silica nanocomposites: roles of number and molecular weight of grafted chains on mechanistic reinforcement. Polymers 2016, 8, 300.

[43] S. Mehdiabadi, J.B.P. Soares. Production of ethylene/α-Olefin/1,9-decadiene copolymers with complex microstructures using a two-stage polymerization process. Macromolecules 2011, 44, 7926–7939.

[44] Q. Guo, P. Zhu, G. Li, D. Lu, R. Sun, C.-P. Wong. Effects of surface-modified alkyl chain length of silica fillers on the rheological and thermal mechanical properties of underfill. IEEE Trans. Compon. Packag Manuf. Technol. 2016, 6, 1796–1803.

[45] A. Sriboonruang, T. Kumpika, E. Kantarak, W. Sroila, P. Singjai, N. Lawan, S. Muangpile, W. Thongsuwan. Isomer effect on chemical reactivity and superhydrophobicity of chlorosilane modified SiO_2 nanoparticles prepared by one-step reaction. Mater. Lett. 2019, 248, 227–230.

[46] T. Glaskova, M. Zarrelli, A. Borisova, K. Timchenko, A. Aniskevich, M. Giordano.

Method of quantitative analysis of filler dispersion in composite systems with spherical inclusions. Compos. Sci. Technol. 2011, 71, 1543–1549.

[47] H. Ogihara, J. Xie, T. Saji. Factors determining wettability of superhydrophobic paper prepared by spraying nanoparticle suspensions. Colloids Surf. A 2013, 434, 35–41.

[48] X. Yang, L. Zhu, Y. Chen, B. Bao, J. Xu, W. Zhou. Controlled hydrophilic/hydrophobic property of silica films by manipulating the hydrolysis and condensation of tetraethoxysilane. Appl. Surf. Sci. 2016, 376, 1–9.

[49] Y. Wang, L. Zhang, Y. Hu, C. Li. In situ surface functionalization of hydrophilic silica nanoparticles via flame spray process. J. Mater. Sci. Technol. 2015, 31, 901–906.

[50] Y. Yuan, Y. Duan, Z. Zuo, L. Yang, R. Liao. Novel, stable and durable superhydrophobic film on glass prepared by RF magnetron sputtering. Mater. Lett. 2017, 199, 97–100.

[51] R. Mueller, H.K. Kammler, K. Wegner, S.E. Pratsinis. OH surface density of SiO_2 and TiO_2 by thermogravimetric analysis. Langmuir 2003, 19, 160–165.

[52] T. Ji, C. Ma, L. Brisbin, L. Mu, C.G. Robertson, Y. Dong, J. Zhu. Organosilane grafted silica: quantitative correlation of microscopic surface characters and macroscopic surface properties. Appl. Surf. Sci. 2017, 399, 565–572.

[53] W. Chen, V. Karde, T.N.H. Cheng, S.S. Ramli, J.Y.Y. Heng. Surface hydrophobicity: effect of alkyl chain length and network homogeneity. Front. Chem. Sci. Eng. 2020, 15, 90–98.

[54] S.H. Tabatabaei, P.J. Carreau, A. Ajji. Rheological and thermal properties of blends of a long-chain branched polypropylene and different linear polypropylenes. Chem. Eng. Sci. 2009, 64, 4719–4731.

[55] J. Tian, W. Yu, C. Zhou. Crystallization behaviors of linear and long chain branched polypropylene. J. Appl. Polym. Sci. 2007, 104, 3592–3600.

[56] W. Zhao, Y. Huang, X. Liao, Q. Yang. The molecular structure characteristics of long chain branched polypropylene and its effects on non-isothermal crystallization and mechanical properties. Polymer 2013, 54, 1455–1462.

Chapter 3

Dual Effects of Side-functional Groups in Compatibilizing and Toughening of Polypropylene Nanocomposites

Chapter 3

Abstract

Addition of nanofillers to polymer offers mechanical reinforcement to the resultant nanocomposites at an expense of deterioration in the elongation at break, and thus the toughness, due to the stiffness of rigid nanoparticles and their agglomeration. A strategy to balance mechanical reinforcement with high toughness is required to prepare performant nanocomposites with improved processability and practicality for applications with high contact loads. In this work, polar functional groups were introduced to polypropylene (PP) by direct copolymerization of propylene and 4-Allyl-1,2-dimethoxybenzene (ADMB) using a Ziegler-Natta catalyst. The functionalized PP containing methoxy-phenyl side-functional groups (PP-ADMB) was employed as a matrix for fabricating PP/SiO_2 nanocomposites. It was found that the incorporation of methoxy-phenyl side-functional groups even at a trace amount not only improved the dispersion of SiO_2 nanoparticles, but also surprisingly enhanced the elongation at break and the toughness without deteriorating the reinforcement. These dual effects on compatibilizing with nanofillers and toughening of polymer make PP-ADMB advantageous over the homopolymer in balancing the mechanical properties of nanocomposites.

Keywords: PP nanocomposites, side-functional group, compatibilizing, toughening, mechanical properties

Chapter 3

3.1. Introduction

Polypropylene (PP), a key member of the polyolefin family, is one of the most widely used commodity plastics in numerous sectors of applications. Due to its good processability, good stability, low cost, and lightweight, PP offers considerable advantages in developing sustainable-by-design materials from flexible and rigid packaging to lightweight structural materials with enhanced functionalities and maximized energy efficiency [1–12]. The introduction of inorganic fillers to polymer is a common method for material property enhancement [13–18]. Compared with micron-sized fillers, nano-sized fillers offer much greater interfacial area for devising novel functionalities synergistically derived from inorganic components and polymer as well as effective load transfer to the matrix to remarkably improve reinforcement. However, the inertness of PP makes it challenging to homogeneously disperse nanofillers, i.e., the dispersion of nanofillers strongly depends on the preparation method in which several techniques, such as the use of compatibilizers [17,19,20], surface modification of nanofillers [21–24], in-situ polymerization in the presence of nanofillers [25], in-situ formation of nanofillers [26–28], polymer grafting [29–32], and so on, have been applied to compromise the lack of PP affinity to nanofillers.

In recent years, functionalized PP having polar functional groups or reactive functional groups has attracted attention in both industries and academia owing to the

opportunity to broaden its properties, especially at the improvement in compatibility with other materials [29,33,34]. Various strategies have been introduced to incorporate functional groups to the PP backbone. For example, Zhou et al. prepared post-functionalized PP by amination in the presence of N-hydroxyphthalimide and bis(2,2,2-trichloroethyl) azodicarboxylate, followed by atom transfer radical polymerization to graft polystyrene (PS) or poly(methyl) methacrylate (PMMA) onto the PP chains [35]. The grafted polymer was employed as a phase compatibilizer in blending PP with PS and PMMA. Our group prepared terminally hydroxylated PP (PP-*t*-OH) by controlled chain transfer reaction in metallocene-catalyzed propylene polymerization [36,37]. Terminally hydroxylated PP having different chain lengths was grafted onto SiO_2 nanoparticles to improve the dispersion of SiO_2 in the fabrication of mechanically-reinforced polymer nanocomposites. Chung's group reported the synthesis of PP containing hydroxyl groups, ester groups, and maleic anhydride using the reactive intermediate approach [38–40]. In this method, propylene was copolymerized with comonomers containing boranes or silanes, followed by interconverting boranes or silanes into the desired functional groups in the post-conversion process. Iizuka et al. synthesized functionalized PP by directly copolymerization of propylene with 5-hexen-1-ol. They found that the resultant copolymer exhibited improved mechanical properties [41]. Among these methods, the direct copolymerization of propylene with polar comonomers appears to be the simplest way to obtain functionalized PP in one step. On the other hand, the catalyst deactivation due to the complexation with functional comonomers remains as a serious issue for

practical applications.

To effectively synthesize and utilize functionalized PP for nanocomposite applications, our research group have previously reported the synthesis of PP having less than one functional group per chain by direct copolymerization of propylene with 7-octenyltrimethoxysilane (OTMS) [42]. Since a trace amount of a polar comonomer is required to incorporate a minute amount of copolymer, a serious issue in polymer productivity could be circumvented. I found that PP bearing less than one reactive side-functional groups did not act as an ordinary compatibilizer, but rather behaved like end-functionalized PP that simultaneously grafted onto SiO_2 nanoparticles during the melting mixing process to endow significant improvement in the reinforcement. On the other hand, the inclusion of rigidly embedded nanoparticles in the matrix caused the deterioration in the elongation at break and the toughness in spite of the improved dispersion of nanoparticles. Combination of the grafting strategy with the surface modification of SiO_2 nanoparticles to exert plasticizing layer was found to provide a way in balancing the stiffness and the toughness of nanocomposites [43].

In this work, an alternative way towards balanced properties of PP/SiO_2 nanocomposites was presented. I found that a choice of comonomer played an important role in balancing the stiffness and toughness of polymer. By exploiting 4-Allyl-1,2-dimethoxybenzene as a comonomer to synthesize PP bearing methoxy-phenyl side-functional groups and exploited as a matrix, the improvement in the nanocomposite properties was achieved not only for the dispersion of nanoparticles, but also the

significant increase in the elongation at break and the toughness without deteriorating the reinforcement. These dual effects on compatibilizing with nanofillers and toughening of polymer were investigated in detail.

3.2. Experimental sections

3.2.1 Materials

PP (M_n = 4.7 × 10^4, M_w/M_n = 3.6, stereoregularity (*mmmm*) = 92 mol%) and PP-ADMB were synthesized using a 5th-generation Ziegler-Natta catalyst according to our previous study [42]. *n*-Heptane was dried by N_2 bubbling in the presence of molecular sieve 3Å prior to use. Propylene of polymerization grade was donated by Japan Polypropylene Corporation and used as received. Dichloromethane was purchased from Kanto Chemical Co., Inc. Triethylaluminum (TEA, donated by Tosoh Finechem Co.) was used as a dilution in heptane. 4-Allyl-1,2-dimethoxybenzene (ADMB, purity > 98%, Tokyo Chemical Industry Co., Ltd.) was used as a comonomer without further purification. Octadecyl-3-(3,5-di-*tert*-butyl-4-hydroxyphenyl)propionate (AO-50, donated by ADEKA Corporation) was used as a stabilizer. SiO_2 nanoparticles (average diameter = 26 nm, specific surface area = 110 m^2 g^{-1}) were purchased from Kanto Chemical Co., Inc.

3.2.2. Synthesis of PP-ADMB

PP-ADMB was synthesized by copolymerization of propylene and ADMB using a Ziegler-Natta catalyst [42]. The polymerization was performed in a semi-batch manner in a 1 L stainless steel reactor equipped with a mechanical stirrer. 500 mL of heptane as a solvent, 5–35 mmol of TEA as a cocatalyst, and 0–30 mmol of ADMB as a comonomer were added to a reactor under N_2 atmosphere. The solvent was saturated with 0.5 MPa of propylene at 50 °C for 30 min. Thereafter, 16 mmol of H_2 was introduced as a chain transfer agent, followed by 50 mg of a catalyst to start the polymerization. After 60 min of polymerization at 50 °C and 0.5 MPa, the reactor was depressurized. The solvent was removed by decantation and the resultant polymer powder was repeatedly washed with ethanol and acetone under N_2. Finally, the polymer powder was washed with dichloromethane and dried in vacuo at room temperature. PP homopolymer (HomoPP) was also synthesized in the absence of ADMB under the same condition with the amount of TEA used at 5.0 mmol.

3.2.3. Preparation of polymer nanocomposites

The following process was used to fabricate PP-ADMB and PP-ADMB/SiO_2 nanocomposites: first, PP-ADMB (3.4 g) was impregnated with 1.0 wt% of AO-50 in 100 mL of acetone as a solvent. The polymer power was dried by purging with N_2 flow, followed by vacuum drying at room temperature for 12 h. Thereafter, it was melt-mixed

with 5.0 wt% of SiO_2 in a Micro Compounder MC5 (Xplore) at 185 °C and 100 rpm for 15 min under N_2 atmosphere. The extrudate was hot-pressed into a 200 μm-thick nanocomposite film at 230 °C and 20 MPa for 5 min, followed by quenching at 100 °C for 5 min and cooling at 0 °C for 3 min.

3.2.4. Characterizations

The ADMB content in PP-ADMB was determined using a ^{1}H NMR (Bruker 400 MHz) at 120 °C with 1000 scans. Approximately 60 mg of a sample was dissolved in 0.7 mL of 1,1,2,2-tetrachloroethane-d_2 as a solvent and an internal lock. A typical ^{1}H NMR spectrum of PP-ADMB is showed in Fig. 3.1, where the peaks at 3.8 ppm and 1.8 ppm are assigned to the methyl protons of the methoxy group in ADMB and the methine protons of the polymer backbone, respectively. The ADMB content was calculated using Eq. (2-1),

$$\text{ADMB content (mol\%)} = \frac{H^a/6}{H^e} \times 100 \quad (2\text{-}1),$$

where H^a and H^e are the peak areas for the methyl protons of the methoxy group in ADMB and the methine protons of the polymer backbone, respectively.

The thermal behavior of a polymer sample was analyzed by differential scanning calorimetry (DSC, Mettler Toledo DSC 822, Mettler Toledo). Approximately 8 mg of a sample was loaded into an aluminum pan and heated to 230 °C at a heating rate of 20 °C min^{-1}. The melting endotherm in the first heating was used to determine the melting

temperature (T_m) and the crystallinity (X_c). After holding the temperature at 230 °C for 10 min, the sample was cooled down to 25 °C at a cooling rate of 20 °C min^{-1} to acquire the crystallization temperature (T_c). The molecular weight and the molecular weight distribution of a polymer sample were analyzed by gel permeation chromatography (GPC, HLC-8321GPC/HT, Tosoh Co.) at 140 °C using *o*-dichlorobenzene as a mobile phase. Polystyrene standards were used for calibration. The dispersion of SiO_2 nanoparticles was observed on a transmission electron microscope (TEM, Hitachi H-7650, Hitachi High-Tech Corporation) operated at an acceleration voltage of 100 kV. A 100 nm-thick specimen was cut from a nanocomposite film using an ultramicrotome instrument (Leica ULTRACUTS FCS, Leica Microsystems GmbH) equipped with a diamond knife. The dispersion of nanoparticles in a macroscopic scale was also observed by scanning electron microscopy (SEM, TM3030Plus, Hitachi Ltd.) coupled with energy dispersive X-ray spectroscopy (EDS, x-stream-2, Oxford Instruments). Tensile properties of a polymer film were acquired at room temperature using a tensile tester (Dat-100, Abecks Inc.) with a crosshead speed of 1 mm min^{-1}. A 200 μm-thick film was die-cut into dumbbell-shaped specimens for the measurement. At least five measurements were performed for each sample and the tensile properties were reported as an average value.

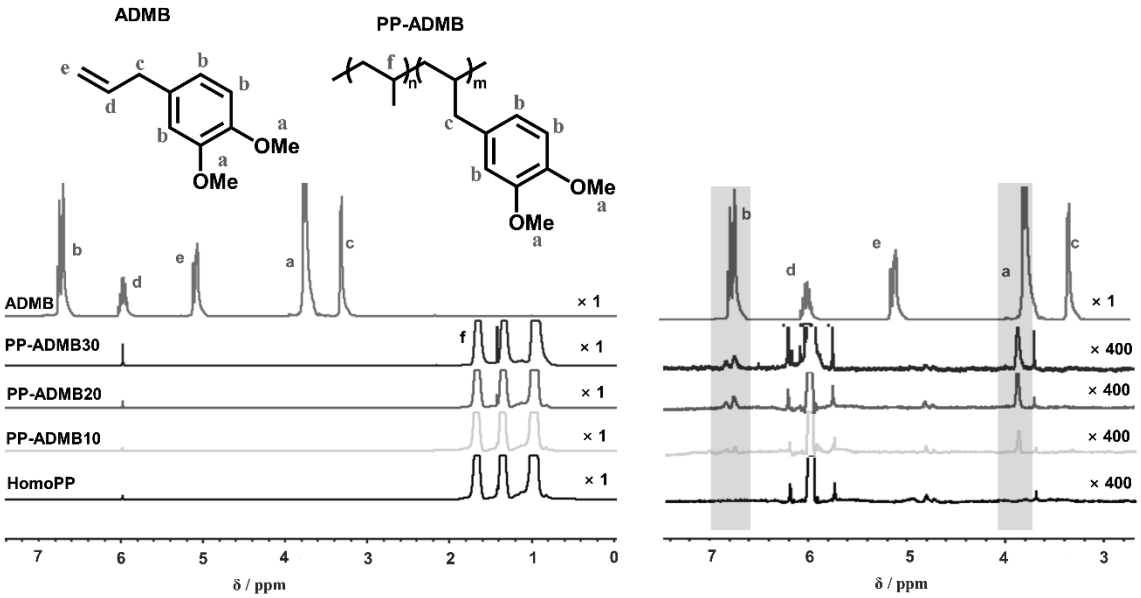

Fig. 3.1. ^{1}H NMR spectra of HomoPP and PP-ADMB.

The right figure shows expanded spectra.

3.3. Results and discussion

3.3.1. Polymerization results of PP-ADMB

The methoxy-phenyl functional group was introduced into a PP chain by copolymerization of propylene and ADMB using a Ziegler-Natta catalyst. In Fig. 3.1, the NMR spectra of PP-ADMB were identical to that of HomoPP, except the presence of extra chemical shifts around 3.8 ppm and 6.8 ppm. These peaks were respectively assigned to the methoxy protons and aromatic protons in ADMB. The absence of methylene and methine protons for the vinyl group of the comonomer at 5.1 and 6.0 ppm confirmed that ADMB was successfully incorporated into the polymer chain. The

polymerization results are summarized in Table 3.1. In general, the introduction of functional comonomers in olefin polymerization causes the deterioration of the activity due to a strong complexation between the non-bonded electron pairs of the functional comonomers and the Lewis acid catalytic sites [44]. The synthetic modification of the functional group by exerting steric and electronic protection is typical required to prevent the coordination of the functional group with the metal center. In our previous work using octenyltrimethoxysilane (OTMS) as a comonomer, the protection of the functional group was simply done through complexation with alkylaluminum, i.e., apart from the portion added as a cocatalyst, alkylaluminum was additionally introduced at an equivalent molar amount to a comonomer [42]. Though the decrease in the activity was still unavoidable, the reasonable yield could be achieved. In the PP-ADMB system under the same practice, the catalytic activity decreased with the addition of ADMB similar to the general trend. However, the activity deterioration was much smaller as compared to our previous work, i.e., 50% decrease in the activity was observed at the ADMB addition amount of 10 mmol as compared to 200% decrease in the activity for OTMS. This plausibly comes from the steric effect of the aromatic ring and/or the conjugative interaction that facilitates the flow of non-bonded valence shell electron pairs on the oxygen atom to the aromatic ring. The stereoregularity (*mmmm*) and the molecular weight of the polymer samples were slightly increased by the addition of ADMB [45]. By increasing the amount of ADMB, the ADMB content in the resultant polymer proportionally increased, and was determined to be in the range of 5.3×10^{-3} mol% to 12.5×10^{-3} mol%, corresponding to 0.06–0.17 functional

groups per chain.

Table 3.1. Results of propylene homo- and copolymerization.

Samples	ADMB [mmol]	Activity[a] [kg-polymer mol-Ti^{-1} h^{-1} atm^{-1}]	*mmmm*[b] [mol%]	M_n[c] [× 10^4]	M_w[c] [× 10^5]	M_w/M_n[c]	ADMB content [× 10^{-3} mol%][d]	ADMB content [Number per main chain][e]
HomoPP	0	605 ± 8	95	4.7	2.0	3.6	n.a.	n.a.
PP-ADMB10	10	277 ± 10	96	5.0	3.2	4.6	5.3	0.06
PP-ADMB20	20	210 ± 9	97	5.1	2.6	4.0	10.6	0.13
PP-ADMB30	30	161 ± 4	97	5.7	3.0	4.6	12.5	0.17

[a]Polymerization conditions: 5 mmol of TEA was used as a cocatalyst with 16 mmol of H_2 as a chain transfer agent and 50 mg of a catalyst. In the case of copolymerization, additional TEA was introduced at an equimolar amount of a comonomer. Polymerization was conducted at 0.5 MPa for 1 h in 500 mL of heptane.

[b]Determined by ^{13}C NMR.

[c]Determined by GPC.

[d]Determined by ^{1}H NMR.

[e]Calculated using the ADMB content and M_n.

3.3.2. DSC results of polymer and its nanocomposites

HomoPP and PP-ADMB samples were melt-mixed in the absence or presence of 5 wt% of SiO_2 nanoparticles, and compressed into films. DSC results of the film samples are shown in Table 3.2. It was evident that the incorporation of ADMB at a small amount had no significant effect on the melting temperature (T_m), the crystallinity (X_c) and non-isothermal crystallization temperature (T_c) of the polymer samples. This indicates that the crystal structure of copolymer and the long sequences of propylene units in the polymer chains remains unchanged from that of homopolymer [45], which is indeed highly desirable to introduce the functional group to the polymer chain while maintaining its basic properties especially at high T_m [46–48]. In the case of nanocomposites, T_m and X_c did not change considerably for HomoPP/SiO_2 and PP-ADMB10/SiO_2, but the T_m values notably increased for PP-ADMB20/SiO_2 and PP-ADMB30/SiO_2. The increase in T_m also accompanied the decrease in the crystallinity and T_c. The ^{1}H NMR spectra of the polymer films are shown in Fig. 3.2 and the ADMB content after melt mixing determined from the methoxy proton is listed in Table 3.2. It was clearly seen that the methoxy group was consumed in the melt mixing process, probably through the reaction with residual water. The decrement became less in the presence of SiO_2. In our previous work, the reaction between hydroxyl groups on SiO_2 surfaces and the methoxysilane-side functional group of copolymer afforded the grafting of polymer chains onto SiO_2 surfaces [42]. It was further observed that the grafted chains acted as the crystallization nuclei to accelerate

crystallization and to increase T_c. Judging from the DSC results and the consumption of the methoxy group, it is likely that the introduction of SiO_2 to PP-ADMB did not consume the methoxy groups, which meant there was no grafting reaction between the polymer and the nanofillers. With regard to crystallization behavior, the T_c was found to decease. It must be noted that dissolution of PP-ADMB and PP-ADMB30 in boiling xylene formed a thick gel instead of a clear solution as in the case of HomoPP and HomoPP/SiO_2 (Fig. 3.3). Considering that all polymer samples possessed the similar molecular weight and stereospecificity, it was speculated that the formation of a thick gel arose from non-crosslinking of polymer through the phenyl side-functional groups. This opened possibility that non-covalent cross-linkage may happen through association of phenyl groups.

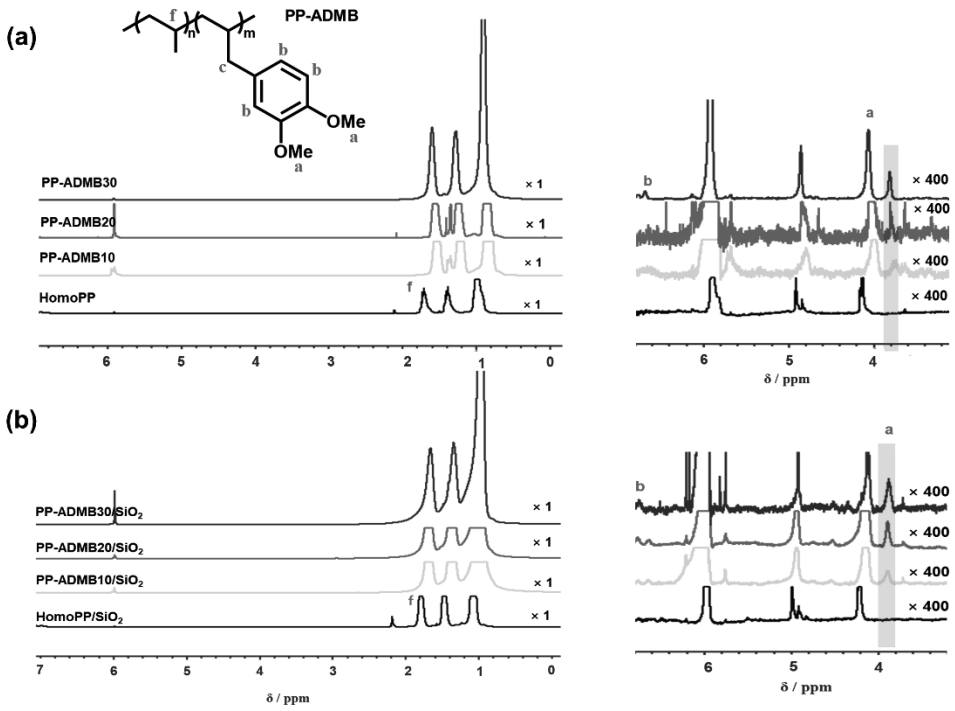

Fig. 3.2. ^{1}H NMR spectra of polymer films after melt mixing: a) HomoPP and PP-ADMB, and b) HomoPP/SiO_2 and PP-ADMB/SiO_2.

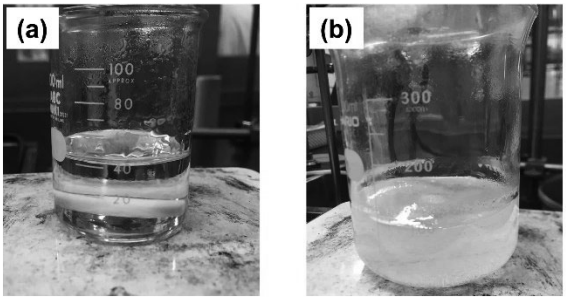

Fig. 3.3. Appearance of polymer samples dissolved in boiling xylene: a) HomoPP, and b) PP-ADMB30.

Table 3.2. DSC results and ADMB contents of film samples.

Samples	T_m[a] (°C)	X_c[a] (%)	T_c[a] (°C)	ADMB content[b] (× 10^3 mol%)
HomoPP	161	49	117	–
PP-ADMB10	162	49	116	4.0
PP-ADMB20	162	49	116	7.1
PP-ADMB30	162	49	116	8.5
HomoPP/SiO_2	161	48	118	–
PP-ADMB10/SiO_2	162	47	116	2.8
PP-ADMB20/SiO_2	164	45	113	6.8
PP-ADMB30/SiO_2	166	36	114	7.5

[a]Determined by DSC and [b]Determined by ^{1}H NMR.

3.3.3. TEM results of nanocomposites

Fig. 3.4 shows TEM images of the nanocomposite films. Huge aggregates of nanoparticles of over 1 μm were observed for the HomoPP/SiO_2 sample due to poor compatibility between the inert PP matrix and SiO_2 nanoparticles. In the case of using PP-ADMB as a matrix, the dispersion was clearly improved and the large aggregates were not anymore evident. Noted that the increase in the ADMB content in the copolymer did not seem to exert an effect on the dispersion of nanoparticles. For all PP-ADMB/SiO_2 nanocomposites, small clusters of SiO_2 were seen, but they were homogeneously distributed throughout the observed area. At the macroscopic scale, Si-mapping observed by SEM-EDS revealed that huge aggregates of nanoparticles in the HomoPP/SiO_2 sample could be concentrated to over a 10 μm-scale (Fig. 3.5a). Contrary, no macroscopic aggregations of nanoparticles were seen for the PP-ADMB/SiO_2 samples (Fig. 3.5b–d). These results point out that the presence of functional groups even at a trace amount improves compatibility between the PP matrix and polar nanofillers to endow a better dispersion of nanoparticles.

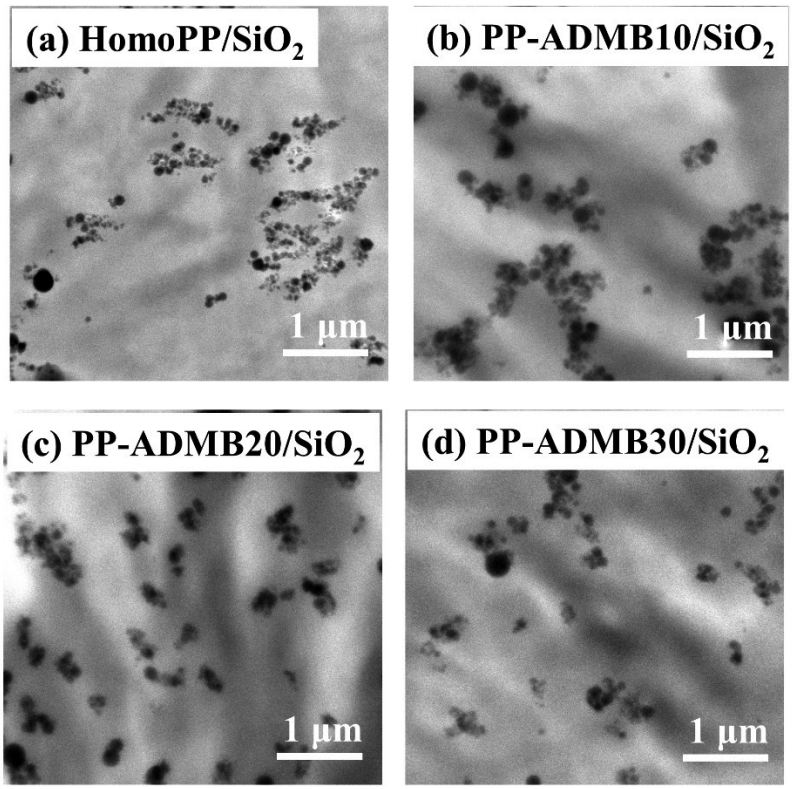

Fig. 3.4. TEM images of nanocomposite films: a) HomoPP/SiO_2, b) PP-ADMB10/SiO_2, c) PP-ADMB20/SiO_2, and d) PP-ADMB30/SiO_2.

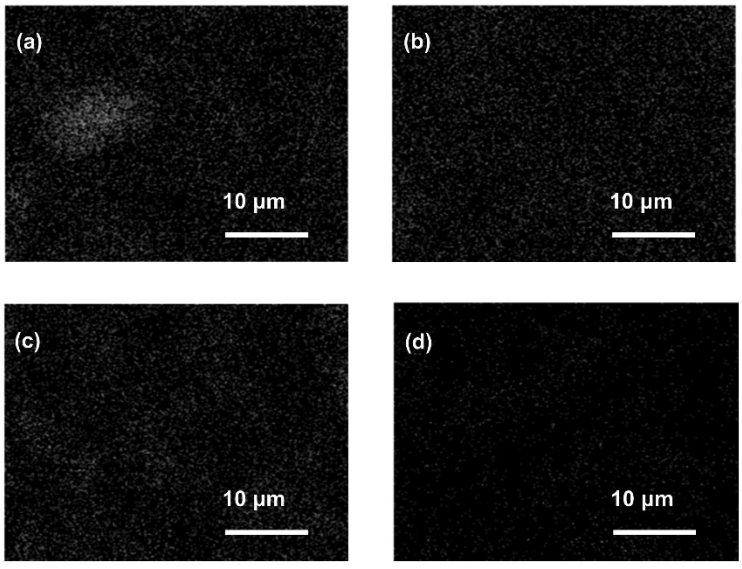

Fig. 3.5. Si-mapping observed by SEM-EDS of nanocomposite films: a) HomoPP/SiO_2,

b) PP-ADMB10/SiO_2, c) PP-ADMB20/SiO_2, and d) PP-ADMB30/SiO_2.

3.3.4. Tensile results of polymer and its relative nanocomposites

Mechanical properties of nanocomposites were acquired using a uniaxial tensile tester. The representative stress-strain curves of the film samples are depicted in Fig. 3.6 and Fig. 3.7. It was found that the incorporation of ADMB to PP surprisingly toughened the polymer. The elongation at break was significantly improved to nearly ten times larger than HomoPP. It is well-known that the strain hardening of polymer is related to connectivity of polymer chains. For semi-crystalline polymer, the strain hardening is mainly governed by the entanglement and physical crosslinkage in the amorphous phase. To understand the origin of toughening mechanism in the PP-ADMB system, the stress-strain curves of PP-OTMS, which was reported to undergo crosslinking through methoxysilane-side functional group, were compared in Fig. 3.6 [42]. However, only small improvement in the elongation at break was observed for PP-OTMS as compared to HomoPP. Hence, the crosslinkage could not explain these unexpected phenomena. Table 3 summarizes the mechanical properties derived from the stress-strain curves. It can be seen that the incorporation of ADMB decreased the Young's modulus, implying that the polymer became softer [49]. Accordingly, it is most plausible that the inclusion of ADMB in the amorphous phase helps in dissipating the energy to improve the toughness of polymer by the non-covalent cross-linkage through association of phenyl

groups. Upon increasing the incorporated amount of the comonomer, the Young's modulus was recovered to a similar level of HomoPP, while the yield strength exceeded that of HomoPP. The introduction of SiO_2 to HomoPP did not significantly improve the mechanical properties of polymer, but rather deteriorated the elongation at break. This was often reported to arise from nanoparticle aggregations, which becomes the fracture initiation sites. The addition of SiO_2 to PP-ADMS, on the other hand, significantly improved the Young's modulus as compared to the base matrices. This is believed to attribute to better dispersion of rigid nanoparticles due to the improved compatibility between the matrices and polar fillers. The yield strength of the PP-ADMB/SiO_2 nanocomposites was found to be similar to that of correspondent PP-ADMB, which made the mechanical properties in both of the Young's modulus and yield strength for the PP-ADMB/SiO_2 system better than HomoPP/SiO_2. Though the deterioration of the elongation at break was also observed for the PP-ADMB/SiO_2 samples, they still exhibited a significantly higher toughness as compared to HomoPP/SiO_2. The improvement in the toughness is indeed very essential for polymer processing, especially for nanocomposite films, as it offers resistance to failure under stretching. Hence the incorporation of a small amount of methoxy-phenyl side-functional group through copolymerization was found to be a promising strategy to prepare a polymer matrix for fabricating PP nanocomposites with well-balance mechanical properties.

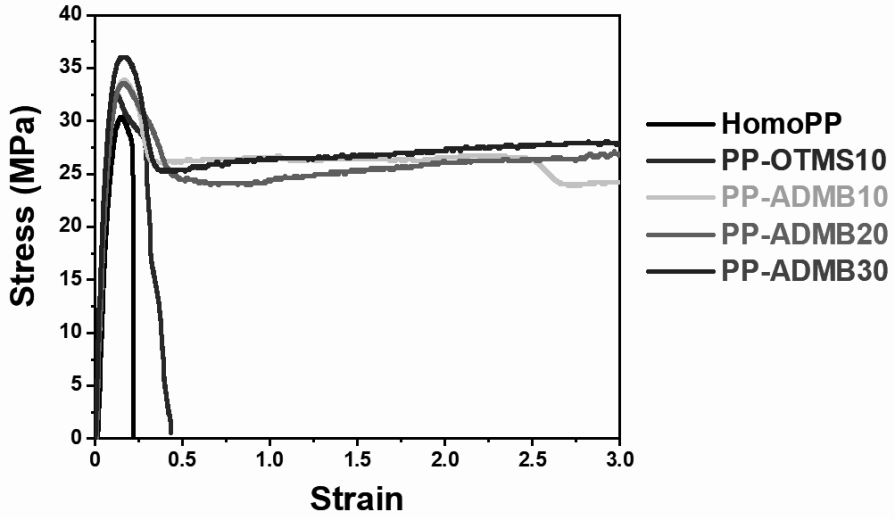

Fig. 3.6. Stress-strain curves of polymer films.

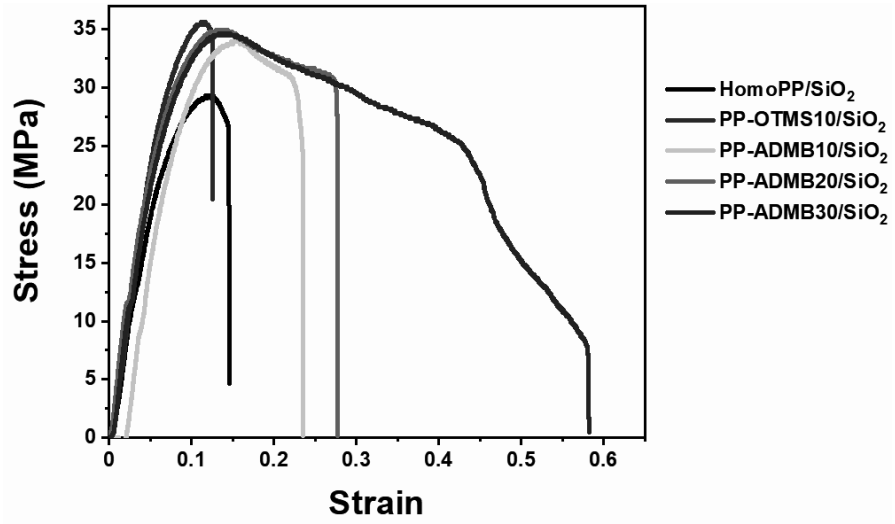

Fig. 3.7. Stress-strain curves of nanocomposites films.

Table 3.3. Tensile properties of copolymer and nanocomposites.

Sample	Young's modulus (MPa)	Yield strength (MPa)	Elongation at break (%)	Toughness (MJ/m^3)
HomoPP	576 ± 18	30.2 ± 0.3	24 ± 3	5.4 ± 0.8

PP-ADMB10	443 ± 80	33.3 ± 3.0	>300[a]	>77
PP-ADMB20	546 ± 106	33.9 ± 1.0	>300[a]	>77
PP-ADMB30	550 ± 25	36.1 ± 0.8	>300[a]	>77
HomoPP/SiO_2	617 ± 46	29.6 ± 0.4	14 ± 1	2.8 ± 0.2
PP-ADMB10/SiO_2	536 ± 21	33.1 ± 0.6	21 ± 3	6.2 ± 0.8
PP-ADMB20/SiO_2	587 ± 49	33.0 ± 1.6	37 ± 17	7.6 ± 3.2
PP-ADMB30/SiO_2	659 ± 25	34.3 ± 0.7	65 ± 19	15.8 ± 4.0

[a]Not break at the instrumental limitation of 470% strain.

3.4. Conclusions

In this study, a small amount of methoxy-phenyl functional groups was introduced to polypropylene (PP) by direct copolymerization of propylene and 4-Allyl-1,2-dimethoxybenzene (ADMB) using a Ziegler-Natta catalyst. By using a functional comonomer with an aromatic group, the deterioration in the activity due to complexation between the polar comonomer and the catalyst was found to be significantly reduced to afford copolymer with reasonable activity for practical application. PP having a trace amount of methoxy-phenyl side-functional groups (PP-ADMB) exhibited the properties similar to that of homopolymer especially at high melting temperature. PP-ADMB was employed as a matrix for the fabrication of PP nanocomposites using SiO_2 as nanofillers. The methoxy groups of the functional copolymer were found to be consumed during the

melt mixing process. However, because the functional groups of copolymers remained largely unreacted after melt mixing, these results indicated that no grafting occurred. With the increase in the incorporated amount of the comonomer, PP-ADMB/SiO_2 nanocomposites exhibited an increase in the melting temperature, while the crystallinity and the crystallization temperature were reduced. The incorporation of methoxy-phenyl side-functional groups even at a trace amount was found not only to improve the dispersion of nanoparticles, but also to soften the polymer which surprisingly improved the toughness and elongation at break without deteriorating the reinforcement. These dual effects on compatibilizing with nanofillers and toughening of polymer make PP-ADMB advantageous over homopolymer in balancing the mechanical properties of nanocomposites.

References

[1] H. Hagihara, K. Tsuchihara, K. Takeuchi, M. Murata, H. Ozaki, T. Shiono. Copolymerization of ethylene or propylene with α-olefins containing hydroxyl groups with zirconocene/methylaluminoxane catalyst. J. Polym. Sci., Part A: Polym. Chem. 2004, 42, 52–58.

[2] Q.-X. Zhang, Z.-Z. Yu, X.-L. Xie, Y.-W. Mai. Crystallization and impact energy of polypropylene/$CaCO_3$ nanocomposites with nonionic modifier. Polymer 2004, 45, 5985–5994.

[3] H.-Y. Yu, L.-Q. Liu, Z.-Q. Tang, M.-G. Yan, J.-S. Gu, X.-W. Wei. Surface modification of polypropylene microporous membrane to improve its antifouling characteristics in an SMBR: air plasma treatment. J. Membr. Sci. 2008, 311, 216–224.

[4] M. Xu, J. Qiu, Y. Lin, X. Shi, H. Chen, T. Xiao. Surface biocompatible modification of polypropylene by entrapment of polypropylene-block-poly(vinylpyrrolidone). Colloids Surf. B 2010, 80, 200–205.

[5] N. Gomathi, R. Rajasekar, R.R. Babu, D. Mishra, S. Neogi. Development of bio/blood compatible polypropylene through low pressure nitrogen plasma surface modification. Mater. Sci. Eng. C Mater. Biol. Appl. 2012, 32, 1767–1778.

[6] H. Hagihara, K. Ito, S. Kimata. Comprehensive study of altered amorphous structure in functionalized polypropylenes exhibiting high tensile strength. Macromolecules 2013, 46, 4432–4437.

[7] X. Wang, Y. Wang, X. Shi, J. Liu, C. Chen, Y. Li. Syntheses of well-defined functional isotactic polypropylenes via efficient copolymerization of propylene with ω-halo-α-alkenes by post-metallocene hafnium catalyst. Macromolecules 2014, 47, 552–559.

[8] J. Shi, J.-Y. Dong. Simultaneous cross-linking as a way to control physical growth of random ethylene-propylene copolymer during formation of high-impact polypropylene. Polymer 2016, 85, 10–18.

[9] T. Yang, Y. Qin, J.-Y. Dong. Nonconjugated α, ω-diolefin/propylene

copolymerization to long chain-branched polypropylene by Ziegler–Natta catalyst: overcoming steric hindrance by introducing an extra electronic pulling effect. Macromolecules 2018, 51, 9234–9249.

[10] X. Huang, J. Zhang, P. Jiang, T. Tanaka. Material progress toward recyclable insulation of power cables part 2: polypropylene-based thermoplastic materials. IEEE Electr. Insul. Mag. 2019, 36, 8–18.

[11] Y. Jing, H. Niu, Y. Li. Improved ethylene-propylene rubber/silica interface via in-situ polymerization. Polymer 2019, 172, 117–125.

[12] H. Huang, H. Niu, J.Y. Dong. Synthesis of azide end-functionalized isotactic polypropylene building block and renewed modular synthesis of diblock copolymers of isotactic polypropylene and poly (ε-caprolactone). J. Polym. Sci., Part A: Polym. Chem. 2011, 49, 2222–2232.

[13] S. Iwamoto, S. Yamamoto, S.-H. Lee, T. Endo. Mechanical properties of polypropylene composites reinforced by surface-coated microfibrillated cellulose. Composites Part A 2014, 59, 26–29.

[14] V. Dougnac, R. Alamillo, B. Peoples, R. Quijada. Effect of particle diameter on the permeability of polypropylene/SiO_2 nanocomposites. Polymer 2010, 51, 2918–2926.

[15] M.Z. Rong, M.Q. Zhang, Y.X. Zheng, H.M. Zeng, K. Friedrich. Improvement of tensile properties of nano-SiO_2/PP composites in relation to percolation mechanism. Polymer 2001, 42, 3301–3304.

[16] P. Song, Z. Cao, Y. Cai, L. Zhao, Z. Fang, S. Fu. Fabrication of exfoliated graphene-

based polypropylene nanocomposites with enhanced mechanical and thermal properties. Polymer 2011, 52, 4001–4010.

[17] D.N. Bikiaris, A. Vassiliou, E. Pavlidou, G.P. Karayannidis. Compatibilisation effect of PP-g-MA copolymer on iPP/SiO_2 nanocomposites prepared by melt mixing. Eur. Polym. J. 2005, 41, 1965–1978.

[18] W. Li, J. Karger-Kocsis, R. Thomann. Compatibilization effect of TiO_2 nanoparticles on the phase structure of PET/PP/TiO_2 nanocomposites. J. Polym. Sci., Part B: Polym. Phys. 2009, 47, 1616–1624.

[19] M.A. Poothanari, J. Abraham, N. Kalarikkal, S. Thomas. Excellent electromagnetic interference shielding and high electrical conductivity of compatibilized polycarbonate/polypropylene carbon nanotube blend nanocomposites. Ind. Eng. Chem. Res. 2018, 57, 4287–4297.

[20] X. Wen, J. Min, H. Tan, D. Gao, X. Chen, K. Szymańska, B. Zielińska, E. Mijowska, T. Tang. Reactive construction of catalytic carbonization system in PP/C_{60}/$Ni(OH)_2$ nanocomposites for simultaneously improving thermal stability, flame retardancy and mechanical properties. Composites Part A 2020, 129, 105722.

[21] R.-J. Zhou, T. Burkhart. Polypropylene/SiO_2 nanocomposites filled with different nanosilicas: thermal and mechanical properties, morphology and interphase characterization. J. Mater. Sci. 2011, 46, 1228–1238.

[22] S. Kango, S. Kalia, A. Celli, J. Njuguna, Y. Habibi, R. Kumar. Surface modification of inorganic nanoparticles for development of organic-inorganic nanocomposites-a

review. Prog. Polym. Sci. 2013, 38, 1232–1261.

[23] F. Ahangaran, A.H. Navarchian. Recent advances in chemical surface modification of metal oxide nanoparticles with silane coupling agents: a review. Adv. Colloid Interface Sci. 2020, 286, 102298.

[24] Y. Zhou, J. Hu, B. Dang, J. He. Effect of different nanoparticles on tuning electrical properties of polypropylene nanocomposites. IEEE Trans. Dielectr. Electr. Insul. 2017, 24, 1380–1389.

[25] M.A. Milani, D. González, R. Quijada, N.R. Basso, M.L. Cerrada, D.S. Azambuja, G.B. Galland. Polypropylene/graphene nanosheet nanocomposites by in situ polymerization: synthesis, characterization and fundamental properties. Compos. Sci. Technol. 2013, 84, 1–7.

[26] X. Zhang, B. Maira, Y. Hashimoto, T. Wada, P. Chammingkwan, A. Thakur, T. Taniike. Selective localization of aluminum oxide at interface and its effect on thermal conductivity in polypropylene/polyolefin elastomer blends. Composites Part B 2019, 162, 662–670.

[27] W. Bahloul, F. Mélis, V. Bounor-Legaré, P. Cassagnau. Structural characterisation and antibacterial activity of PP/TiO_2 nanocomposites prepared by an in situ sol-gel method. Mater. Chem. Phys. 2012, 134, 399–406.

[28] M.M. Adnan, A.R.M. Dalod, M.H. Balci, J. Glaum, M.A. Einarsrud. In situ synthesis of hybrid inorganic-polymer nanocomposites. Polymers 2018, 10, 1129.

[29] M.-C. Hsiao, S.-H. Liao, Y.-F. Lin, C.-A. Wang, N.-W. Pu, H.-M. Tsai, C.-C.M. Ma.

Preparation and characterization of polypropylene-graft-thermally reduced graphite oxide with an improved compatibility with polypropylene-based nanocomposite. Nanoscale 2011, 3, 1516–1522.

[30] R. Watanabe, M. Kunioka, J. Mizukado, H. Suda, H. Hagihara. Highly ductile polypropylene-based nanocomposites by dispersing monodisperse silica nanospheres in functionalized polypropylene containing hydroxyl groups. Polymer 2016, 99, 63–71.

[31] W. Yuan, F. Wang, Z. Chen, C. Gao, P. Liu, Y. Ding, S. Zhang, M. Yang. Efficient grafting of polypropylene onto silica nanoparticles and the properties of PP/PP-g-SiO_2 nanocomposites. Polymer 2018, 151, 242–249.

[32] R. Watanabe, H. Shinzawa, M. Kunioka, J. Mizukado, H. Suda, H. Hagihara. Reinforcement mechanism of functionalized polypropylene containing hydroxyl group nanocomposites studied by rheo-optical near-infrared spectroscopy. Eur. Polym. J. 2017, 92, 86–96.

[33] X.Y. Wang, Y.Y. Long, Y.X. Wang, Y.S. Li. Insights into propylene/ω-halo-α-alkenes copolymerization promoted by rac-Et$(Ind)_2ZrCl_2$ and (pyridyl-amido)hafnium catalysts. J. Polym. Sci., Part A: Polym. Chem. 2014, 52, 3421–3428.

[34] D. Zhang, L. Pan, Y. Li, B. Wang, Y. Li. Synthesis and reaction of anthracene-containing polypropylene: a promising strategy for facile, efficient functionalization of isotactic polypropylene. Macromolecules 2017, 50, 2276–2283.

[35] H. Zhou, C.M. Plummer, H. Li, H. Huang, P. Ma, L. Li, L. Liu, Y. Chen.

Regioselective post-functionalization of isotactic polypropylene by amination in the presence of N-hydroxyphthalimide. Polym. Chem. 2019, 10, 619–626.

[36] T. Taniike, M. Toyonaga, M. Terano. Polypropylene-grafted nanoparticles as a promising strategy for boosting physical properties of polypropylene-based nanocomposites. Polymer 2014, 55, 1012–1019.

[37] M. Toyonaga, P. Chammingkwan, M. Terano, T. Taniike. Well-defined polypropylene/polypropylene-grafted silica nanocomposites: roles of number and molecular weight of grafted chains on mechanistic reinforcement. Polymers 2016, 8, 300.

[38] G. Zhang, C. Nam, T.M. Chung, L. Petersson, H. Hillborg. Polypropylene copolymer containing cross-linkable antioxidant moieties with long-term stability under elevated temperature conditions. Macromolecules 2017, 50, 7041–7051.

[39] M. Zhang, R.H. Colby, S.T. Milner, T.M. Chung, T. Huang, W. Degroot. Synthesis and characterization of maleic anhydride grafted polypropylene with a well-defined molecular structure. Macromolecules 2013, 46, 4313–4323.

[40] T.M. Chung. Functional polyolefins for energy applications. Macromolecules 2013, 46, 6671–6698.

[41] Y. Iizuka, J.-i. Sugiyama, H. Hagihara. Unexpected mechanical properties of functionalized polypropylene: tensile test, Charpy impact tensile test, DSC, and WAXD analysis of poly (5-hexen-1-ol-co-propylene). Macromolecules 2009, 42, 2321–2323.

[42] E. Kurahashi, T. Wada, T. Nagai, P. Chammingkwan, M. Terano, T. Taniike. Synthesis of polypropylene functionalized with a trace amount of reactive functional groups and its utilization in graft-type nanocomposites. Polymer 2018, 158, 46–52.

[43] D. Zhu, E. Kurahashi, H. You, T. Wada, P. Chammingkwan, T. Taniike. Enhancing mechanical properties of graft-type nanocomposites using organically modified SiO_2 and polypropylene containing reactive methoxy groups. Polymers 2022, 14, 563.

[44] J.-Y. Dong, Y. Hu. Design and synthesis of structurally well-defined functional polyolefins via transition metal-mediated olefin polymerization chemistry. Coord. Chem. Rev. 2006, 250, 47-65.

[45] H. Lu, S. Hong, T. Chung. Synthesis of polypropylene-co-p-methylstyrene copolymers by metallocene and Ziegler-Natta catalysts. J. Polym. Sci., Part A: Polym. Chem. 1999, 37, 2795–2802.

[46] J. Yang, C. Wang, K. Wang, Q. Zhang, F. Chen, R. Du, Q. Fu. Direct formation of nanohybrid shish-kebab in the injection molded bar of polyethylene/multiwalled carbon nanotubes composite. Macromolecules 2009, 42, 7016–7023.

[47] S.L. Kodjie, L. Li, B. Li, W. Cai, C.Y. Li, M. Keating. Morphology and crystallization behavior of HDPE/CNT nanocomposite. J. Macromol. Sci. Part B Phys. 2006, 45, 231–245.

[48] T. Fornes, D.R. Paul. Crystallization behavior of nylon 6 nanocomposites. Polymer 2003, 44, 3945–3961.

[49] R. Ohnishi, S. Yukimasa, T. Konakazawa. Synthesis of elastomeric poly

(propylene)(ELPP) using the highly active $TiCl_4$/dibutyl phthalate (DBP)/$MgCl_2$-$Al(i\text{-}C_4H_9)_3$/1-allyl-3, 4-dimethoxybenzene (ADMB) catalyst. Macromol. Chem. Phys. 2002, 203, 1003–1010.

Chapter 4

Dielectric Properties of Biaxially Oriented Polypropylene Nanocomposites Prepared Based on Reactor Granule Technology

Chapter 4

Abstract

The addition of inorganic nanoparticles is one of the most widely studied strategies to improve dielectric properties of thin film capacitors, but its application to biaxially oriented polypropylene (BOPP) has rarely been reported due to the difficulty of stretching without break. Here, I have investigated dielectric properties of BOPP/TiO_2 nanocomposites prepared by a reactor granule technology, in which precursors impregnated in the pores of PP reactor granule are converted into highly dispersed oxide nanoparticles during melt mixing. The permittivity of the nanocomposites was greatly enhanced beyond classical mixing rules by the addition of a small amount of TiO_2 nanoparticles (1–5wt %), and the enhancement was very sensitive to the stretching ratio. A critical role of the interphase region was suggested. The AC breakdown voltage (BDV) of the BOPP/TiO_2 nanocomposites decreased sharply with respect to the amount of TiO_2 added. The detailed analysis suggested the roughening of the film surface around the nanoparticles due to stretching as the main cause of the BDV reduction.

Keywords: biaxially oriented polypropylene; dielectric properties; nanocomposites; reactor granule technology; titanium dioxide

4.1. Introduction

Thin film capacitors are electrical capacitors, where an insulating polymer film

working as the dielectric is metalated typically by Al and rolled into a cylindrical shape. Among plastics used for this purpose, biaxially oriented polypropylene (BOPP) has advantages such as high dielectric strength, low dielectric loss, and high moisture resistance [1,2]. It is commonly employed in electronic and electrical devices, for example, film capacitors for switched-mode power supplies, converters and inverters, high-voltage capacitors, smoothing capacitors, and so on. In these applications, there is a continuous demand to make film capacitors smaller in size and larger in capacitance, that is, to improve their energy density.

Polymer nanocomposites are materials where filler particles having at least one dimension below 100 nm are dispersed at a nanoscale in polymer matrices. Since the synthesis of a nylon 6-clay hybrid in 1993 [3],they have been targets of extensive research in various applications, as a means of modifying relevant properties of polymers by adding a small amount of fillers [4–7].In the field of thin film capacitors, modification of dielectric properties of polymers by dispersing insulating oxide nanoparticles with high relative permittivity has been actively researched [8–13].The size of filler particles must be well below the film thickness, and highly dispersed nanoparticles are required for creating a uniform electric field throughout the material. It has been reported for various polymer/filler combinations that nanocomposites show improvements in both the permittivity and the electric breakdown strength as compared to the original polymer [14–16], as long as nanoparticles are sufficiently dispersed with appropriate filler selection and/or proper interfacial design in respective considerations of the dielectric contrast and

leakage current/dielectric loss. Similar results have been reported for polypropylene nanocomposites, but most of them were for unstretched nanocomposites [17], and far fewer cases have been reported for BOPP nanocomposites in spite of their industrial significance [18]. This problem is likely rooted to the well-known incompatibility of PP and inorganic fillers. It is difficult to control the dispersion of oxide nanoparticles in chemically inactive and hydrophobic PP and even more difficult to stretch it without break [19,20].

Reactor granule is in the form of porous polyolefin powder that is directly obtained after catalyzed olefin polymerization and prior to pelletization for shipping. The reactor granule technology (RGT) is a technique for in situ conversion of precursors, which are impregnated in the polyolefin reactor granule, into highly dispersed nanoparticles at the temperature of melt compounding [21]. The RGT is applicable to preparing polyolefin nanocomposites filled with various types of nanoparticles from low to high content up to 40 wt % without the need of a compatibilizer. Our research group have reported PP-based nanocomposites with excellent dispersion and functions, such as transparent UV shielding (TiO_2) [22], heat releasing (Al_2O_3) [23], flame retardant [$Mg(OH)_2$] [24], and antimicrobial properties (Ag).25 Moreover, controlled migration of Al_2O_3 nanoparticles at the interface between PP and an elastomer was realized based on the RGT [26–28].

Here, dielectric properties of BOPP/TiO_2 nanocomposites prepared by the RGT are reported. TiO_2 was chosen not only for its low price but also for its high relative permittivity in contrast to relatively low electrical conductivity [29]. The effects of

various factors such as the TiO_2 content, interfacial design, and drawing ratio on the permittivity, BDV, and dielectric loss of the nanocomposites were investigated in detail, so as to figure out potentials and problems of BOPP nanocomposites.

4.2. Experimental section

4.2.1. Raw materials

PP reactor granule (M_w = 2.6 × 10^5, M_w/M_n = 5.7, *mmmm* = 98 mol %) was synthesized by propylene polymerization using a fourth-generation Ziegler−Natta catalyst [30,31]. The median size (D_{50}) and the pore volume of the granule were determined as 480 μm and 0.56 mL/g based on laser scattering in ethanol (HORIBA partica, LA-950V2) and mercury porosimetry (Shimazu, Autopore IV 9505), respectively. Titanium isopropoxide [Ti(O*i*Pr)$_4$] was supplied by Sigma-Aldrich and used as a precursor. n-Octdecyl-3-(3',5'-di-t-butyl-4'-hydroxyphenyl)propionate (AO-50) and bis(1,2,2,6,6-pentamethyl-4-piperidyl)sebacate (LA-77) were donated by ADEKA. They were used as an antioxidant stabilizer and a catalyst for the sol−gel reaction, respectively [22]. TiO_2 nanoparticles (AEROXIDE TiO_2 P25) was used to prepare reference nanocomposites. Trimethoxy(2-phenylethyl)-silane, trimethoxy(methyl)silane, and triethoxy(hexyl)silane were purchased from TCI and used as surface modifiers for in situ-generated TiO_2 nanoparticles. These silane coupling agents are denoted as PE, Me, and Hex according to the organic group, respectively.

4.2.2. Sample preparation

In order to clarify factors that affect dielectric properties of BOPP/TiO_2 nanocomposites, various samples were prepared. The scheme of the preparation and the varied parameters are shown in Scheme 4.1. The prepared samples are listed in Tables 4.2 and 4.3. In the following, a typical preparation method is described, followed by information on the varied parameters.

In a typical preparation, the PP reactor granule was impregnated with a solution of Ti(O*i*Pr)$_4$ in heptane at 50 °C under nitrogen for 12 h. The amount of Ti(O*i*Pr)$_4$ was determined so as to obtain the TiO_2 loading of 2.0 wt % in the resultant PP/TiO_2 nanocomposite, under the assumption of full conversion of the metal alkoxide to oxide. This assumption has been shown to be reasonable in the previous studies [21–28]. Indeed, thermogravimetric measurements for selected samples gave almost completely same amount of produced TiO_2 as the theoretical one. Hence, the theoretical loading is adopted in this paper. After solvent removal in vacuo, the granule was held at 50 °C and 100% relative humidity for 24 h to promote the hydrolysis and solidification of Ti(O*i*Pr)$_4$ in the pores, followed by melt mixing at 185 °C and 200 rpm for 15 min using a twin-screw micro compounder (Xplore MC5). The extrudate was hot-pressed into a film with a thickness of 300 μm at 230 °C and 10 MPa for 5 min and subsequently quenched at 0 °C for 5 min. Biaxial sequential stretching was performed using a laboratory stretching

machine (KARO, Brückner Maschinenbau). A sample film was preheated at 165 °C and stretched at the same temperature first in the machine direction (MD) and then in the transverse direction (TD), where the stretching rate was fixed at 600%/s for MD and 300%/s for TD. Further details are described elsewhere [32]. The film thickness was measured by a micrometer according to method A in IS K 7130:1999. The thickness of biaxially stretched films at a drawing ratio of 4 × 7 mostly fell in the range of 10−13 μm with a standard deviation of 0–1 μm. Photographs of film samples before and after stretching are given in Fig. 4.1.

The loading of TiO_2 was varied in the range of 0.1–5 wt % through the addition amount of Ti(O*i*Pr)$_4$ to the PP reactor granule. The loading of TiO_2 was kept relatively low, first, to enable stretching without break and, second, to suppress an electric field concentration and leakage current due to clustering/agglomeration of nanoparticles. In a previous study, it was reported that impregnation and reaction of Al(OiPr)$_3$ in the presence of a silane coupling agent resulted in organically modified Al_2O_3 nanoparticles, which significantly improved the interfacial bonding with the PP matrix for thermal conduction [23]. Accordingly, samples were prepared by adding a silane coupling agent (PE, Me, or Hex) to the heptane solution of Ti(O*i*Pr)$_4$ at a Si/Ti molar ratio of 0.06. Samples were also prepared at different drawing ratios from 2 × 5 to 4 × 7.

As a reference sample, biaxially oriented films were obtained for neat PP in the above-mentioned conditions. A PP/TiO_2 nanocomposite (termed PP/TiO_2-NP) was also prepared by melt mixing 2.0 wt % of preformed TiO_2 nanoparticles. However, biaxial

stretching of this film failed due to break.

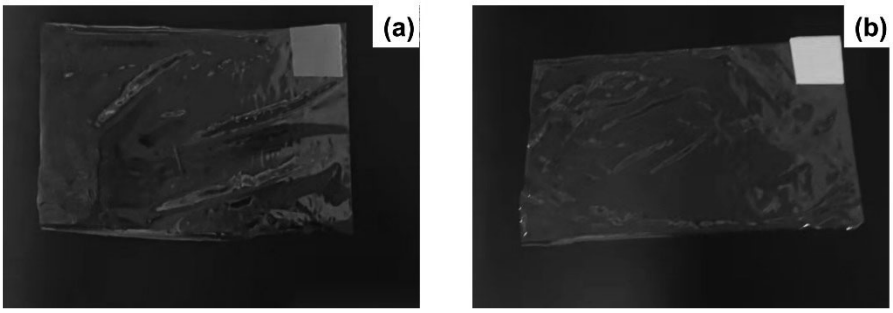

Fig. 4.1. Photographs of neat PP and PP/PE-TiO_2 (2.0) before and after stretching at the drawing ratio of 4 × 7. Note that the unstretched film is placed on the top right of the stretched film.

4.2.3. Dielectric measurements

Dielectric properties of BOPP nanocomposites were measured as follows. Au electrodes were formed on both sides of a sample by sputtering (MSP-20-TK, VACUUM DEVICE) (30 mmφ, 2.0 Ω/sq). A brass plate was placed on top of an insulating rubber, and a conductive rubber (40 mmφ) was placed on top of it. The sample was sandwiched between a brass cylinder (27 mmφ, 250 g) and the said conductive rubber. Electrodes were connected to the brass plate and the brass cylinder, and the capacitance (C) of the sample was measured at 23 °C, an applied voltage of 1 V, and a frequency range of 20 Hz to 20 kHz. The relative permittivity (ε_r) of the sample was obtained by the following equation (4-1),

$$\varepsilon_r = \frac{C \times t}{\varepsilon_0 \times A} \quad (4\text{-}1),$$

where t, ε_0, and A are the thickness of the sample, the permittivity of the vacuum, and the area of the electrode, respectively. The measurements were taken at least 3 times, and the relative permittivity is reported as the average value. The loss factor (tan δ) was also obtained in these measurements. Regardless of the samples, the relative permittivity and the loss factor were almost independent of the frequency in the measured range. Therefore, the data at 1 kHz were taken as representative due to high practical relevance.

The AC breakdown voltage of BOPP nanocomposites was obtained using a withstanding voltage tester (TOS5051A, Kikusui Electronics) based on the electrode configuration of the flat-plate electrode method described in JIS C 2151:2006. AC voltage of 60 Hz was increased at a rate of 100 V/s at 100 °C in air. The voltage at which the leakage current reached a threshold value of 5.0 mA was measured 12 times, and the average voltage of 8 measurements, excluding 2 measurements with the highest voltages and the lowest voltages, was defined as BDV after being normalized by the sample thickness. Due to the configuration of the electrode, breakdown by surface discharges was unlikely to occur, but if it occurred, such measurements were discarded. The measurement temperature of 100 °C and the normal atmosphere were assumed to be used in automobiles.

4.2.4. Characterization

The size distribution and dispersion of TiO_2 nanoparticles in the unstretched nanocomposites were observed using a transmission electron microscope (Hitachi H-7650) operated at an acceleration voltage of 100 kV. TEM specimens with the thickness of 100 nm were prepared by an ultramicrotome (Reichent Ultracut FCS, Leica) equipped with a diamond knife (Diatome). Particle size distribution profiles were acquired by measuring the size of TiO_2 in the TEM images at a fixed magnification. The dispersion was quantified based on a dispersion index (DI) as,

$$\mathrm{DI} = \frac{0.2}{\sqrt{2\pi}} \times \frac{\mu}{\sigma} \quad (4\text{-}2),$$

where μ and σ are the average and the standard deviation of the area of TiO_2 nanoparticles or their aggregates, respectively [33]. The analysis of the TEM images was performed by imageJ software. The analysis covered at least 200 nanoparticles (or their aggregates) per sample.

Wide-angle X-ray diffraction (WAXD) measurements were taken on a Rigaku MiniFlex 300 diffractometer in a reflection mode at room temperature with graphite monochromated Cu Kα radiation operating at 30 kV and 10 mA. The crystallite dimension (D) was estimated for the α(040) reflection based on the Scherrer equation,

$$D = \frac{K \times \lambda}{\beta \times \cos\theta} \quad (4\text{-}3),$$

where K is the shape factor set to 0.94, β is the full width at half maximum of the peak, and θ is the Bragg angle.

The volume resistivity of BOPP/TiO_2 nanocomposites was measured according to JIS C 2139-3-1:2018. Briefly, main and guard electrodes were closely contacted to one side of a sample film, and the counter electrode to the other side of the film, at a fixed load of 5.0 kgf. The setup was kept at 100 °C for 30 min. Then, a DC voltage was applied to the sample to achieve a potential gradient of 40 V/μm. The volume resistivity (ρ_v) was calculated using the following formula,

$$\rho_v = R \times \frac{A}{t} \quad (4\text{-}4),$$

where R is the measured resistance, A is the effective electrode area, and t is the sample thickness.

Surface topographic information of BOPP/TiO_2 nanocomposites was acquired on a non-contact 3D optical profilometer (R5500GML, Ryoka Systems) in a WAVE mode using a 530 white optical filter and a 10X objective lens. Measurements were taken at 10 locations per sample with a field of view of 353.16 μm × 470.92 μm. The acquired images were pre-processed by a median filter (3 × 3) and a Gaussian filter with a cutoff value of 30 μm to remove noise and undulation components. Biaxially stretch nanocomposites exhibited crater-like roughness around nanoparticles. The reduced valley depth *(*Rvk), a measure of surface roughness, was determined as an average of 10 images per sample.

Scheme 4.1. Preparation of BOPP/TiO_2 nanocmposites. Three kinds of parameters are varied: 1) TiO_2 loading, 2) surface modifier, and 3) drawing ratio.

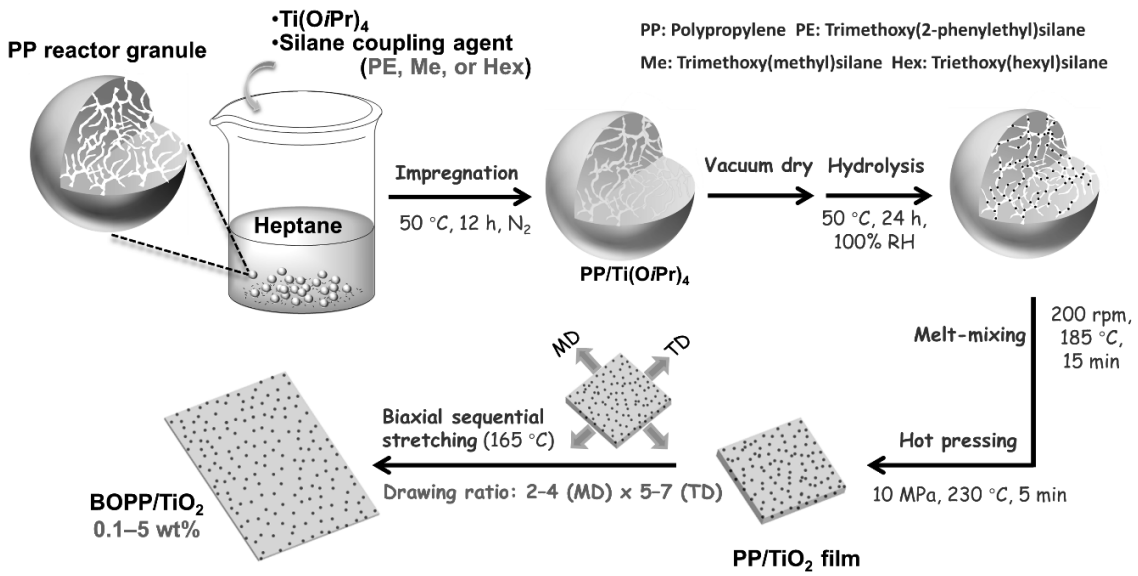

4.3. Results and discussions

4.3.1. Morphology of PP/TiO_2 nanocomposites

Fig. 4.2 shows TEM images of the PP/TiO_2 nanocomposites before stretching. The analytical results for the size distribution of TiO_2 nanoparticles and the dispersion index (DI) are shown in Fig. 4.3. and Table 4.1, respectively. The most important characteristic of RGT-based nanocomposites is uniform dispersion of in-situ generated nanoparticles over a wide range of loading, which is ascribed to the pore confinement of precursors [21]. The same characteristic was observed in the TEM images for the RGT-based nanocomposites (Fig. 4.2a-e). The in-situ generated nanoparticles possessed the average size of ca. 50–100 nm, which increased by increasing the TiO_2 loading. The dispersion index, where a larger value manifests more uniform dispersion, was above 0.65 when the

surface modifier was employed. In comparison, when preformed TiO_2 nanoparticles were melt-mixed, the nanocomposite possessed huge aggregates and the smallest DI value (Fig. 4.2f).

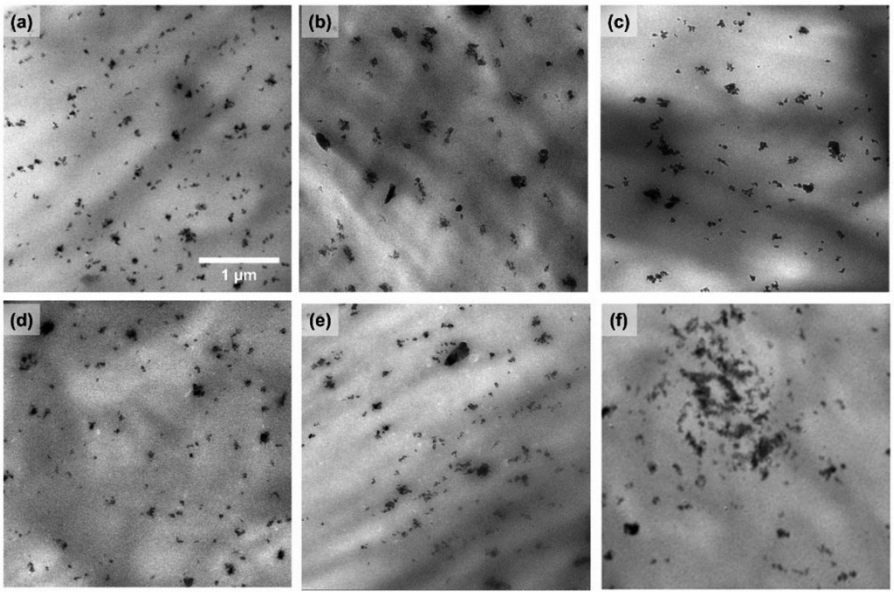

Fig. 4.2. TEM images of PP/TiO_2 nanocomposites before stretching: a) PP/PE-TiO_2 (2.0), b) PP/PE-TiO_2 (5.0), c) PP/TiO_2 (2.0), d) PP/Me-TiO_2 (2.0), e) PP/Hex-TiO_2 (2.0), and f) PP/TiO_2-NP (2.0). The same scale bar is applied to all the images.

The particle size distribution profiles and the dispersion parameters are shown in Fig. 4.3 and Table 4.1, respectively.

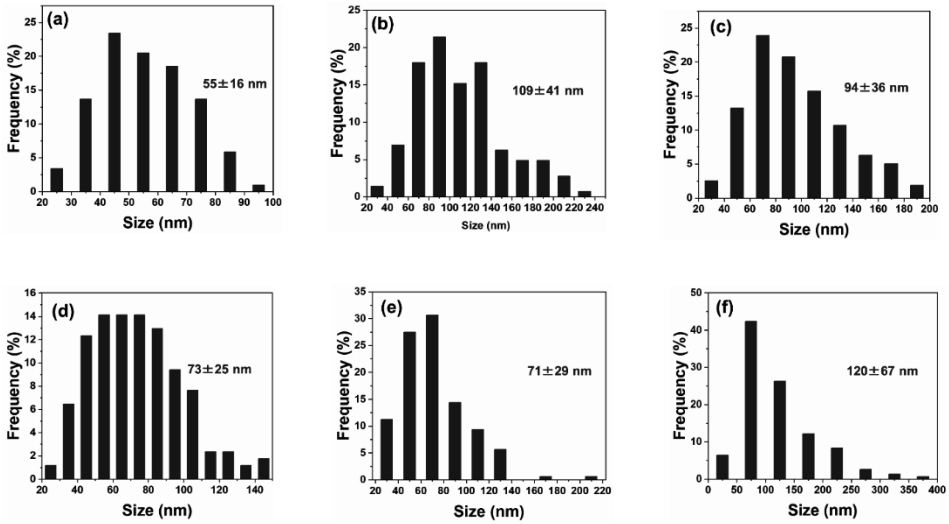

Fig. 4.3. Size distribution of TiO_2 nanoparticles in PP/TiO_2 nanocomposites: a) PP/PE-TiO_2 (2.0), b) PP/PE-TiO_2 (5.0), c) PP/TiO_2 (2.0), d) PP/Me-TiO_2 (2.0), e) PP/Hex-TiO_2 (2.0), and f) PP/TiO_2-NP (2.0).

Table 4.1. Dispersion parameters for PP/TiO_2 nanocomposites.[a]

Sample	μ^b [μm^2]	σ^b [μm^2]	DI^b
PP/PE-TiO_2 (2.0)	0.0029	0.0029	0.080
PP/PE-TiO_2 (5.0)	0.0133	0.0145	0.073
PP/TiO_2 (2.0)	0.0090	0.0229	0.031
PP/Me-TiO_2 (2.0)	0.0051	0.0056	0.073
PP/Hex-TiO_2 (2.0)	0.0079	0.0097	0.065

PP/TiO_2-NP (2.0)	0.0189	0.0582	0.026

[a] Acquired by analyzing the TEM images using ImageJ software.

[b] μ and σ correspond to the average area of TiO_2 nanoparticles and its standard deviation, respectively. The dispersion index (DI) is as defined in Equation (2).

4.3.2. Dielectric and related properties of BOPP/TiO_2 nanocomposites

Surface modification of nanoparticles is very important for the dielectric properties of resultant nanocomposites. First, it facilitates the dispersion of inorganic nanoparticles in matrices; poor dispersion causes a significant decrease in BDV [34], and even break during stretching. Second, improved interfacial adhesion prevents the formation of microvoids, which can cause the premature breakdown. Third, it reduces permittivity contrast between the matrix and high-permittivity inclusions like TiO_2 [29]. Last, it affects the interfacial layers in the framework of a multicore model [18,34]. Recent studies have shown that polymer-coated nanoparticles are promising not only in attaining the above advantages but also in imparting a feature arising from the properties of the coating polymer [35,36]. RGT provides good dispersion on its own based on pore confinement. Meanwhile, the coexistence of a silane coupling agent in the sol-gel reaction of metal alkoxides restricts the growth of particles. As a result, the size of the nanoparticles became smaller in the presence of the silane coupling agents (Fig. 4.3). The capping efficiency or

the efficiency to restrict the particle growth was far greater for PE than for Me and Hex, which is consistent with our previous results on PP/Al_2O_3 nanocomposites [23].

Table 4.2. Dielectric and related properties of BOPP/TiO_2 nanocomposites.[a]

Sample	TiO_2 loading [wt%]	Surface modifier[b]	ε_r[c]	tan δ × 10^4 [c]	BDV[d] [V_{AC}/μm]	ρ_v[e] [Ω·cm]	Rvk[f] [μm]
Neat PP	n.a.	n.a.	2.27±0.06	5±3	245±10	1.54×10^{16}	0.011±0.001
PP/PE-TiO_2 (0.1)	0.1	PE	2.31±0.01	5±1	223±11	3.19×10^{15}	0.019±0.002
PP/PE-TiO_2 (0.5)	0.5	PE	2.41±0.01	7±0	194±17	2.28×10^{15}	0.034±0.008
PP/PE-TiO_2 (1.0)	1.0	PE	2.84±0.05	11±3	160±10	1.44×10^{15}	0.097±0.028
PP/PE-TiO_2 (2.0)	2.0	PE	3.10±0.06	20±1	119±15	1.13×10^{15}	0.264±0.063

PP/PE-TiO_2 (5.0)	5.0	PE	3.20±0.04	101±4	89±10	1.63×10^9	0.852±0.168
PP/TiO_2 (2.0)	2.0	n.a.	2.87±0.03	18±2	148±6	n.d.	0.129±0.025
PP/Me-TiO_2 (2.0)	2.0	Me	2.76±0.05	32±3	126±12	n.d.	0.278±0.112
PP/Hex-TiO_2 (2.0)	2.0	Hex	2.67±0.04	35±9	124±7	n.d.	0.270±0.126

[a] The PP/TiO_2 nanocomposites were prepared based on RGT, where the TiO_2 loading and the surface modifier were varied. All the samples were biaxially stretched at 165 °C and at the drawing ratio of 4 × 7, with the stretching rate of 600%/s for MD and 300%/s for TD.

[b] Either trimethoxy(2-phenylethyl)silane (PE), trimethoxy(methyl)silane (Me), or triethoxy(hexyl)silane (Hex) was added at a Si/Ti molar ratio of 0.06.

[c] Measured at least 3 times per sample at 23 °C, an applied voltage of 1 V, and a frequency of 1 kHz.

[d] Measured based on JIS C 2151:2006. AC voltage of 60 Hz was increased at a rate of 100 V/s at 100 °C in air. Out of 12 measurements, 8 measurements with middle BDV values were used for deriving the average.

[e] Measured based on JIS C 2139-3-1:2018 at 100 °C under a DC voltage gradient of 40 V/μm.

[f] Determined based on optical profilometry; 10 images acquired at different locations were analyzed to obtain the Rvk value.

Table 4.2 summarizes the dielectric properties of PP and PP/TiO_2 nanocomposites stretched at the drawing ratio of 4 × 7. Note that the relative permittivity and BDV were measured at different temperatures, 23 and 100 °C, respectively, from a practical viewpoint in automotive film capacitors, where a high relative dielectric constant under normal operation and high breakdown strength at an elevated temperature in the case of abnormal operation are required. In Fig. 4.4, the dielectric properties of PP/PE-TiO_2 nanocomposites are plotted against the TiO_2 loading. The relative permittivity (ε_r) and the loss factor (tan δ) of neat PP were 2.27 and 5.0×10^{-4}, respectively, in agreement with reported values in literature. The BDV at 100 °C was 245 V_{AC}/μm. The ε_r value increased proportionally with the addition of phenylethyl-modified TiO_2 (PE-TiO_2) up to 1.0 wt% (Fig. 4.4a). After that, the increment became smaller and almost saturated at 2.0 wt%, where the ε_r value became as high as 3.1. This improvement was much greater than

estimations from the ε_r value of TiO_2 (about 100) and its small fraction less than 1 vol%, which will be discussed later. The reason for the increase in the loss factor is attributed to the lossy nature of TiO_2 itself and the interfacial polarization called Maxwell-Wagner-Sillars (MWS) effect caused by the permittivity/conductivity contrast between PP and TiO_2 [34]. The saturation of the ε_r value and the sharp increase in the loss factor at 5.0 wt% both suggest the occurrence of clustering/agglomeration at this loading, which provides conduction pathways [18,29]. The BDV value decreased inversely with the TiO_2 loading (Fig. 4.4c), and at 2.0 wt%, it became almost half of that of neat PP. Though the fraction of TiO_2 nanoparticles is the main factor of the dielectric properties, the presence and the type of surface modifiers is also important. Modification with saturated alkyl groups lowers the effective relative permittivity of nanoparticles [29], and in turn the ε_r values of the nanocomposites (PP/Me-TiO_2 or Hex-TiO_2) as compared to that of the non-modified sample (PP/TiO_2). It is reasonable that the longer alkyl chain caused the lower permittivity due to the larger organic content. Contrary to these results, phenylethyl-modified TiO_2 (PE-TiO_2) showed a higher ε_r value than unmodified TiO_2. This could be attributed to the unique effect of the phenylethyl group in RGT. In our past study for PP/Al_2O_3 nanocomposites based on RGT, when trimethoxy(2-phenylethyl)silane was used as a modifier, the particle size of Al_2O_3 produced became significantly smaller. Furthermore, the dispersion and interfacial bonding were largely improved as compared to the other modifiers [23]. Indeed, the PP/PE-TiO_2 sample exhibited the smallest particle size as well as the largest DI at 2.0 wt% (Fig. 4.3 and Table 4.1). The decrease in BDV

was smaller for unmodified TiO_2 when compared to the modified TiO_2 samples. This suggests that electric field concentration by permittivity contrast and space charge accumulation by conductivity contrast are not the main cause of the BDV decrease.

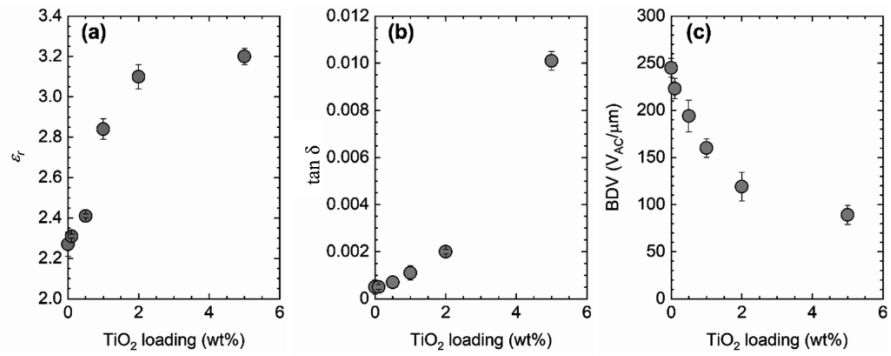

Fig. 4.4. Dielectric properties of BOPP/PE-TiO_2 nanocomposites along with the TiO_2 loading: a) Relative permittivity, b) loss factor, and c) breakdown voltage. All the samples were biaxially stretched at 165 °C and at the drawing ratio of 4 × 7.

Table 4.3. Effect of the drawing ratio on dielectric and related properties.[a]

Sample	Drawing ratio	ε_r	tan δ × 10^4	BDV [V_{AC}/μm]	D[c] [nm]	ρ_v [Ω·cm]	Rvk [μm]
Neat PP	1 × 1	2.20±0.04	9±2	n.d.[b]	n.d.	n.d.	n.d.
	2 × 5	2.29±0.05	3±1	n.d.[b]	17.3±0.3	n.d.	n.d.
	3 × 6	2.28±0.02	3±1	n.d.[b]	16.6±0.6	8.10×10^{15}	n.d.

	4 × 7	2.27±0.06	5±3	245±10	14.9±0.3	1.54×10^{16}	0.011±0.001
	1 × 1	2.17±0.01	42±4	n.d.[b]	n.d.	n.d.	0.069±0.021
PP/PE-TiO_2 (2.0)	2 × 5	2.58±0.04	23±2	120±5	18.5±0.4	n.d.	0.223±0.051
	3 × 6	2.83±0.05	22±2	117±5	15.5±0.8	8.87×10^{14}	0.236±0.051
	4 × 7	3.10±0.06	20±1	119±15	15.1±0.3	1.13×10^{15}	0.264±0.063

[a] Neat PP and a PP/PE-TiO_2 nanocomposite (2.0 wt%) were biaxially stretched at 165 °C and at different drawing ratios, where the stretching rate was fixed at 600%/s for MD and 300%/s for TD.

[b] Not determined because the electric breakdown did not occur at 5 kV as the instrumental upper limit.

[c] Estimated from the α(040) reflection in WAXD based on the Scherrer equation.

Stretching transforms the spherulitic structure into a highly oriented fibrillar morphology, which is the origin of the high BDV of BOPP [37]. For instance, the BDV of unstretched PP sheets at room temperature was reported to be 360–400 V/μm compared to ~700 V/μm for BOPP [38]. In addition to this, it is expected that biaxial stretching of nanocomposites causes the elongation of interparticle distances and non-uniform deformation near nanoparticles. However, few studies have investigated changes in the

dielectric properties of PP nanocomposites upon stretching. Table 4.3 and Fig. 4.5 summarize the dielectric properties of neat PP and PP/PE-TiO_2 (2.0) biaxially stretched at different drawing ratios. The relative permittivity of neat PP was almost constant before and after stretching. The decrease in the loss factor due to stretching is attributed to the orientation and higher crystallinity. Unfortunately, BDV could not be evaluated for the films with low stretching ratios because of their large thickness and the instrumental limitation. The response of the dielectric properties of the nanocomposite to the stretching ratio was quite different from that of neat PP. The ε_r value of the unstretched nanocomposite was almost the same as that of neat PP. However, that of the stretched films increased proportionally to the degree of stretching. The reason for this will be discussed later. The decrease in the loss factor due to stretching was also observed in the nanocomposite, but it was more pronounced than that for neat PP. This corresponds to the fact that the clustering/agglomeration of TiO_2 forms conduction pathways, and the increase in the distance between the nanoparticles due to stretching partially eliminates such pathways. The value of BDV was about 120 V/μm, almost independent of the stretching ratio.

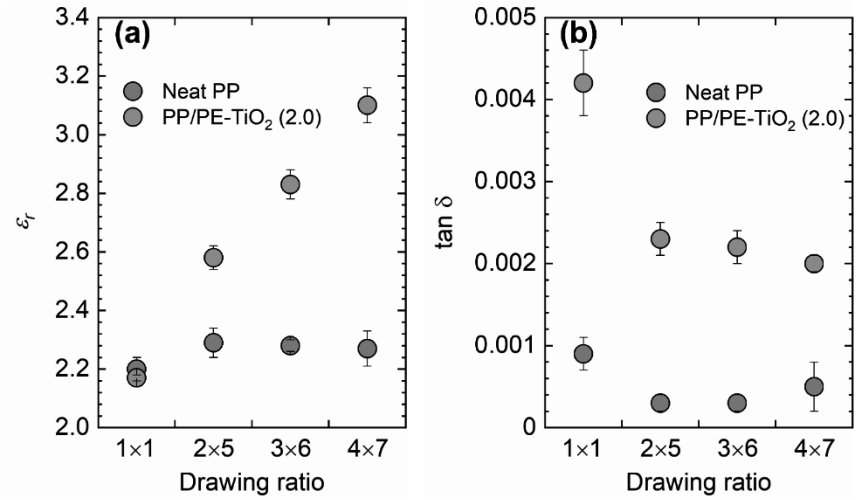

Fig. 4.5. Variation in dielectric properties of neat PP and a PP/PE-TiO_2 nanocomposite (2.0 wt%) in biaxial stretching: a) Relative permittivity, and b) loss factor. 1 × 1 corresponds to unstretched films.

Hereafter, we will discuss the two interesting results found in this study, namely, the unexpected increase in the relative permittivity and the decrease in BDV. As for the relative permittivity, the observed increase due to the addition of TiO_2 (up to 2.0 wt%) is much greater than classical volume average-based predictions (Fig. 4.6 and Table 4.4). The Maxwell-Garnett equation and the Bruggeman self-consistent effective medium approximation [39] predict that the addition of TiO_2 below 1.1 vol% (corresponding to 5.0 wt%) has marginal impacts on the relative permittivity of the composites. The Wiener upper bound (parallel model) [39], which is equivalent to the upper limit of the Lichtenecker logarithmic law ($\alpha = 1$) [40], is the closest to the observations, and it explains about 87% of the observed increase. The Maxwell-Garnett and Bruggeman

models have been widely and successfully used in a variety of polymer nanocomposites, in most of which the fractions of nanoparticles are greater than 10 vol%. Deviation of the relative permittivity of polymer nanocomposites from the classical mixing rules has been often reported, and this has been attributed to the effect of the interphase region around nanoparticles, which increases dramatically as the particle size decreases [34]. The interphase is explicitly taken into consideration by the Lewis double-layer model [41], or by the modified Tanaka multicore model [42], and the latter has been particularly successful in cases when the classical rules fail. According to these models, depending on the nature of the interphase, the relative permittivity of polymer nanocomposites can exceed the classical mixing rules, or conversely, it can even be lower than the relative permittivity of the matrix. It has also been recently reported that the relative permittivity of nanocomposites can be dramatically improved at very low loadings below 1 vol% [43,44]. Inspired by the multicore model, Li et al. proposed a model, in which the existence of a three-layered interphase is incorporated into the logarithmic mixture formula, and succeeded in explaining the dramatic improvement of the relative permittivity at ultra-low loadings [43]. As shown in Fig. 4.6, the relative permittivity of BOPP/PE-TiO_2 nanocomposites can be well reproduced by Li's model below 0.44 vol% (corresponding to 2.0 wt%). This strongly suggests the importance of the interphase region in the nanocomposites, which is consistent with the fact that the relative permittivity values were relatively sensitive to the presence and the type of surface modifiers (cf. Table 4.2). Li's model predicts that the relative permittivity begins to

decrease when the TiO_2 loading exceeds 0.5 vol%. This is due to the overlap of the interphase regions as the distance between the nanoparticles decreases under the assumption of random dispersion. The reason why the actual results did not show such a decrease was probably due to the fact that the clustering/agglomeration of TiO_2 nanoparticles became more prominent at 5.0 wt%, as was evident from the TEM images (Fig. 4.2b) and the loss factor (Table 4.2). In other words, if the number of isolated TiO_2 nanoparticles with a sufficient interphase region remains largely unchanged due to the clustering/agglomeration of excessive nanoparticles, the saturation of the relative permittivity value can be understood. Likewise, the dramatic increase in the relative permittivity of the nanocomposite along with the biaxial stretching can be easily explained. Without stretching, the distance between nanoparticles was too short, so the contribution of the interphase became negligible, as a result of which the relative permittivity followed the classical mixing rules. As the distance between the nanoparticles increased with the stretching ratio, the contribution of the interphase, which plays a major role in improving the relative permittivity, increased. From these considerations, it is concluded that the relative permittivity of BOPP/TiO_2 nanocomposites is dominated by the interphase region.

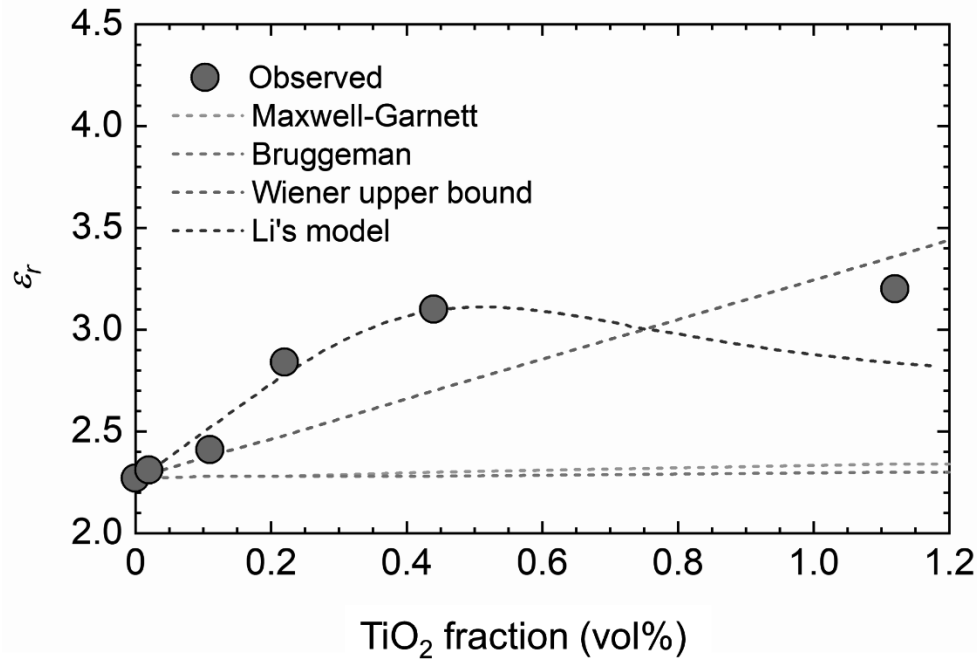

Fig. 4.6. Comparison of the measured relative permittivity of BOPP/PE-TiO_2 nanocomposites with theoretical models. The relative permittivity and the density used for the calculations are 2.27 and 0.91 g/cm^3 for PP and 100 and 4.23 g/cm^3 for TiO_2, respectively. Bruggeman means the Bruggeman's self-consistent effective medium approximation. Li's model takes into account the contribution of the interphase region composed by three layers [43]. Relevant internal parameters, that is the thickness of the interface (t = 2.23 nm) and the best filling fraction (φ_0 = 0.00524), were determined to fit the measured relative permittivity up to 2.0 wt%.

Table 4.4. Measured and predicted relative permittivity of PP/PE-TiO_2 nanocomposites biaxially stretched at the drawing ratio of 4 × 7.[a]

Sample	TiO_2 loading [vol%][a]	ε_r				
		Measured	Maxwell-Garnett	Bruggeman[b]	Wiener upper bound	Li's model[c]
Neat PP	n.a.	2.27	2.27	2.27	2.27	2.27
PP/PE-TiO_2 (0.1)	0.02	2.31	2.27	2.27	2.29	2.32
PP/PE-TiO_2 (0.5)	0.11	2.41	2.28	2.27	2.38	2.53
PP/PE-TiO_2 (1.0)	0.22	2.84	2.28	2.28	2.48	2.78
PP/PE-TiO_2 (2.0)	0.44	3.10	2.30	2.28	2.70	3.10
PP/PE-TiO_2 (5.0)	1.12	3.20	2.34	2.30	3.36	2.84

[a] The relative permittivity and the density used for the calculations are 2.27 and 0.91 g/cm^3 for PP; 100 and 4.23 g/cm^3 for TiO_2, respectively.

[b] Corresponds to the Bruggeman self-consistent effective medium approximation.

[c] It takes into account the contribution of the interphase region composed by three layers. Relevant internal parameters, i.e. the thickness of the interface (t = 2.23 nm) and the best filling fraction (φ_0 = 0.00524), were determined so as to fit the measured relative permittivity up to 2.0 wt%.

4.3.3. Factors for affecting BDV

Various factors are known to affect the BDV of nanocomposites. Each of the potential factors that could explain the observed decrease in BDV is discussed. To start, nanoinclusions can exert influences on the crystallization process of a matrix through nucleation, confinement of polymer chains, and viscosity increase, which can in turn affect the orientation and miniaturization of crystallites by biaxial stretching. As shown in Fig. 4.7, no significant difference was observed in the WAXD patterns of neat PP and PP/PE-TiO_2 (2.0). Stretching made the α(040) reflection evident due to the orientation, and the crystallite dimension (D) became smaller as the drawing ratio increased (Table 4.3). Second, in-situ synthesis of PP/TiO_2 can leave impurities such as unreacted Ti(O*i*Pr)$_4$, alcohol, water, and so on that adversely affect BDV. In this light, a PP/PE-TiO_2 (1.0) nanocomposite was newly prepared according to same procedure except the fact that the sample obtained immediately after the pre-hydrolysis treatment was stirred in ethanol 3 times to wash out potential impurities. The washed sample was then subjected to the melt-compounding, hot pressing, and biaxial stretching at a drawing ratio of 4 × 7. The BDV value of this washed sample was 153 V_{AC}/μm, similar to 160 V_{AC}/μm for the

unwashed one. This ruled out impurities as a cause of BDV decrease. Third, the interfacial polarization, which originates from permittivity/conductivity contrast, causes a local electric field enhancement around nanoparticles. In particular, a field enhancement amplified by clustering/agglomeration of nanoparticles leads to the deterioration of BDV [29]. As shown in Table 4.2, modification of the TiO_2 surface with alkyl groups, which have low relative permittivity and insulating properties, did not improve the BDV. Also, as shown in Table 4.3, separation of the nanoparticles by stretching did not improve the BDV. These observations suggest that the local electric field enhancement by interfacial polymerization is not the cause of the BDV decrease.

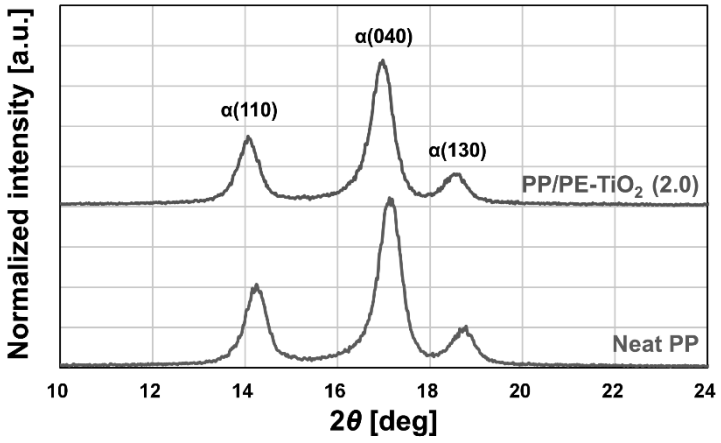

Fig. 4.7. WAXD patterns of neat PP and a PP/PE-TiO_2 nanocomposite (2.0 wt%) biaxially stretched at the drawing ratio of 4 × 7.

The patterns are vertically translated for clarity.

From the above, the possibilities are narrowed down to Joule heating due to leakage current, which causes premature breakdown [11,45], and a rough film surface, which causes an electric field enhancement between the electrode and the surface [18,38]. Thus, volume resistivity and profilometer measurements were taken, and the results are summarized in Tables 4.2 and 4.3. The volume resistivity decreased with the addition of TiO_2, which has a higher electrical conductivity than PP (Table 4.2). In particular, the extent of the decrease was large from 0 to 0.1 wt% and from 2.0 to 5.0 wt%. The former might be explained by residual impurities due to the in-situ synthesis of TiO_2. The latter was obviously from the formation of conduction pathways due to the clustering/agglomeration. The volume resistivity decreased monotonically with the amount of TiO_2, as did BDV. However, two inconsistent cases were found: the addition of 0.1 wt% TiO_2 caused 79% decrease in the volume resistivity from that of neat PP, in contrast to only 10% decrease in BDV; the volume resistivity of the nanocomposite increased along with the drawing ratio, but the BDV did not (Table 4.3). Hence, the volume resistivity alone cannot explain the decrease in the breakdown voltage. The surface roughness (Rvk) of BOPP increased with the addition of TiO_2 and by increasing the drawing ratio (Tables 4.2 and 4.3). Fig. 4.8 shows optical profilometry images for biaxially stretched films of neat PP and PP/PE-TiO_2 nanocomposites. In contrast to the smooth surface of neat PP, the surface of the nanocomposites showed characteristic roughness with prominent spots surrounded by low areas, which became more and more evident at a higher TiO_2 loading. In general, the surface of BOPP tends to exhibit

craterlike roughness, which is caused by the density difference that occurs when β-crystals (lower density) turn into α-crystals (higher density) during stretching above the melting point of β-crystals [46]. Because β-crystals did not exist in the hot-pressed films regardless of the presence of TiO_2, uneven stress and deformation occurred around the nanoparticles to cause the said roughness. Fig. 4.9 shows the relationship between surface roughness and BDV, where Rvk correlated well with BDV without obvious exception. An additional experiment supported that the roughening was the main cause of the BDV decrease, where PP/PE-TiO_2 (2.0) was biaxially stretched at 165 °C and at the drawing ratio of 4 × 7, and subsequently held at the same temperature for 60 s on the tenter. As can be seen in Figure 5 (the star mark), such post-annealing reduced the roughness and partially recovered the BDV, where the data point still followed the same trend. The reason why the BDV value of the unmodified TiO_2 sample [PP/TiO_2 (2.0)] was higher than those of the modified samples in Table 4.2 can also be explained by the surface roughness, where the Rvk value of the unmodified sample was less than half of those of the modified samples. It is likely that surface modification strengthens the interfacial connection, and this causes increased strain at the interface during stretching.

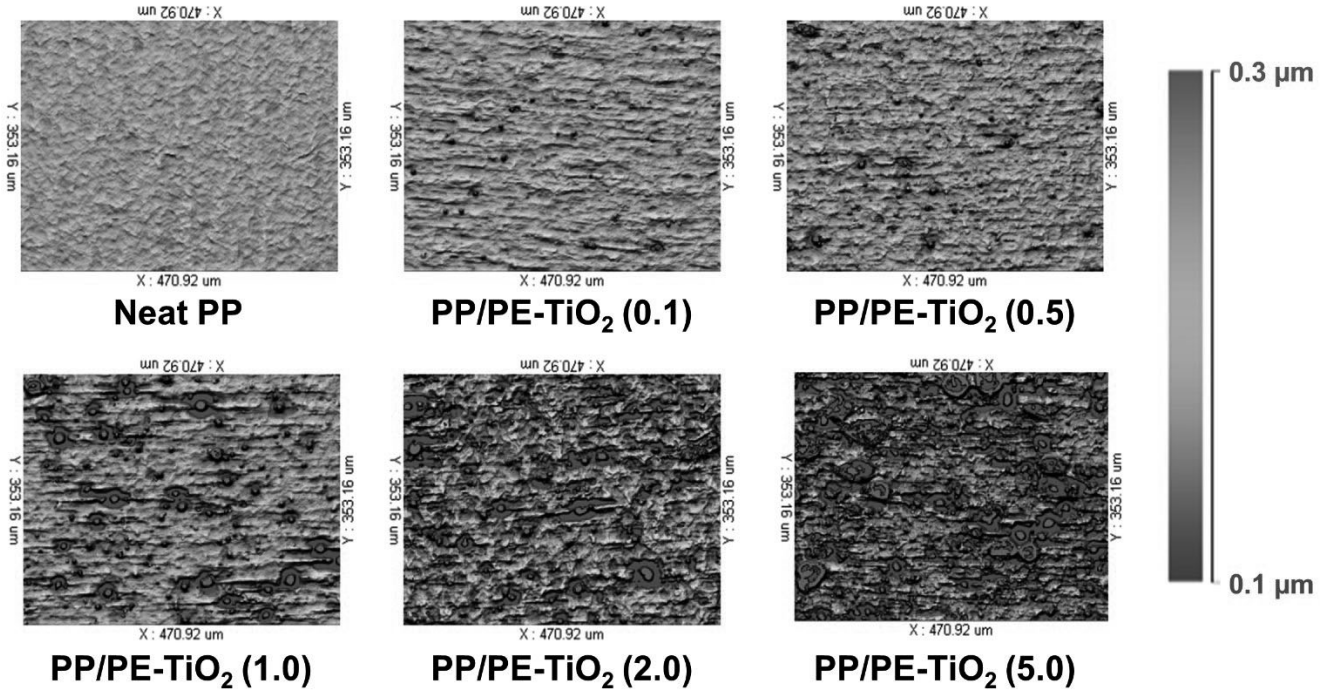

Fig. 4.8. Optical profilometry images for neat PP and PP/PE-TiO_2 nanocomposites biaxially stretched at the drawing ratio of 4 × 7.

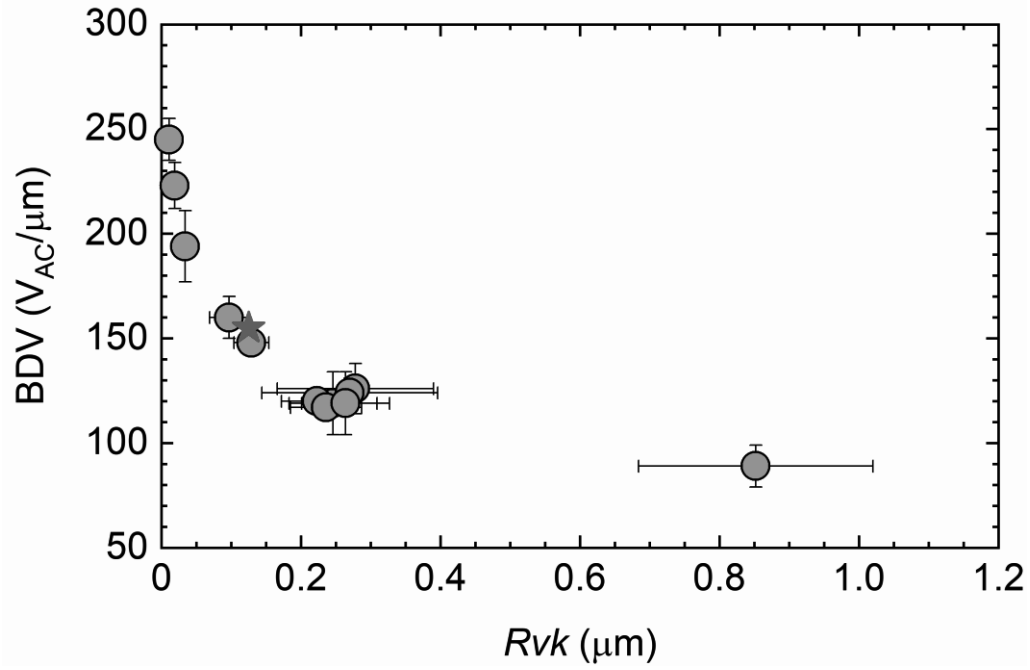

Fig. 4.9. Relationship between surface roughness and breakdown voltage. The reduced valley depth (Rvk) is used as a measure of the surface roughness. The star symbol (red) corresponds to the data for PP/PE-TiO_2 (2.0), which was biaxially stretched at 165 °C and at the drawing ratio of 4 × 7, and subsequently

held at the same temperature for 60 s on the tenter.

4.4. Conclusions

In this study, BOPP/TiO_2 nanocomposite films were prepared, and their dielectric properties were analyzed to figure out potentials and problems of BOPP nanocomposites. Major findings and suggestions are summarized below.

- Biaxial stretching without break presumes good dispersion of nanoparticles. This is usually difficult when preformed nanoparticles are directly melt-blended with PP. The RGT provided nanocomposites with uniformly dispersed TiO_2 nanoparticles of about 50–100 nm, which enabled biaxial stretching.

- The relative permittivity of BOPP nanocomposites increased with the addition amount of TiO_2, which, however, accompanied an increase in the loss factor and a decrease in the BDV. The relative permittivity was relatively sensitive to the type of surface modification, and the greatest improvement was obtained with phenylethyl modification.

- Excessive addition of nanoparticles leads to clustering/agglomeration of nanoparticles, which has significant adverse effects on the loss factor, BDV, and leakage current. In the present study, such phenomena were observed at 1.0 vol% of TiO_2.

- The relative permittivity of the nanocomposites was much higher than predictions based on classical mixing rules. A critical role of the interphase around nanoparticles was suggested. In order to exploit the positive contribution of the interphase, nanoparticles must be well separated from each other, and this was accomplished by stretching at a higher drawing ratio.

- The plausible cause of the BDV decrease in the BOPP nanocomposites was the surface roughening that occurred around the nanoparticles during stretching. In fact, post-annealing reduced the surface roughness and partially recovered BDV.

These provide useful insights for research of BOPP nanocomposites. In a practical viewpoint, it is important to pursue materials and processes to reduce surface roughening during biaxial stretching. Understanding and optimization of the interphase will play an essential role in achieving required relative permittivity even at a lower filler amount, which will in turn minimize the demerits associated with the addition of nanoparticles.

References

[1] M. Rabuffi, G. Picci. Status quo and future prospects for metallized polypropylene energy storage capacitors. IEEE Trans. Plasma Sci. 2002, 30, 1939–1942.

[2] Y. Zhou, C. Yuan, S. Wang, Y. Zhu, S. Cheng, X. Yang, Y. Yang, J. Hu, J. He, Q. Li. Interface-modulated nanocomposites based on polypropylene for high-temperature energy storage. Energy Storage Mater. 2020, 28, 255–263.

[3] A. Usuki, Y. Kojima, M. Kawasumi, A. Okada, Y. Fukushima, T. Kurauchi, O. Kamigaito. Synthesis of nylon 6-clay hybrid. J. Mater. Res. 1993, 8, 1179–1184.

[4] M. Castro, J. Lu, S. Bruzaud, B. Kumar, J.-F. Feller. Carbon nanotubes/poly(ε-caprolactone) composite vapour sensors. Carbon 2009, 47, 1930–1942.

[5] B. Luo, X. Wang, Y. Wang, L. Li. Fabrication, characterization, properties and theoretical analysis of ceramic/PVDF composite flexible films with high dielectric constant and low dielectric loss. J. Mater. Chem. A 2014, 2, 510–519.

[6] P. Barber, S. Balasubramanian, Y. Anguchamy, S. Gong, A. Wibowo, H. Gao, H. Ploehn, H.-C. Zur Loye. Polymer composite and nanocomposite dielectric materials for pulse power energy storage. Materials 2009, 2, 1697–1733.

[7] S. K. Kumar, B. C. Benicewicz, R. A. Vaia, K. I. Winey. 50th anniversary perspective: are polymer nanocomposites practical for applications? Macromolecules 2017, 50, 714–731.

[8] T. Iizuka, T. Tanaka. Comparison of partial discharge resistance of several nanocomposites. Electr. Eng. Jpn. 2013, 182, 1–9.

[9] I. Rytoluoto, K. Lahti, M. Karttunen, M. Koponen, S. Virtanen, M. Pettersson. Large-area dielectric breakdown performance of polymer films-part II: interdependence of filler content, processing and breakdown performance in polypropylene-silica nanocomposites. IEEE Trans. Dielectr. Electr. Insul. 2015, 22, 2196–2206.

[10] A. B. Poda, R. Dhara, M. A. Rab, P. Basappa. Evaluation of aging in nanofilled polypropylene by surface discharges. IEEE Trans. Dielectr. Electr. Insul. 2016, 23, 275–287.

[11] G. C. Montanari, D. Fabiani, F. Palmieri, D. Kaempfer, R. Thomann, R. Mulhaupt. Modification of electrical properties and performance of EVA and PP insulation through nanostructure by organophilic silicates. IEEE Trans. Dielectr. Electr. Insul. 2004, 11, 754–762.

[12] M. Takala, M. Karttunen, P. Salovaara, S. Kortet, K. Kannus, T. Kalliohaka. Dielectric properties of nanostructured polypropylene-polyhedral oligomeric silsesquioxane compounds. IEEE Trans. Dielectr. Electr. Insul. 2008, 15, 40–51.

[13] M. Takala, H. Ranta, P. Nevalainen, P. Pakonen, J. Pelto, M. Karttunen, S. Virtanen, V. Koivu, M. Pettersson, B. Sonerud. Dielectric properties and partial discharge endurance of polypropylene-silica nanocomposite. IEEE Trans. Dielectr. Electr. Insul. 2010, 17, 1259–1267.

[14] D. He, Y. Wang, X. Chen, Y. Deng. Core-shell structured $BaTiO_3$@Al_2O_3 nanoparticles in polymer composites for dielectric loss suppression and breakdown strength enhancement. Compos. Part A Appl. Sci. Manuf. 2017, 93, 137–143.

[15] R. Su, Z. Luo, D. Zhang, Y. Liu, Z. Wang, J. Li, J. Bian, Y. Li, X. Hu, J. Gao, Y. Yang. High energy density performance of polymer nanocomposites induced by designed formation of $BaTiO_3$@sheet-likeTiO_2 hybrid nanofillers. J. Phys. Chem. C 2016, 120, 11769–11776.

[16] D. Kang, G. Wang, Y. Huang, P. Jiang, X. Huang. Decorating TiO_2 nanowires with $BaTiO_3$ nanoparticles: A new approach leading to substantially enhanced energy storage capability of high-*k* polymer nanocomposites. ACS Appl. Mater. Interfaces 2018, 10, 4077–4085.

[17] N. Guo, S. A. DiBenedetto, P. Tewari, M. T. Lanagan, M. A. Ratner, T. J. Marks. Nanoparticle, size, shape, and interfacial effects on leakage current density, permittivity, and breakdown strength of metal oxide-polyolefin nanocomposites: experiment and theory. Chem. Mater. 2010, 22, 1567–1578.

[18] M. Streibl, S. Werner, J. Kaschta, D. W. Schubert, R. Moos. The influence of nanoparticles and their functionalization on the dielectric properties of biaxially oriented polypropylene for power capacitors. IEEE Trans. Dielectr. Electr. Insul. 2020, 27, 468–475.

[19] M. Toyonaga, P. Chammingkwan, M. Terano, T. Taniike. Well-defined polypropylene/polypropylene-grafted silica nanocomposites: roles of number and

molecular weight of grafted chains on mechanistic reinforcement. Polymers 2016, 8, 300.

[20] T. Taniike, M. Toyonaga, M. Terano. Polypropylene-grafted nanoparticles as a promising strategy for boosting physical properties of polypropylene-based nanocomposites. Polymer 2014, 55, 1012–1019.

[21] B. Maira, P. Chammingkwan, M. Terano, T. Taniike. Reactor granule technology for fabrication of functionally advantageous polypropylene nanocomposites with oxide nanoparticles. Compos. Sci. Technol. 2017, 144, 151–159.

[22] K. Kaneko, N. Yadav, K. Takeuchi, B. Maira, M. Terano, T. Taniike. Versatile strategy for fabrication of polypropylene nanocomposites with inorganic network structures based on catalyzed in-situ sol-gel reaction during melt mixing. Compos. Sci. Technol. 2014, 102, 120–125.

[23] B. Maira, K. Takeuchi, P. Chammingkwan, M. Terano, T. Taniike. Thermal conductivity of polypropylene/aluminum oxide nanocomposites prepared based on reactor granule technology. Compos. Sci. Technol. 2018, 165, 259–265.

[24] B. Maira, P. Chammingkwan, M. Terano, T. Taniike. New reactor granule technology for highly filled nanocomposites: effective flame retardation of polypropylene/magnesium hydroxide nanocomposites. Macromol. Mater. Eng. 2015, 300, 679–683.

[25] A. Qiagedeer, B. Maira, R. Strauss, Y. Zhao, P. Chammingkwan, G. Mizutani, T. Taniike. Preparation and characterization of polypropylene/noble metal nanocomposites based on reactor granule technology. Polymer 2017, 127, 251–258.

[26] X. Zhang, T. Wada, P. Chammingkwan, A. Thakur, T. Taniike. Cooperative influences of nanoparticle localization and phase coarsening on thermal conductivity of polypropylene/polyolefin elastomer blends. Compos. Part A Appl. Sci. Manuf. 2019, 126, 105602.

[27] X. Zhang, B. Maira, Y. Hashimoto, T. Wada, P. Chammingkwan, A. Thakur, T. Taniike. Selective localization of aluminum oxide at interface and its effect on thermal conductivity in polypropylene/polyolefin elastomer blends. Compos. Part B Eng. 2019, 162, 662–670.

[28] X. Zhang, X. Xia, H. You, T. Wada, P. Chammingkwan, A. Thakur, T. Taniike. Design of continuous segregated polypropylene/Al_2O_3 nanocomposites and impact of controlled Al_2O_3 distribution on thermal conductivity. Compos. Part A Appl. Sci. Manuf. 2020, 131, 105825.

[29] G. Zhang, D. Brannum, D. Dong, L. Tang, E. Allahyarov, S. Tang, K. Kodweis, J.-K. Lee, L. Zhu. Interfacial polarization-induced loss mechanisms in polypropylene/$BaTiO_3$ nanocomposite dielectrics. Chem. Mater. 2016, 28, 4646–4660.

[30] T. Taniike, T. Funako, M. Terano. Multilateral characterization for industrial Ziegler-Natta catalysts toward elucidation of structure-performance relationship. J. Catal. 2014, 311, 33–40.

[31] T. Wada, T. Funako, P. Chammingkwan, A. Thakur, A. Matta, M. Terano, T. Taniike. Structure-performance relationship of $Mg(OEt)_2$-based Ziegler-Natta catalysts. J. Catal. 2020, 389, 525–532.

[32] T. Taniike, X. Zhang, Y. Hashimoto, M. Sueyoshi, T. Ishiwata, D. Zhu. Biaxially oriented polypropylene film. WO 2021205908A1. 14th October **2021**.

[33] T. Glaskova, M. Zarrelli, A. Borisova, K. Timchenko, A. Aniskevich, M. Giordano. Method of quantitative analysis of filler dispersion in composite systems with spherical inclusions. Compos. Sci. Technol. 2011, 71, 1543–1549.

[34] M. Streibl, R. Karmazin, R. Moos. Materials and applications of polymer films for power capacitors with special respect to nanocomposites. IEEE Trans. Dielectr. Electr. Insul. 2018, 25, 2429–2442.

[35] B. Liu, M. Yang, W.-Y. Zhou, H.-W. Cai, S.-L. Zhong, M.-S. Zheng, Z.-M. Dang. High energy density and discharge efficiency polypropylene nanocomposites for potential high-power capacitor. Energy Stor. Mater. 2020, 27, 443–452.

[36] M.-S. Zheng, Y.-T. Zheng, J.-W. Zha, Y. Yang, P. Han, Y.-Q. Wen, Z.-M. Dang. Improved dielectric, tensile and energy storage properties of surface rubberized $BaTiO_3$/polypropylene nanocomposites. Nano Energy 2018, 48, 144–151.

[37] T. Lüpke, S. Dunger, J. Sänze, H. Radusch. Sequential biaxial drawing of polypropylene films. Polymer 2004, 45, 6861–6872.

[38] I. Rytöluoto, A. Gitsas, S. Pasanen, K. Lahti. Effect of film structure and morphology on the dielectric breakdown characteristics of cast and biaxially oriented polypropylene films. Eur. Polym. J. 2017, 95, 606–624.

[39] C.-W. Nan. Physics of inhomogeneous inorganic materials. Prog. Mater Sci. 1993, 37, 1–116.

[40] T. Zakri, J. P. Laurent, M. Vauclin. Theoretical evidence for `Lichtenecker's mixture formulae based on the effective medium theory. J. Phys. D: Appl. Phys. 1998, 31, 1589–1594.

[41] T. Lewis. Nanometric dielectrics. IEEE Trans. Dielectr. Electr. Insul. 1994, 1, 812–825.

[42] T. Tanaka, M. Kozako, N. Fuse, Y. Ohki. Proposal of a multi-core model for polymer nanocomposite dielectrics. IEEE Trans. Dielectr. Electr. Insul. 2005, 12, 669–681.

[43] L. Li, J. Cheng, Y. Cheng, T. Han, Y. Liu, Y. Zhou, G. Zhao, Y. Zhao, C. Xiong, L. Dong, Q. Wang. Significant improvements in dielectric constant and energy density of ferroelectric polymer nanocomposites enabled by ultralow contents of nanofillers. Adv. Mater. 2021, 33, 2102392.

[44] Y. Thakur, T. Zhang, C. Iacob, T. Yang, J. Bernholc, L. Q. Chen, J. Runt, Q. M. Zhang. Enhancement of the dielectric response in polymer nanocomposites with low dielectric constant fillers. Nanoscale 2017, 9, 10992–10997.

[45] Y. Abdullahi Hassan, H. Hu. Current status of polymer nanocomposite dielectrics for high-temperature applications. Compos. Part A Appl. Sci. Manuf. 2020, 138, 106064.

[46] M. Fujiyama, Y. Kawamura, T. Wakino. Study on rough-surface biaxially oriented polypropylene film. II. influence of stretching conditions. J. Appl. Polym. Sci. 1988, 36, 995–1009.

Chapter 5

General Conclusion

Chapter 5

Polypropylene (PP), as one of the most commonly used commercial plastics with excellent chemical resistance and especially low cost, is very promising for use in fabricating polymer nanocomposites. Nanoparticles are introduced to the matrix with the aim of improving properties or introducing extra functionalities for the further applications of PP. However, the addition of nanoparticles usually sacrifices the ductility of the material, which limits the applications of PP-based nanocomposites. In this thesis, I prepared PP nanocomposites by chemically modifying both the nanoparticles and the PP chain, as well as by reactor granule technology, aiming at clarifying key factors for achieving desired properties, including the ductility. The main conclusions are as follows:

In **Chapter 2**, catalyzed copolymerization between propylene and 7-octenyltrimethoxysilane (OTMS) was used to prepare PP with less than one functional group per chain. The advantage of the combination of surface modification and in-situ grafting was evidenced by the mechanical properties, in which the efficient grafting of the reactive chains strengthened the interfacial interaction between the matrix and SiO_2 to improve the reinforcement. In addition, the modification with long alkyl chains also helped to recover the elongation deterioration due to its plasticizing ability. This provided an opportunity to balance the reinforcement and the toughness of the materials, which is rarely achieved by in-situ grafting alone.

In **Chapter 3**, novel functionalized PP containing methoxy groups was synthesized by copolymerization of propylene with 4-Allyl-1,2-dimethoxybenzene (ADMB). PP-ADMB was blended with SiO_2 to fabricate PP nanocomposite. It was found that even

with a trace amount, ADMB, imparted unexceptionally high toughness for PP. These dual effects on compatibilizing with nanoparticles and toughening of polymer make PP-ADMB advantageous over the homo PP in balancing the mechanical properties of nanocomposites.

In **Chapter 4**, a reactor granule technology (RGT) was used to develop biaxially oriented polypropylene (BOPP)/TiO_2 nanocomposites to effectively improve the dielectric properties of PP. The effects of several parameters on the permittivity, BDV, and dielectric loss of the nanocomposites were explored in depth, including TiO_2 content, interfacial design, and drawing ratio. The RGT provided nanocomposites with uniformly dispersed TiO_2 nanoparticles, which enabled biaxial stretching. The permittivity of nanocomposites was greatly enhanced by a small amount of TiO_2 (2 wt%) beyond classical mixing rules, and the enhancement was very sensitive to the stretching ratio.

In conclusion, for the application of PP nanocomposites, balanced mechanical properties of nanocomposites, in particular the toughness, must be preserved or improved. In this thesis, I have successfully shown three different strategies to achieve PP-based nanocomposites with balanced mechanical properties. Furthermore, I have clarified key factors affecting final properties of nanocomposites, which are expected to be useful for the future design of nanocomposites.

Achievements

Main Publication

1. **D. Zhu,** E. Kurahashi, H. You, T. Wada, P. Chammingkwan, T. Taniike, Enhancing mechanical properties of graft-type nanocomposites using organically modified SiO_2 and polypropylene containing reactive methoxy groups, Polymers 2022, 14, 563, (Selected as Editor's Choice articles).

Other Publications

1 **X. Zhang**, **D. Zhu,** H. You, Y. Hashimoto, T. Miyata, P. Chammingkwan, T. Taniike, Dielectric properties of biaxially oriented polypropylene nanocomposites prepared based on reactor granule technology, ACS Appl. Electron. Mater. 2022, 2022, 4, 1257-1265, (Co-first author).

2 H. You, X. Zhang, **D. Zhu**, C. Yang, P. Chammingkwan, T. Taniike, Advantages of polydopamine coating in the design of ZIF-8-filled thin-film nanocomposite (TFN) membranes for desalination, Colloids Surf. A 2021, 629, 127492.

3 A. Piovano, T. Wada, A. Amodio, G. Takasao, T. Ikeda, **D. Zhu**, M. Terano, P. Chammingkwan, E. Groppo, T. Taniike. Formation of highly active Ziegler-Natta catalysts clarified by a multifaceted characterization approach. ACS Catal. 2021, 11, 13782–13796.

Conferences

1. **D. Zhu,** E. Kurahashi, T. Wada, P. Chammingkwan, T. Taniike, Improving mechanical properties of grafttype nanocomposites using silane modified SiO_2 and reactive polypropylene prepared by a Ziegler-Natta catalyst, Hakodate Conv. of JPI (51^{st} Petrol-Petrochem. Symposium of JPI), Hokkaido, Japan, November 11–12, 2021.

2. **D. Zhu,** T. Wada, P. Chammingkwan, T. Taniike, Enhancing mechanical properties of graft-type nanocomposites using silane modified SiO_2 and polypropylene containing reactive methoxy groups, 7^{th} Nano Today Conference, Guangzhou, China, November 16–18, 2021.